

No.1/2015

HYDRAULICA

HYDRAULICS-PNEUMATICS-TRIBOLOGY-ECOLOGY-SENSORICS-MECHATRONICS

ISSN 1453 - 7303
ISSN-L 1453 - 7303

CONTENTS

<ul style="list-style-type: none"> • EDITORIAL: Ce ne sfatuiti? / What Would You Advise Us? Ph.D. Petrin DRUMEA 	5 - 6
<ul style="list-style-type: none"> • High Order Dynamic Model and Control Strategy of Automotive Powertrain System with Electro-hydraulic Driven Dry-clutch Dr. Mario PISATURO, Prof. Dr. Adolfo SENATORE 	7 - 18
<ul style="list-style-type: none"> • Axial Balance in Centrifugal Pumps – Back Labyrinth Versus Dorsal Vanes Lecturer Ph.D. Eng. Sanda BUDEA 	19 - 24
<ul style="list-style-type: none"> • Considerations Regarding the Behavior to Cavitation Erosion of Two Carbon Alloy Stainless Steels Used in the Manufacturing of Hydraulic Equipment Drawers of Command, Adjustment and Distribution PhD.stud. eng. Cristian GHERA, Prof. PhD. eng. Ilare BORDEASU, PhD.stud. eng. Laura SALCIANU, Lecturer PhD. eng. Sebastian Titus DUMA, PhD.stud. eng. Ștefan-Eusebiu KATONA, Assoc. Prof. PhD. eng. Adrian PUGNA, PhD.stud. eng. Lavinia Madalina MICU, PhD. eng. Luoana Florentina PASCU 	25 - 31
<ul style="list-style-type: none"> • Pneumatic Tracking System for Photovoltaic Panel Dr. Eng. Ionel Laurentiu ALBOTEANU 	32- 39
<ul style="list-style-type: none"> • Process Study on the Work of a Dough Kneader with a Planetary Motion of the Kneading Arm PhD. Eng. Dorel STOICA, PhD. Eng. Gheorghe CONSTANTIN 	40 - 45
<ul style="list-style-type: none"> • Determining the Response of a Pneumatic System with Medium and High Pressure Actuators to Step Signal PhD. eng. Gheorghe SOVAIALA, PhD. eng. Radu RADOI, PhD. eng. Gabriela MATACHE, Tech. Ioan PAVEL 	46 - 51
<ul style="list-style-type: none"> • Kinematic and dynamic irregularities of roller pumps Part I. Modeling of kinematic and dynamic irregularities Prof. MSc. Gencho POPOV PhD, MSc. Yuliyen ANGELOV PhD 	52 - 59
<ul style="list-style-type: none"> • Hydrostatic Transmissions Used to Drive Electric Generators in Wind Power Plants Ph.D. eng. Corneliu CRISTESCU, Ph.D. eng. Catalin DUMITRESCU, Ph.D. stud.eng. Ioana ILIE, Dipl. eng. Liliana DUMITRESCU 	60 - 72

MANAGER OF PUBLICATION

- PhD. Eng. Petrin DRUMEA - Hydraulics and Pneumatics Research Institute in Bucharest, Romania

EDITOR IN CHIEF

- PhD. Eng. Gabriela MATAACHE - Hydraulics and Pneumatics Research Institute in Bucharest, Romania

EXECUTIVE EDITOR

- Ana-Maria POPESCU - Hydraulics and Pneumatics Research Institute in Bucharest, Romania

SPECIALIZED REVIEWERS

- PhD. Eng. Heinrich THEISSEN – Scientific Director of Institute for Fluid Power Drives and Controls IFAS, Aachen - Germany

- Prof. PhD. Eng. Henryk CHROSTOWSKI – Wrocław University of Technology, Poland

- Prof. PhD. Eng. Pavel MACH – Czech Technical University in Prague, Czech Republic

- Prof. PhD. Eng. Alexandru MARIN – POLITEHNICA University of Bucharest, Romania

- Assoc. Prof. PhD. Eng. Constantin RANEA – POLITEHNICA University of Bucharest, Romania

- Lecturer PhD. Eng. Andrei DRUMEA – POLITEHNICA University of Bucharest, Romania

- PhD. Eng. Ion PIRNA - General Manager - National Institute Of Research - Development for Machines and Installations Designed to Agriculture and Food Industry – INMA, Bucharest- Romania

- PhD. Eng. Gabriela MATAACHE - Hydraulics & Pneumatics Research Institute in Bucharest, Romania

- Lecturer PhD. Eng. Lucian MARCU - Technical University of Cluj Napoca, ROMANIA

- PhD. Eng. Corneliu CRISTESCU - Hydraulics & Pneumatics Research Institute in Bucharest, Romania

- Prof. PhD. Eng. Dan OPRUTA - Technical University of Cluj Napoca, ROMANIA

Published by:

Hydraulics and Pneumatics Research Institute, Bucharest-Romania

Address: 14 Cuțitul de Argint, district 4, Bucharest, post code 040558, ROMANIA

Phone: +40 21 336 39 90; +40 21 336 39 91 ; Fax: +40 21 337 30 40 ;

e-Mail: ihp@fluidas.ro

Web: www.ihp.ro

with support of:

National Professional Association of Hydraulics and Pneumatics in Romania - FLUIDAS

e-Mail: fluidas@fluidas.ro

Web: www.fluidas.ro

HIDRAULICA Magazine is indexed by the international databases:



HIDRAULICA Magazine is indexed by the Romanian Editorial Platform:



ISSN 1453 – 7303; ISSN – L 1453 – 7303

EDITORIAL

Ce ne sfatuiti?

Inceputul de an reprezinta de obicei perioada de asezare a lucrurilor pentru programul anual al fiecărei unitati de productie. In aceste cateva saptamani fiecare firma isi definitiveaza planul de afaceri, cu precadere care sa fie nivelul numeric al personalului si chiar care sa fie structura profesionala si nivelul de pregatire al acestuia. Pentru aceasta conducatorii fac tot felul de analize, pornind de la studiile de marketing ale lor si ale altora, unii incercand sa se foloseasca de experienta lor anterioara, chiar daca situatia pietei nu mai este cea traditionala. Ca urmare, numarul celor care ne intreaba “ce ne sfatuiti?” este foarte mare, iar eu ma gandesc destul de serios ca



Dr.ing. Petrin DRUMEA
DIRECTOR DE PUBLICATIE

ne-am putea intreba “care sunt elementele care ne permit sa avem niste pareri autorizate?” Ideea cum ca noi am sti ce trebuie facut pentru ca lucram in Bucuresti, ca avem contacte cu multe firme din tara, ca avem contacte internationale, ca avem acces direct la datele furnizate de CETOP si ca stim ce noutati sunt de perspectiva, este o idee corecta pana intr-un punct, pentru ca partea economica a raspunsului ne depaseste.

Aspectul economic din tara este cunoscut de noi in principiu, fara a avea capacitatea de analiza amanuntita si eventual corecta, asa ca de obicei ramanem doar la aspectul tehnic. Ca urmare a modificarilor structurale din economia nationala, cea mai importanta activitate pe care o poate desfasura un IMM din Romania care activeaza in domeniul hidropneumaticii este activitatea de mentenanta si de reparatii. Pentru aceasta activitate, unitatea trebuie sa dispuna de cativa specialisti cu pregatire adecvata; de asemenea, trebuie sa dispuna de mici standuri de verificare si de aparatura de masura si control a parametrilor hidraulici, pneumatici si chiar si mecanici. Trebuie mare atentie ca nu orice unitate poate face reparatii de echipamente complexe, ca de exemplu pompele si servovalvele.

Mentenanta si reparatia trebuie sa se refere cu prioritate la instalatiile hidraulice, indiferent de complexitatea acestora. Revenind la activitatea de reparatii a echipamentelor ar trebui retinut ca marii producatori ofera kit-uri de reparatii, care usureaza munca si asigura un nivel de calitate destul de bun. Pentru activitatea de productie recomandarea noastra se indreapta spre subansamble si echipamente care nu se regasesc in fabricatia de serie a marilor producatori si, de asemenea, spre producerea unor instalatii de complexitate mica si medie pe baza unor proiecte bine conturate.

Toate aceste directii de activitate ar trebui dublate obligatoriu de o perfectionare tehnica si manageriala adecvata a tuturor specialistilor din intreprindere. Nu cred ca se poate face o activitate eficienta in domeniu fara a dispune de un personal cu buna calificare, indiferent de pregatirea scolara, desi bine ar fi sa existe un anumit dezechilibru care sa incline balanta catre absolventii de cursuri universitare de specialitate sau de specialitati apropiate.

EDITORIAL

What would you advise us?

The beginning of the year is usually the period when things are settled with regard to the annual schedule of each production entity. During these few weeks each company finalizes its business plan elaboration, especially deciding which should be the number of the staff and even its professional structure and training level. For that leaders are doing all sorts of analyzes, based on their own marketing studies and studies belonging to others, some trying to use their previous experience, even if the situation on the market is no longer the traditional one. As a result, the number of people who ask us "What would you advise us?" is very large, and I think quite seriously



Ph.D.Eng. Petrin DRUMEA
MANAGER OF PUBLICATION

that we could ask ourselves: "Which elements allow us to have some competent opinions?" The idea that we are very likely to know what is best to be done as we work in Bucharest, we have contacts with many companies in the country, we also have international contacts, we have direct access to data provided by CETOP and we know which are the forward-looking new issues, is an accurate idea up to a point, because the economic side of the answer is beyond us.

The economic aspect in the country is known to us virtually, with no ability of ours to make a detailed and possibly proper analysis, so we usually just stick to the technical side. As a result of structural changes in the national economy, the most important activity that can be performed by an SME in Romania working in the field of hydro pneumatics is the maintenance and repair activity. For this activity, the unit must have a couple of specialists with suitable education and training; it must also have small testing stands and devices for measuring and controlling the hydraulic and pneumatic parameters, and even the mechanical ones. Much care is needed, as not any unit can repair complex equipment, such as pumps and servo valves.

Maintenance and repair must refer prevalently to hydraulic installations, regardless of their complexity. Coming back to the activity of equipment repairing, it should be noted that large manufacturers offer repair kits, which facilitate work and ensure a quality good enough. Our recommendation for production operations targets parts and equipment which are not found in mass production of large manufacturers, and it also targets the development of small and medium complexity equipment based on well-defined projects.

All these activity directions should necessarily be accompanied by a suitable technical and managerial training for all professionals in the company. I do not think anyone can do efficient work in the field without having a well-trained staff, regardless of its school education, although it would be better for a certain imbalance to exist, turning the scale in favour of those professionals who have graduated from university courses in the specific field or adjacent areas.

High Order Dynamic Model and Control Strategy of Automotive Powertrain System with Electro-hydraulic Driven Dry-clutch

Dr. Mario PISATURO¹, Prof. Dr. Adolfo SENATORE^{1,*}

¹ Department of Industrial Eng., University of Salerno, {mpisaturo,a.senatore}@unisa.it

* corresponding author

Abstract: *In Automated Manual Transmissions (AMTs) based on electro-actuated dry-clutch design the frictional material properties, the sensors accuracy, the response of the throwout bearing actuator, and the control strategies to drive the engagement operation are mutual interdependent and only an optimized mechatronic design could lead to an effective target from several points of view: passengers' comfort, fuel economy, system reliability, performance, driving feeling, etc.*

In such transmissions, the quality of the vehicle propulsion as perceived by driver and passengers is largely dependent on either the quality of the control strategies and the fast dynamics of the clutch subsystems. Furthermore, sensitivity analyses on control schemes for this type of transmissions have shown that uncertainties on the prediction of the actual torque transmitted by the clutch can severely affect the engagement performance.

In this paper a high order dynamic model of the powertrain system which includes the electro-hydraulic actuator dynamics has been analysed to design a feedback controller based on multiple Model Predictive Controller (MPC). Simulations of start-up manoeuvres prove the effectiveness of the proposed control strategy and encourage the development of real-time routines for the testing on transmission control unit.

Keywords: *electro-hydraulic actuator, dry-clutch control, mechatronic transmission, simulation*

1. Introduction

An Automated Manual Transmission (AMT) is directly derived from a manual one through the integration of actuators. In this way, development and production costs are generally lower than other automatic transmissions, while the reliability and durability are at highest level. For high class sport cars, vehicle dynamic performances and driving quality can be strongly improved with respect to automatic transmissions [1,2].

In AMTs the clutch engagement during gearshift is managed by an actuator driven by the Transmission Control Unit (TCU). Consequently, high importance is assumed by the actuator positioning accuracy along with the reliability of the control algorithm implemented in the TCU. Several models of control strategies for dry clutches in AMTs have been proposed in the literature, e.g., classical controller [2], decoupling control [3], optimal control [4,5], predictive control [6,7], and robust control [8,9]. However, as explained in [10] effective AMTs controllers are difficult to be designed without having a physical model to predict the actual frictional torque transmitted by the clutch.

On the other hand, the improvement of the engagement smoothness has driven the vehicle designers to deepen about vibrations that arise during the clutch operations to prevent poor ride quality, discomfort and noise. The control systems in modern automated manual transmission systems couldn't provide good improvement of vehicle longitudinal dynamics during gearshifts without a deep knowledge of the driveline stiffness and damping parameters, along with the frictional conjunction between its main subparts. To this end, more phenomena about vibrations and actuation noises in clutch and gearbox (e.g., judder, shuffle, eek, whoop, clunk, scratch, etc.) have been identified and analyzed [11-17].

In this paper a high order dynamic model of the powertrain system which includes the electro-hydraulic actuator dynamics has been analyzed to design a feedback controller based on multiple Model Predictive Controller (MPC) [6,18]. The MPC is developed to comply with constraints both on the inputs and the outputs. The controller aims at ensuring a comfortable lock-up by avoiding

the engine stall as well even with reduced engagement time. One of the main factors which have led to use the MPC approach could be found in its ability to explicitly handle the constraints. This means that the controller allows for input constraints, like for example actuator saturation constraints, and it never generates input signal that attempt to violate them. Thus, with predictive control the wind-up problem does not arise [19]. Furthermore, with the rapid development of computing, MPC becomes more and more attractive feedback strategy in fast dynamics systems [20].

Simulations of start-up manoeuvres prove the effectiveness of the proposed control strategy and encourage the development of real-time routines for the testing on transmission control unit.

2. Driveline Model

This section describes a model for simulating the driveline dynamic behaviour; the Fig. 1 shows the driveline main subparts on the left side and its model, on the right. The subscripts e, f, c, g, w are referred to engine, flywheel, clutch disc, (primary shaft of) gearbox, and wheels, respectively. A dynamic model of the driveline can be obtained by applying the d'Alembert equilibrium at the nodes of the driveline scheme, where T indicates the torques, J the inertias and θ the angles.

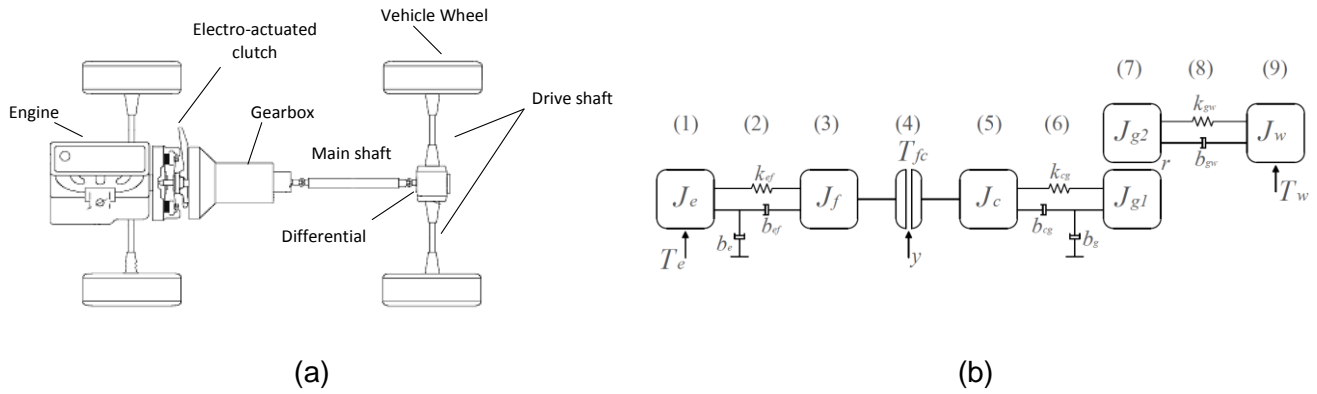


Fig. 1. (a) car driveline and (b) 5 degree-of-freedom driveline model

The equations which model the driveline are:

$$J_e \dot{\omega}_e = T_e(\omega_e) - b_e \omega_e - T_{ef}(\vartheta_{ef}, \omega_{ef}) \quad (1)$$

$$J_f \dot{\omega}_f = T_{ef}(\vartheta_{ef}, \omega_{ef}) - T_{fc}(x_{io}) \quad (2)$$

$$J_c \dot{\omega}_c = T_{fc}(x_{io}) - T_{cg}(\vartheta_{cg}, \omega_{cg}) \quad (3)$$

$$J_g(r) \dot{\omega}_g = T_{cg}(\vartheta_{cg}, \omega_{cg}) - b_g \omega_g - \frac{1}{r} T_{gw}(\vartheta_{gw}, \omega_{gw}) \quad (4)$$

$$J_w \dot{\omega}_w = T_{gw}(\vartheta_{gw}, \omega_{gw}) - T_w(\omega_w) \quad (5)$$

and the angular speeds are:

$$\dot{\vartheta}_e = \omega_e \quad (6)$$

$$\dot{\vartheta}_{ef} = \omega_{ef} = \omega_e - \omega_f \quad (7)$$

$$\dot{\vartheta}_{cg} = \omega_{cg} = \omega_c - \omega_g \quad (8)$$

$$\dot{\vartheta}_{gw} = \omega_{gw} = \omega_g - \omega_w \quad (9)$$

where T_e is the engine torque (assumed to be a control input of the model), T_{fc} is the torque transmitted by the clutch (the second control input), y is the throwout bearing position, and T_w is the equivalent load torque at the wheels (a measured disturbance). The gear ratio is r (which here includes also the final conversion ratio), and J_c is an equivalent inertia, which includes the masses of the clutch disc, friction pads and the cushion spring.

Furthermore the following equations also hold:

$$J_g(r) = J_{g1} + \frac{J_{g2}}{r^2} \quad (10)$$

$$T_{ef}(\vartheta_{ef}, \omega_{ef}) = k_{ef}\vartheta_{ef} + b_{ef}\omega_{ef} \quad (11)$$

$$T_{cg}(\vartheta_{cg}, \omega_{cg}) = k_{cg}\vartheta_{cg} + b_{cg}\omega_{cg} \quad (12)$$

$$T_{gw}(\vartheta_{gw}, \omega_{gw}) = k_{gw}\vartheta_{gw} + b_{gw}\omega_{gw} \quad (13)$$

$$T_w(\omega_w) = T_{w0} + \frac{1}{2}\rho_a A c_d R_w^3 \omega_w^2 \quad (14)$$

where k are torsional stiffness coefficients, b viscous damping, T_{w0} a constant load torque, ρ_a the air density, A the front surface vehicle area, c_d the air drag-resistance coefficient, R_w the wheels radius.

These equations represent the driveline system during the slipping phase, whereas, during the engaged phase, the flywheel angular speed ω_f and the clutch angular speed ω_c are the same: thus, the equations (2) and (3) can be summed each other, which yields:

$$(J_c + J_f)\dot{\omega}_c = T_{ef}(\vartheta_{ef}, \omega_{ef}) - T_{cg}(\vartheta_{cg}, \omega_{cg}) \quad (15)$$

The driveline parameters used for the simulation are typical for a mid-size car and can be found in literature. An alternative mathematical representation of the driveline useful for the Model Predictive Control (MPC) approach is the State-Space representation. In the continuous domain the driveline model can be written as follows:

$$\dot{\mathbf{x}}(t) = [\mathbf{A}_{sl}d + \mathbf{A}_{eng}(1-d)]\mathbf{x}(t) + [\mathbf{B}_{sl}d + \mathbf{B}_{eng}(1-d)]\mathbf{u}(t) \quad (16a)$$

$$\mathbf{y}(t) = \mathbf{C}\mathbf{x}(t) \quad (16b)$$

where the state, input and output vectors are respectively:

$$\mathbf{x} = \{\omega_e \quad \vartheta_e \quad \omega_f \quad \vartheta_f \quad \omega_c \quad \vartheta_c \quad \omega_g \quad \vartheta_g \quad \omega_w \quad \vartheta_w\} \quad (17)$$

$$\mathbf{u} = \{T_e \quad T_{fc} \quad T_w\}^T \quad (18)$$

$$\mathbf{y} = \{\omega_e \quad \omega_c\}^T \quad (19)$$

and d is a switching integer equal to 1 when the system is in the slipping phase and 0 otherwise. The subscript *sl* and *eng* indicate the slipping and the engaged system matrices, respectively, and the matrices can be simply deduced from equation (1)-(15).

The MPC has been designed with the discrete time version of the driveline model (16) obtained by using the zero-order hold method with a sampling time of 0.01s. This value is compatible for automotive applications. In fact, as reported in [21] the computational cycle adopted for these applications is set as 5 to 10ms.

3. Actuator Model

In this section a model of the hydraulic actuator system with the usual features of those coupled to AMT systems is introduced. As previously explained, the aim of the actuator is to throwout bearing position and, consequently, the torque transmitted from the engine to the wheels. In this way it is possible to disengage and engage the clutch during the start-up and the gear-shifts manoeuvres.

The actuator is mainly composed by a hydraulic piston connected to a diaphragm spring by the way of a roller bearing ("throwout-bearing") and other springs that keep the clutch closed when no pressure is applied to the piston, Fig. 2. The piston chamber is connected to a servovalve by means of pipeline. The other two-way of the servovalve are connected to a supply circuit and to a discharge circuit, see Fig. 2 for details. The position of the spool valve, which is controlled by an electromagnetic circuit, determines if the hydraulic circuit is in the filling phase or in the dumping phase. The servovalve connects the piston chamber to the discharging circuit in order to disengage the clutch. The springs push the piston back and the oil flows to the tank. Conversely, to engage the clutch the servovalve connects the piston chamber to the supply circuit in this way the piston force overcomes the springs reactions. The servovalve displacement is controlled in current and to keep the clutch at a certain position, an offset current is needed to hold the spool in its neutral point, that corresponds to no oil flowing in the circuit. For currents greater than this offset value, the actuator is connected to the high pressure power supply, while for currents smaller than the offset value, the actuator is connected to the low-pressure circuit [2].

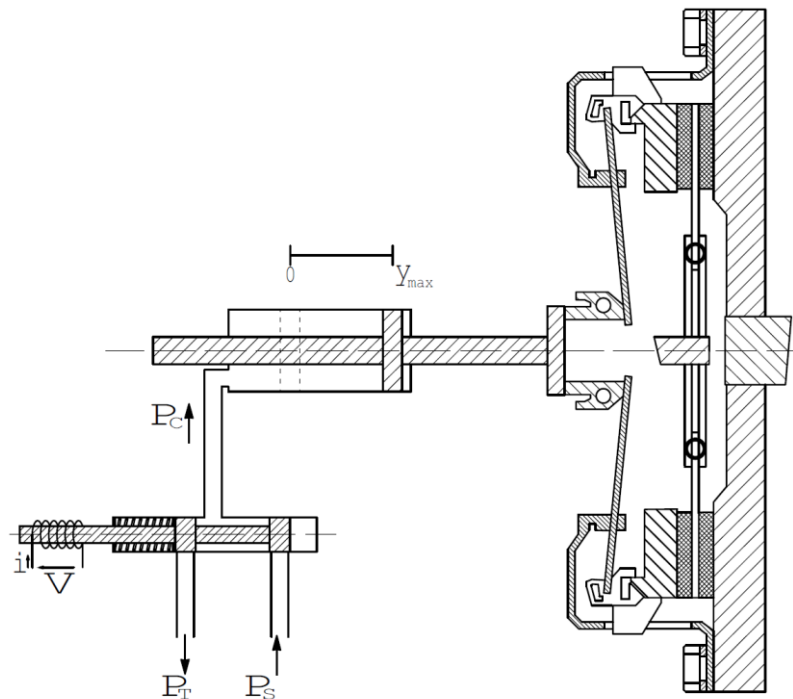


Fig. 2. Actuator scheme and clutch at open position

The clutch actuator is mainly constituted by a mass m_p driven by the springs forces $F_{to}(y)$, friction damping forces and hydraulic forces. The mathematical model which describes the piston dynamics is:

$$m_p \ddot{y} + b_p \dot{y} = A_p P_C - F_{to}(y) \quad (20)$$

$$\dot{P}_C = \frac{\beta}{V_t + A_p y} (q(x, P_C) - A_p \dot{y}) \quad (21)$$

where y is the piston position, P_C is the pressure in the actuator chamber, m_p is the actuator mass, b_p is the viscous damping, A_p is the actuator cross-sectional area, $F_{to}(y)$ is the diaphragm spring and pre-load force as function of the actuator position (see Fig. 3), V_t is the minimum volume of the chamber at $y=0$, $q(x, P_C)$ is the oil flow given by the eq. (24) and finally β is the bulk modulus of the oil.

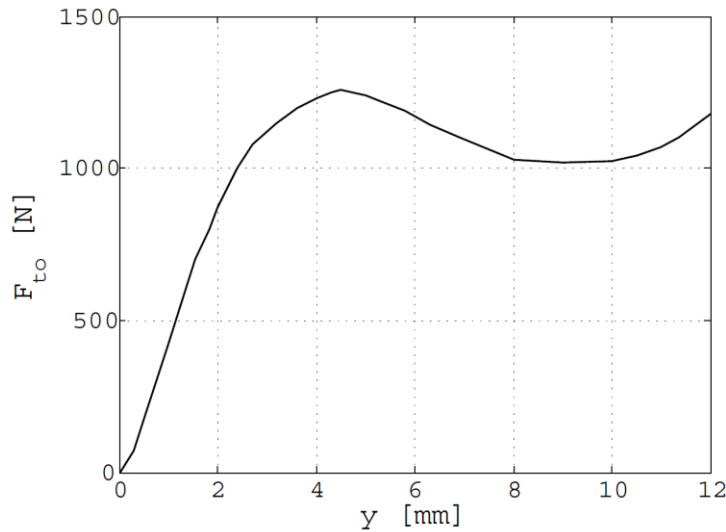


Fig. 3. Diaphragm reaction vs. actuator position

3.1 Servovalve model

A three-way spool flow servovalve with the plunger driven by an electromagnetic actuator has been considered. The servovalve scheme is reported in the Fig. 2 and the mathematical model of the plunger motion is reported below:

$$m_v \ddot{x} + b_v \dot{x} - k_v x = F_M(x, \varphi) + F_B(x, P_C) - F_0 \quad (22)$$

where x is the plunger position, m_v the plunger mass, b_v is the viscous damping, k_v is the stiffness coefficient, F_M is the magnetic force, is the magnetic flux, F_B is the Bernoulli force due to fluid flow through the orifices and F_0 is the spring pre-load.

Under usual operating conditions, the magnetic force acting on the servovalve plunger is considered proportional to the valve current. Moreover, by neglecting the Bernoulli force and by designing a high gain current controller, the servovalve can be considered a current-driven actuator [2]. Under this light the relationship between the servovalve current and the plunger position is given by the following equation:

$$x = \frac{-F_0 + k_f i}{k_v} \quad (23)$$

3.2 Hydraulic model

By considering an overlapped valve, i.e. the land width is greater than the port width when the plunger is in the neutral position and consequently no oil flows through the orifices. This means that there is a dead-band in the orifice area vs. plunger position as described in the equation (24). The oil flow through the servovalve can be written according to Bernoulli's equation:

$$q = \begin{cases} \text{sgn}(P_s - P_c) C_d \sqrt{\frac{2|P_s - P_c|}{\rho}} f_f(x) \\ 0 \\ -\text{sgn}(P_c - P_T) C_d \sqrt{\frac{2|P_c - P_T|}{\rho}} f_d(x) \end{cases} \quad (24)$$

where the first case represents the filling phase ($x > x_f$), the second case represents the dead-zone ($x_d \leq x \leq x_f$) and the last case represents the dumping phase ($x < x_d$). C_d is the discharge coefficient, ρ is the oil density, P_s is the supply pressure and P_T is the tank pressure. The functions f_f and f_d describe the relationship between the orifice area vs. plunger position.

$$\begin{cases} f_f(x) = 1.3796x^2 - 1.4197x + 0.1335 \\ f_d(x) = 1.3371x^2 - 3.0447x + 1.4799 \end{cases} \quad (25)$$

The actuator parameters used for the simulations are listed in [2].

4. Controller Design

In order to manage the engagement phases two closed loops have been designed, Fig. 4. The outer closed loop manages the driveline dynamics and a multiple Model Predictive Control (MPC) strategy has been implemented. The inner loop supervises the actuator position tracking: a PI controller has been designed by neglecting the sensor dynamics.

The electro-hydraulic actuator dynamics depicted in the section 3 is represented by the block $A(z)$ whereas the "Clutch torque model" introduces the frictional torque based on the elastic properties of diaphragm and cushion springs, the clutch disk geometry and the friction coefficient of the disk facings according to the models and outcomes in [22-24].

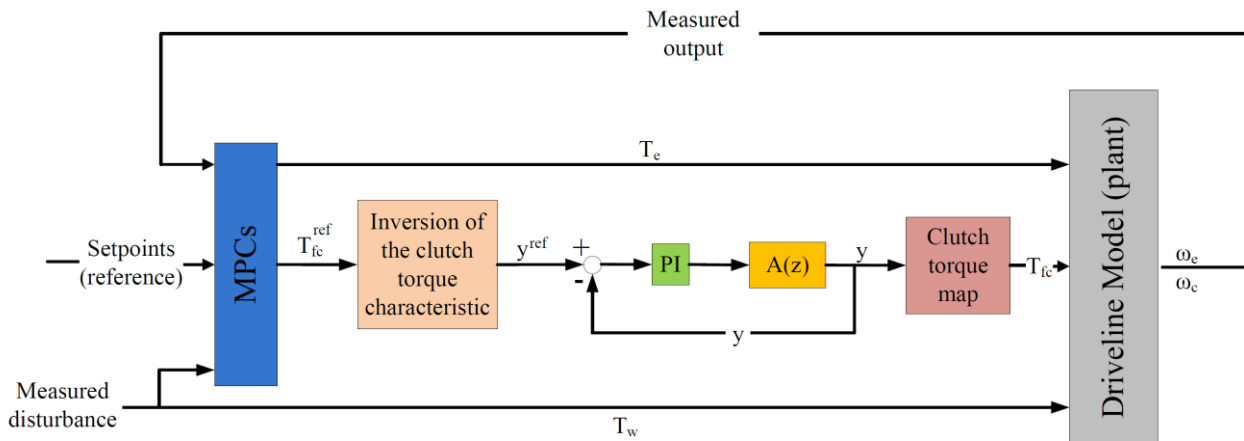


Fig. 4. Block-diagram with MPC-based controller, clutch and driveline models

4.1 Multiple Model Predictive Control

In this section the control approach through MPC theory is explicated. This kind of algorithm provides numerous advantages over the conventional control algorithms. Indeed, it handles multivariable control problem naturally, it can take account of actuator limitations, it allows the system to operate closer to constraints than conventional control, and finally control update rates are relatively low in these applications, so that there is plenty of time for the necessary on-line computations [19].

As explained above, the clutch operates in two different working conditions: the slipping phase and the engaged phase. That is why two different controllers for each phase have been designed. The switching parameter d selects the controller by considering the absolute value of the difference between the engine and the clutch angular speed. Particularly, the switching condition is attained when $\omega_{sl} = \omega_e - \omega_c \leq 1$ rad/s.

It is important to emphasize that in no way the two controllers can work simultaneously and so any conflict between them is avoided *a priori*.

The MPC has been designed with the discrete time version of the driveline model (16) obtained by using the zero-order hold method with a sampling time of 0.01 s. As explained above, this value is compatible for automotive applications.

$$\begin{aligned} \mathbf{x}_{k+1} &= [\bar{\mathbf{A}}_{sl}d + \bar{\mathbf{A}}_{eng}(1-d)]\mathbf{x}_k + [\bar{\mathbf{B}}_{sl}d + \bar{\mathbf{B}}_{eng}(1-d)] \\ \mathbf{y}_k &= \bar{\mathbf{C}}\mathbf{x}_k \end{aligned} \quad (26)$$

The MPC aims at finding the output y_k by tracking the reference trajectory r_k and fulfilling the constraints seen above for any time step $k \geq 0$.

Under the assumption that the estimate of \mathbf{x}_k is available at time k , the cost function to be optimized is:

$$J_i(\Delta u, \varepsilon) = \mathbf{u}_i^T \mathbf{W}_{u,i}^2 \mathbf{u}_i + \Delta \mathbf{u}_i^T \mathbf{W}_{\Delta u,i}^2 \Delta \mathbf{u}_i + [\mathbf{y}_i - \mathbf{r}_i]^T \mathbf{W}_{y,i}^2 [\mathbf{y}_i - \mathbf{r}_i] + \varepsilon \quad (27)$$

where:

$$\mathbf{u}_i = [u_i(0) \quad \dots \quad u_i(P-1)]^T \quad (28)$$

is the input vector;

$$\Delta \mathbf{u}_i = [\Delta u_i(0) \quad \dots \quad \Delta u_i(P-1)]^T \quad (29)$$

is the input increment vector;

$$\mathbf{y}_i = [y_i(1) \quad \dots \quad y_i(P)]^T \quad (30)$$

is the output vector;

$$\mathbf{r}_i = [r_i(1) \quad \dots \quad r_i(P)]^T \quad (31)$$

is the reference trajectory vector. $W_{u,i}$, $W_{\Delta u,i}$ and $W_{y,i}$ are, respectively, the input, input increment and output weights matrices (diagonals and squares); the subscript $i=1,2$ accounts for the two inputs and two outputs of the "plant". The constraints on u , Δu , y are softened by introducing the slack variable $\varepsilon \geq 0$. In (27), the weight ρ_ε on the slack variable ε penalizes the violation of the constraints. As ρ_ε increases with respect to the input and output weights, the controller gives higher priority to the minimization of constraint violations [7].

4.2 Closed-loop actuator control

A classical regulator PI has been designed on the basis of a linearised model of the actuator. In particular, from the non-linear actuator model described by equations (20)-(25) a simplified linear model has been achieved by using a built-in function in MATLAB/SIMULINK[®]. The local feedback control on the throwout bearing position provides robustness to the closed loop system. The reference bearing position is obtained by inverting the clutch torque signal output of the MPC by a look-up table which represents the inversion of the static clutch torque characteristic as show in the Fig. 4.

The PI parameters $K_P=1.2$ and $K_I=0.5$ have been obtained by trial and error procedure looking for the best trade-off between a fast response and the restriction of the wind up problem.

5. Simulation Results

The simulation results have been obtained by implementing the driveline and the actuator models in the MATLAB/SIMULINK[®] environment. Two typical vehicle launch manoeuvres has been considered: *slow* and *fast*. The switch between the slipping and the engaged phase is selected by a Stateflow finite state machine. This signal is used both to select the MP controller suitable to manage each phase and to select the part of the driveline model to activate. The switching condition is reached when the value of the slip speed is less than 1 rad/s. Once the clutch is engaged, the throwout bearing position is rapidly increased to its maximum value by the control algorithm. In other words the clutch actuator reaches the rest position.

Figs. 5, 6 and 7 show the results of the controlled AMT in a slow start-up manoeuvre. The behaviours of the engine and angular velocity, set-points and plant outputs, and those of the engine torque and throwout bearing position are depicted. The comparison between the set-points and the plant outputs shows the good performances of the MPC both before that after the clutch engagement. In fact, the clutch speed set-point trajectory is well tracked by the plant output during the engagement phase and together with the engine speed reach in few seconds the regime value. Moreover in the Fig. 6 the effectiveness of the constraints on the engine torque and on its rate have highlighted showing again the good performance of the MPC.

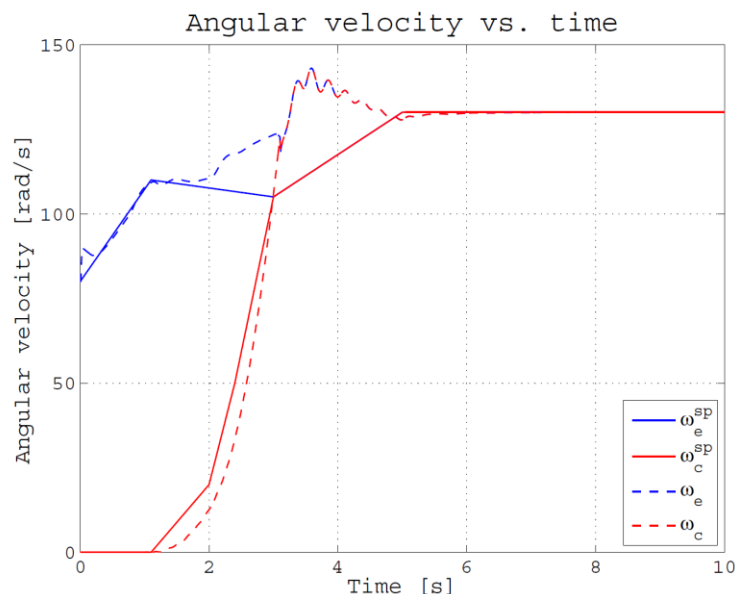


Fig. 5. Slow start-up manoeuvre: angular velocity, set-point trajectory and plant outputs

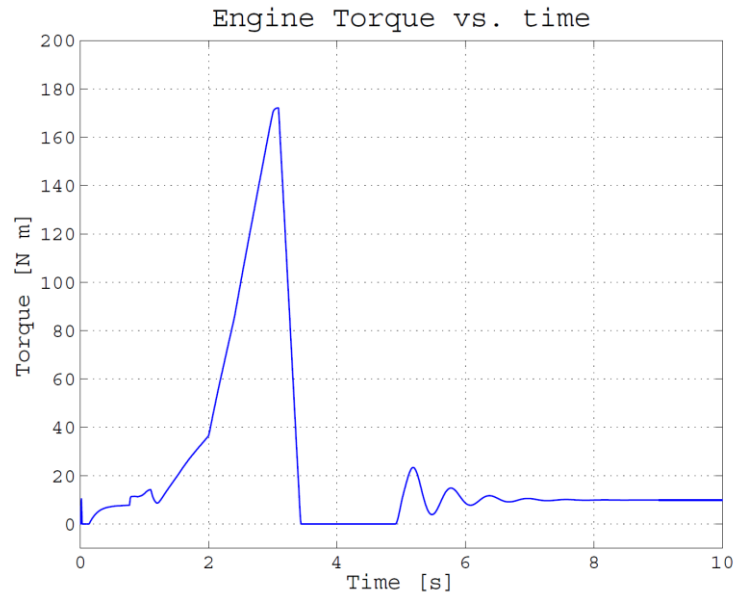


Fig. 6. Slow start-up manoeuvre: engine torque

Finally, in the Fig. 7 the good performance of the PI inner loop on the throwout bearing position is depicted. It is worth noting that with a good choice of the PI parameters K_P and K_I the wind-up does not arise.

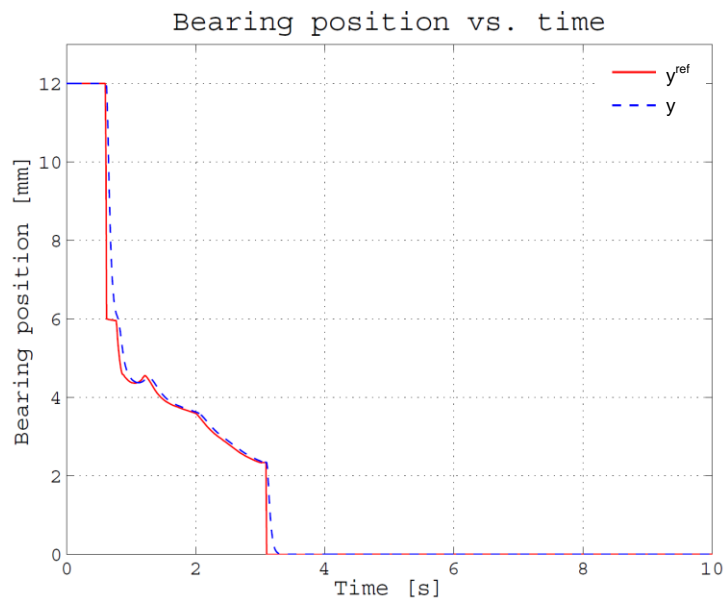


Fig. 7. Slow start-up manoeuvre: throwout bearing position

Figs. 8, 9 and 10 show the results of the controlled AMT in a fast start-up manoeuvre. In this case the comparison between the set-points and the plant outputs shows that for a fast manoeuvre there is an increment of the jerks after that the engagement condition is reached. The Fig. 9 highlights the effectiveness of the constraints on the engine torque and on its rate. Finally, in the Fig. 10 is reported that, also in a fast manoeuvre, the PI controller on the throwout bearing position attains good performances. Indeed, also in this case the wind up does not occur. This means that the throwout bearing position never reaches dangerous and unwanted condition, i.e. excessive stress on the actuator that may be damaged, without the necessity of a saturation on the actuator output highlighting the robustness of the inner closed loop. Figs. 7 and 10 depicts as after that the

engaged condition is attained, the throwout bearing position reaches its rest position. Simulations of the actuator dynamics in open-loop, whose results are not reported here for the sake of brevity, have proven the limits of such industrial cheaper approach concerning the poor tracking of the reference clutch torque.

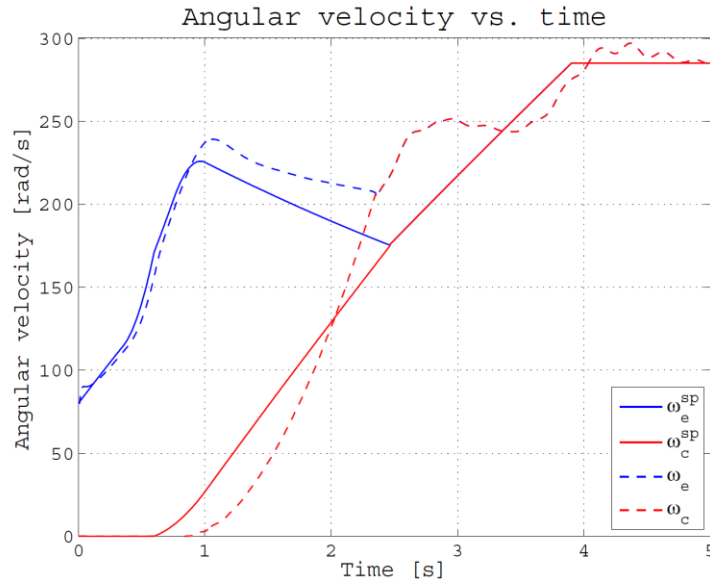


Fig. 8. Fast start-up manoeuvre: angular velocity, set-point trajectory and plant outputs

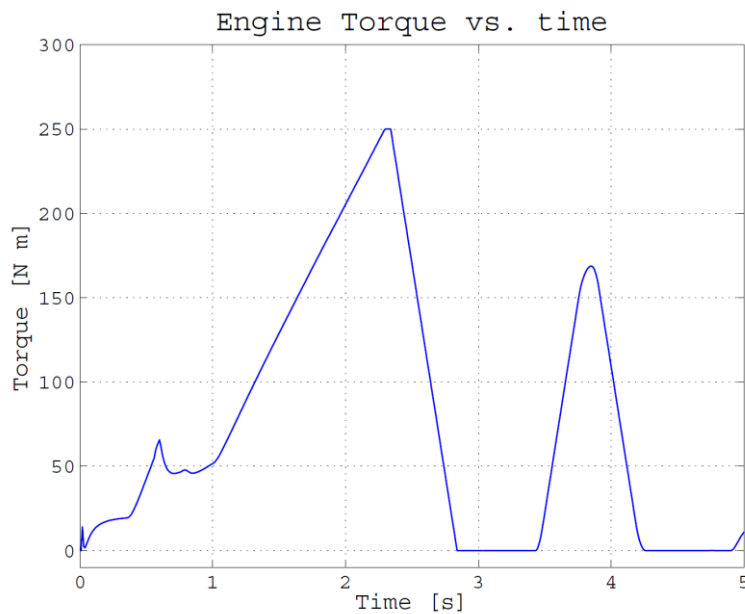


Fig. 9. Fast start-up manoeuvre: engine torque

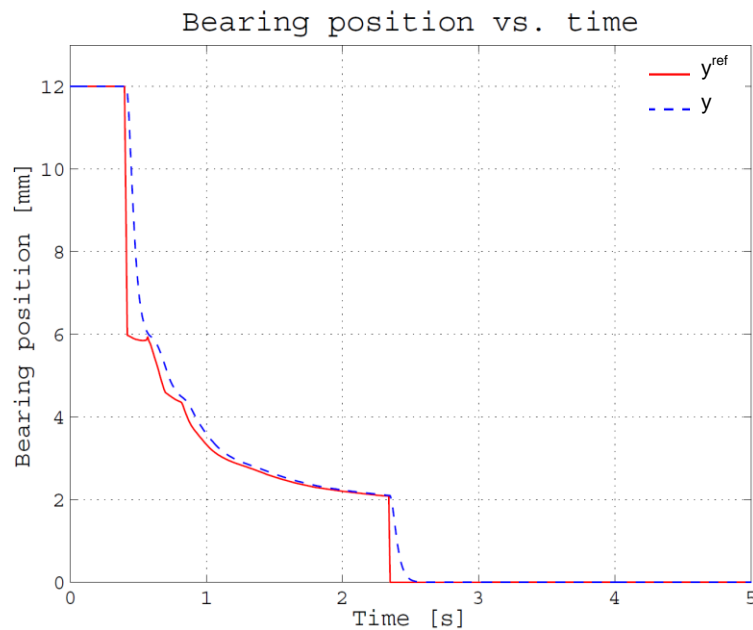


Fig. 10. Fast start-up manoeuvre: throwout bearing position

6. Concluding remarks

In this paper the dynamics of a high-order automotive driveline coupled to dry-clutch system driven by electro-hydraulic actuator has been analyzed to simulate the launch transient manoeuvres of vehicles equipped with robotized (or AMTs) transmission. The frictional torque transmitted from the engine to the vehicle wheels through the dry clutch disks is governed by the constrained multiple model predictive control and its output signals provided to the actuator. Two controllers have been designed: the first one manages the slipping phase whereas the second one manages the engaged phase. Moreover, the clutch actuator dynamics is managed by position-sensing closed loop control by using a PI regulator.

The simulations results have showed the good performances of the MPC especially for a slow start-up manoeuvre. Moreover, the robustness of the PI regulator has been highlighted for both the start-up manoeuvres. Indeed, the good performances exhibited by the PI controller in both the cases is confirmed by the good tracking of the reference signal, by the fast actuator response and by the evidence of the throwout bearing positions which never exceed their limits making the saturation unnecessary. The simulation of the actuator dynamics in open-loop control has showed poor tracking of the reference clutch torque.

Future studies will focus on the role of fast temperature changes due to the huge amount of heat generated at clutch disk facings' interface and the influence of such behaviour on frictional characteristics and actuator response modification.

References

- [1] A. Senatore, "Advances in the automotive systems: an overview of Dual-Clutch Transmissions", *Recent Patents on Mechanical Engineering*, vol. 2, pp. 93–101, 2 2009, ISSN: 2212-7976;
- [2] M. Montanari, F. Ronchi, C. Rossi, A. Tilli, and A. Tonielli, "Control and performance evaluation of a clutch servo system with hydraulic actuation", *Control Engineering Practice*, vol. 12, no. 11, pp. 1369–1379, 2004, *Mechatronic Systems*, ISSN: 0967-0661;
- [3] L. Glielmo, L. Iannelli, V. Vacca, and F. Vasca, "Gearshift control for Automated Manual Transmissions", *IEEE/ASME Transactions on Mechatronics*, vol. 11, no. 1, pp. 17–26, 2006, ISSN: 1083-4435;

- [4] L. Glielmo, F. Vasca, "Optimal control of dry clutch engagement". Proc. of SAE 2000 World Congr, (2000) March 6-9; Detroit, MI, USA;
- [5] P. Dolcini, C. Canudas de Wit, and H. Bechart, "Lurch avoidance strategy and its implementation in AMT vehicles, *Mechatronics*", vol. 18, pp. 289–300 (2008);
- [6] A. Bemporad, F. Borrelli, L. Glielmo, and F. Vasca, "Hybrid control of Dry Clutch engagement", in *European Control Conference*, Porto, Portugal, 2001, pp. 635–639.
- [7] M. Pisaturo, M. Cirrincione, and A. Senatore, "Multiple constrained MPC design for automotive dry clutch engagement", *IEEE/ASME Transactions on Mechatronics*, vol. 20, no. 1, pp. 469 - 480, 2005, ISSN: 1083-4435;
- [8] L. Glielmo, P.O. Gutman, L. Iannelli, and F. Vasca, "Robust smooth engagement of an Automotive Dry Clutch", *Proc. 4th IFAC Symp. Mechatronics Syst.*, September 12 - 14; Heidelberg, Germany, 2006;
- [9] G.J.L. Naus, M. Beenackers, R. Huisman, M.J.G. van de Molengraft, and M. Steinbuch, "Robust control to suppress clutch judder". *Proc. of 8th Int. Symp. Adv. Veh. Control*, October 6-9; Kobe, Japan, 2008;
- [10] F. Vasca, L. Iannelli, A. Senatore, and G. Reale, "Torque transmissibility assessment for automotive Dry-Clutch engagement", *Mechatronics, IEEE/ASME Transactions on*, vol. 16, no. 3, pp. 564–573, 2011, ISSN: 1083-4435.
- [11] A. Senatore, "Vibrations induced by electro-actuated dry clutch in the Eek frequency: excitation in gear-shifting operations", *Journal of Mechatronics*, Vol. 2, No. 4, 2014, pp. 301-311, ISSN 2326-2885;
- [12] H.H. Miyasato, V.G. Segala Simionatto, and M.J. Dias, "Linear powertrain models for NVH phenomena evaluation, *Proc. of the XV International Symposium on Dynamic Problems of Mechanics*", DINAME 2013, February 17-22; Buzios, Brazil, 2013;
- [13] V.G. Segala Simionatto, H.H. Miyasato, and M.J. Dias, "On the influence of the clutch disk's pre-damper parameters on shuffle and clunk phenomena in powertrains", *Proc. of the XV International Symposium on Dynamic Problems of Mechanics*, DINAME 2013, February 17-22; Buzios, Brazil, 2013;
- [14] A. Myklebust, L. Eriksson, "Road slope analysis and filtering for driveline shuffle simulation", *Proc. of IFAC Workshop on Engine and Powertrain Control Sim. and Mod.*, Rueil-Malmaison, France, 2012, pp. 176-183;
- [15] D. Centea, H. Rahnejat, M.T. Menday, "Non-linear Multi-Body dynamic analysis for the study of clutch torsional vibrations (Judder)", *Applied Mathematical Modelling*, vol. 25, pp. 177-192, 2001, ISSN: 0307-904X;
- [16] A. Crowther, N. Zhang, D.K. Liu, J. Jeyakumaran, "Analysis and simulation of clutch engagement judder and stick-slip in automotive powertrain systems", *Proc. IMechE Part D - J. of Automobile Eng.*, vol. 218(12), pp. 1427–1446, 2004, ISSN: 0954-4070;
- [17] A. Senatore, D. Hochlenert, V. D'Agostino, U. von Wagner, "Driveline dynamics simulation and analysis of the dry clutch friction-induced vibrations in the Eek frequency range", *Proc. of ASME-IMECE 2013*, November 15-21; San Diego, CA, USA, 2013;
- [18] R. Amari, M. Alamir, and P. Tona, "Unified MPC strategy for idle speed control, vehicle start-up and gearing applied to an Automated Manual Transmission", in *17th IFAC World Congress*, Seoul, South Korea, 2008;
- [19] J. M. Maciejowski, *Predictive Control with Constraints*, P. Hall, Ed. 2000;
- [20] X. Lu, P. Wang, B. Gao, and H. Chen, "Model Predictive Control of AMT clutch during start-up process", in *Control and Decision Conference (CCDC)*, 2011 China, pp. 3204–3209, 2011;
- [21] H. Quanan, S. Jian, and L. Lei, "Research on Rapid Testing Platform for TCU of Automated Manual Transmission", in *Proceedings of the 2011 Third International Conference on Measuring Technology and Mechatronics Automation - Volume 03*, ser. ICMTMA'11, Washington, DC, USA: IEEE Computer Society, 2011, pp. 67–70, ISBN: 978-0-7695-4296-6.
- [22] N. Cappetti, M. Pisaturo, and A. Senatore, "Modelling the cushion spring characteristic to enhance the Automated Dry-Clutch performance: the temperature effect", *Proc. of the Institution of Mechanical Engineers, Part D: Journal of Automobile Engineering*, vol. 226, no. 11, pp. 1472–1482, 2012, ISSN: 0954-4070.
- [23] V. D'Agostino, N. Cappetti, M. Pisaturo, and A. Senatore, "Improving the engagement smoothness through multi-variable frictional map in automated dry clutch control", *Proc. of the ASME 2012 International Mechanical Engineering Congress and Exposition - November 9-15*, Houston, Texas, 2012;
- [24] A. Senatore, V. D'Agostino, R. Di Giuda, and V. Petrone, "Experimental investigation and neural network prediction of brakes and clutch material frictional behaviour considering the sliding acceleration influence", *Tribology International*, Vol. 44, pp. 1199-1207, 2011, ISSN: 0301-679X.

Axial Balance in Centrifugal Pumps – Back Labyrinth Versus Dorsal Vanes

Lecturer PhD Sanda BUDEA¹

¹ University Politehnica of Bucharest, Hydraulics, Hydraulic Machines and Environmental Engineering Department, 313, Spl. Independentei, 060042, Bucharest, email: s_budea@yahoo.com

Abstract: Redesign and correct sizing of hydraulic machines, like centrifugal pumps, must take account of hydraulic thrusts. This is useful to minimize the components wear and properly size of bearings and extending the bearings durability. These are minimal conditions for pumps optimal working.

The article analyzes two methods of balancing the axial forces - first with front and back labyrinths and wear rings of impeller, the second using dorsal vanes. The article presents the calculation procedure of axial forces customized for these two balancing methods. Calculations are exemplified for a multistage pump with 2-7 stages.

Variations of axial forces are analyzed with the number of stages of multistage pumps, with labyrinth positioning or dorsal vanes diameter, width vanes diameter and clearance between vanes and casing and with the suction pressure of the pump. It also indicates the axial thrust reversal and most convenient rotor geometry.

Keywords: centrifugal pump, axial thrust, front and back labyrinths, dorsal vanes

1. Introduction

For a correct design of the hydraulic machines' impellers, should be considered the axial and radial forces, their size and direction occurring in the working process. Reliability and correct rating of hydraulic machines like centrifugal pumps must take account of hydraulic thrusts. This is useful to minimize the components wear and properly size of bearings and extending the bearings durability. This article proposes a calculation procedure based on information from the literature [1- 5], [7-9], to determine the correct axial thrust in centrifugal pump impellers, single stage and multistage and comparative analyses of axial balance with wear ring and back labyrinth versus dorsal vanes on the impeller. Axial force variations are analyzed with the number of stages of multistage pumps, diameter of positioning the dorsal vanes, width of vanes and clearance between vanes and casing. Also, the pump suction pressure was varied in the case of balancing with back labyrinth on the impeller and was established when the axial forces are canceled.

All numerical examples were performed on a horizontal multistage pumps manufactured in Aversa Manufactory SRL company.

Axial thrust depends on several parameters: the impeller geometry through the suction and discharge diameters, the hub diameter, the diameter of the front and back labyrinths of the impeller, diameter of dorsal vanes, dorsal vanes width and clearance between it and the casing, the pressure discharged by the pump, also specific operating speed, pump suction pressure or the existence or not of discharge holes on the back disk. By determination of axial forces of centrifugal pumps and by finding solutions to its decrease by a correct geometry of the impeller, increases bearing durability and improves hydrodynamic behaviour of the pump in its ensemble.

2. Axial thrust – theoretical approach

In centrifugal pumps, axial forces occur due to asymmetries of the impeller - the back disk higher than the face disk generates a greater thrust in reverse fluid entry. The clearance between the casing and the impeller that turns fluid in the discharge generates swirls and hydraulic losses. Such effects create four components of axial forces: F_1 due to fluid pressure on the front disc, F_2 on the back disc, due to discharge pressure fluid that penetrates the space between the impeller and casing. F_3 is the force due to the difference of pressure on the shaft end as a result of pump suction pressure and axial impulse force F_4 , as the effect of change in flow direction. These components can be seen in figures 1 and 2.

In figure 1, the axial thrust balancing by using back labyrinth, wear ring and discharge holes can be seen. To eliminate the axial thrust of a single suction impeller, the diameter of the both front and back wearing rings can be equal.

In figure 2, the axial thrust balancing using impeller with back vanes is exemplified.

The pressure axial forces, indicated in the literature, [1-5], [7-9] have the form of equation (1):

$$F_{1,2} = \int_{R_1}^{R_2} p_p \cdot 2\pi r \cdot dr \tag{1}$$

$$p_p = p_r - \frac{\rho \cdot \omega^2}{8} (R_2^2 - r^2) \tag{2}$$

Rotational speed is

$$\omega = \frac{2 \cdot \pi \cdot n}{60}$$

(3)

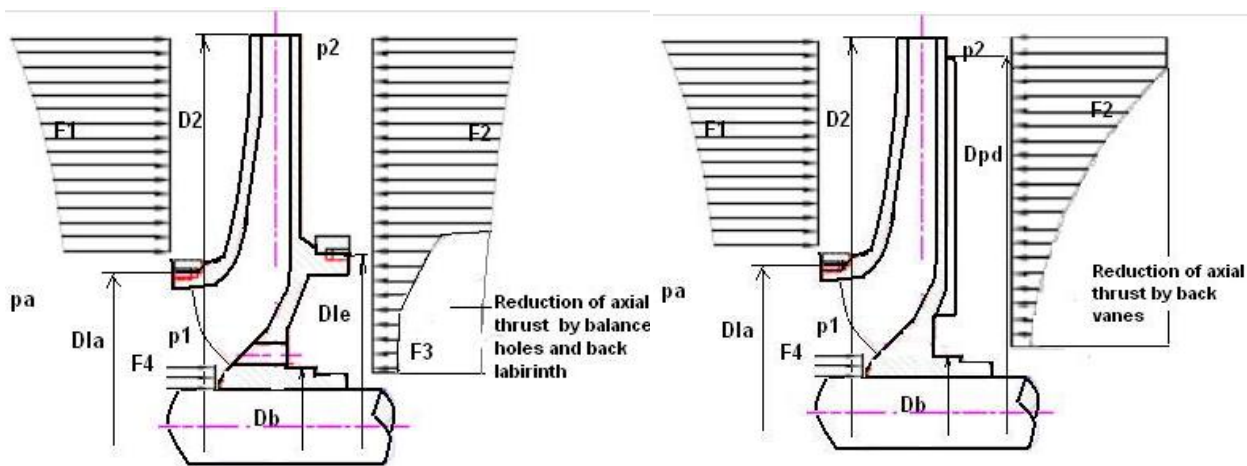


Fig.1. Back side labyrinth and discharge holes

Fig.2. Radial back vanes for axial thrust balancing

Axial force generated by the pump suction pressure has the form of equation (4):

$$F_3 = \frac{\pi \cdot d_b^2}{4} (p_a - p_1) \tag{4}$$

Axial force of impulse has the form of equation (5) or (5') :

$$F_4 = \rho Q c_0 \tag{5}, \text{ for radial impeller}$$

$$F_4 = \rho Q (c_0 - c_{m2} \cos \gamma_2) \tag{5'}, \text{ for mixed flow impeller}$$

The pressure at the discharge depends on the number of pump impellers in Figure 3 is an example CFD modelling to increased pressure in the case of two impellers, leading to increased axial force default. CFD approaches are found in the paper [10].

Analytical set up

Analysed pump is centrifugal multistage with 2÷7 stages, the impeller having the dimensions:

$$D_2 = 128 \text{ mm}, D_b = 33 \text{ mm}, D_{1a} = 78 \text{ mm} = D_{1e}, n = 2900 \text{ rpm}, H = (28, 43, 57, 70, 85, 100) \text{ m}$$

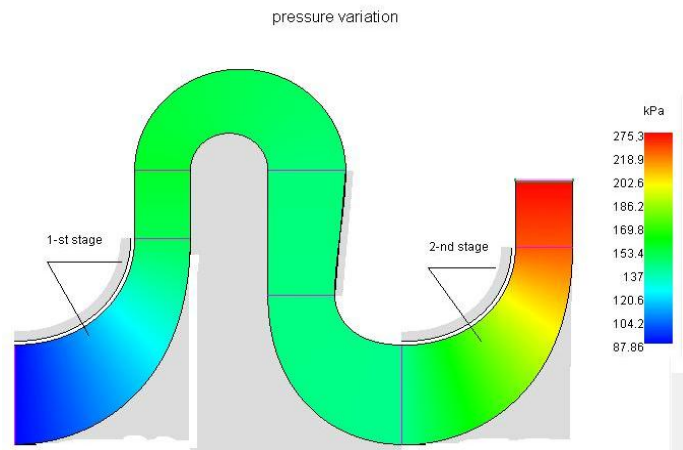


Fig. 3. Pressure variation for two stages of centrifugal pump cu H=28 m and impeller geometry are given below.

3. Axial thrust balanced by back labyrinth and wearing

Relationships above proper for balancing with back labyrinth of the impeller [6], give an axial force like in equation (6):

$$F_{ax} = \frac{\pi}{4} \left[\gamma H_p + \frac{\rho}{8} \omega^2 (D_2^2 - D_{le}^2) (D_{le}^2 - D_b^2) - \frac{\rho}{16} \omega^2 (2D_2^2 - D_{la}^2 - D_b^2) (D_{la}^2 - D_b^2) \right] \quad (6)$$

The diameter of the back labyrinth of impeller can be calculated so as to decrease the axial force, a good balance being provided with the same diameter for the front and the back labyrinths. The both labyrinth are equipped with wearing rings. In the space between the back labyrinth and the impeller’s hub are made n_g discharge holes for a fluid flow from discharge to suction, with diameter d_g . The flow losses by discharge holes are in equation (7):

$$q = n_g \frac{\pi}{4} \cdot d_g^2 \sqrt{\frac{2\Delta p_g}{\rho}} \quad (7)$$

Variation of axial thrust with the number of stages is presented in figure 4. The chart indicates trend line equation for a quickly axial thrust calculus.

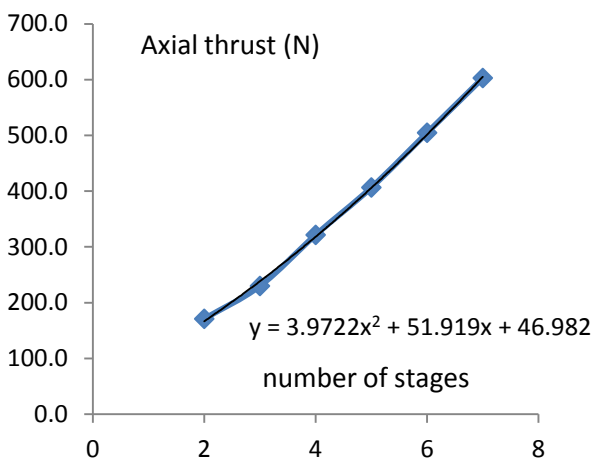


Fig. 4. Axial thrust for back labyrinth vs number of stages

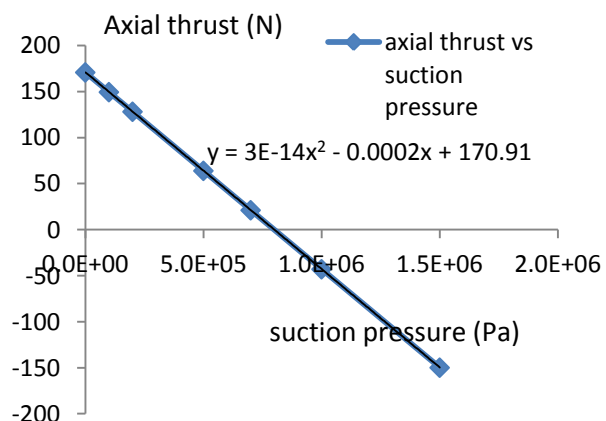


Fig. 5. Axial thrust variation vs suction pressure for a single stage

Figure 5 presents the variation of axial thrust with the suction pressure of the pump and the pressure value that balances the impeller and change the thrust direction. A convenient geometry

in radial and diagonal impeller design has the front and back labyrinth diameters equal. Sign convention is: axial thrust positive in the suction direction and negative to the coupling of the pump.

4. Axial thrust balanced by back vanes

In the balancing of axial thrust with back vanes, the axial resultant force [6] has the particular equation (8):

$$F_{ax} = \frac{\pi}{4} \left[\gamma p_1 + \frac{\rho}{8} \omega^2 (D_2^2 - D_{la}^2) \left(p_2 - \frac{\rho}{16} \omega_1^2 (D_2^2 - D_{la}^2) - (D_2^2 - D_{pd}^2) \left(p_2 - \frac{\rho}{16} \omega_1^2 (D_2^2 - D_{la}^2) - (D_{pd}^2 - D_b^2) \left(D_b^2 - \frac{\rho \omega_2^2}{2} (D_2^2 - D_{la}^2) \right) \right) \right] \right] \quad (8)$$

The rotational speeds of the fluid on the impeller disk, respectively on the dorsal vanes are (9):

$$\omega_1 = 0.5 \frac{\pi \cdot n}{30}, \omega_2 = \frac{\pi \cdot n}{60} \left(1 + \frac{B}{B+j} \right) \quad (9)$$

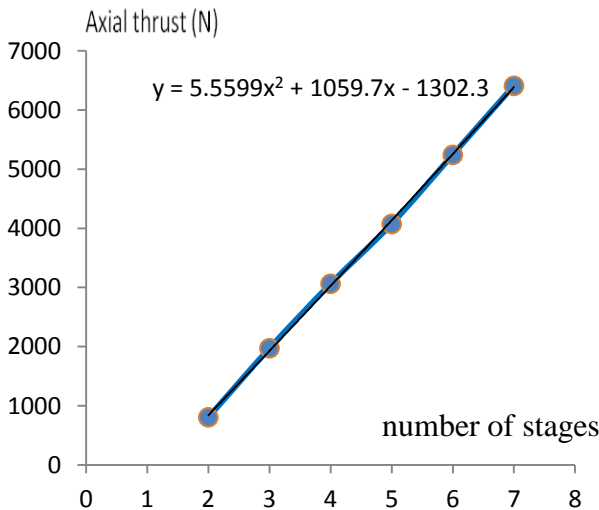


Fig.6. Axial thrust balanced by back blades vs number of stages

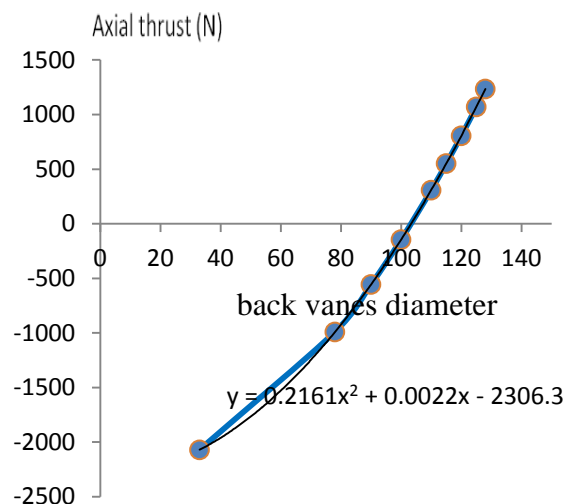


Fig.7. Axial thrust vs back vanes diameter

In figure 6 is analysed the variation of axial thrust using back vanes to balance the impeller versus number of stages of centrifugal pump. The diameter of dorsal vanes to which the axial thrust is zero – the impeller is balanced, can be established, as can see in figure 7. In both cases, trend line equation allows to determine more accurate values and extension of calculation, useful information for centrifugal pump impellers design.

Dorsal blade width B is important to balance the axial impeller. Same the gap j between dorsal vanes and casing must be properly chosen. The values of axial thrust using dorsal vanes were calculate for four widths (4, 5, 6, and 7 mm) of vanes and three gaps (1, 2, 3 mm) between impeller and casing, resumed in figure 8. Similar analyzes regarding the variation of axial thrust width and dorsal vanes diameter meet also in the paper [9].

5. Discussions and Conclusions

Reason to correct design of the impellers of centrifugal pumps must be calculated radial and axial hydraulic forces. The axial thrusts are great in the case of multistage pumps, in direct proportionality with the number of the stages. Hydraulic forces must be reduced by structural elements of the impeller and / or casing, to ensure the best possible durability of bearings.

This paper analyses two methods regarding the axial thrust balance – the first using front and back labyrinths, the second using dorsal vanes.

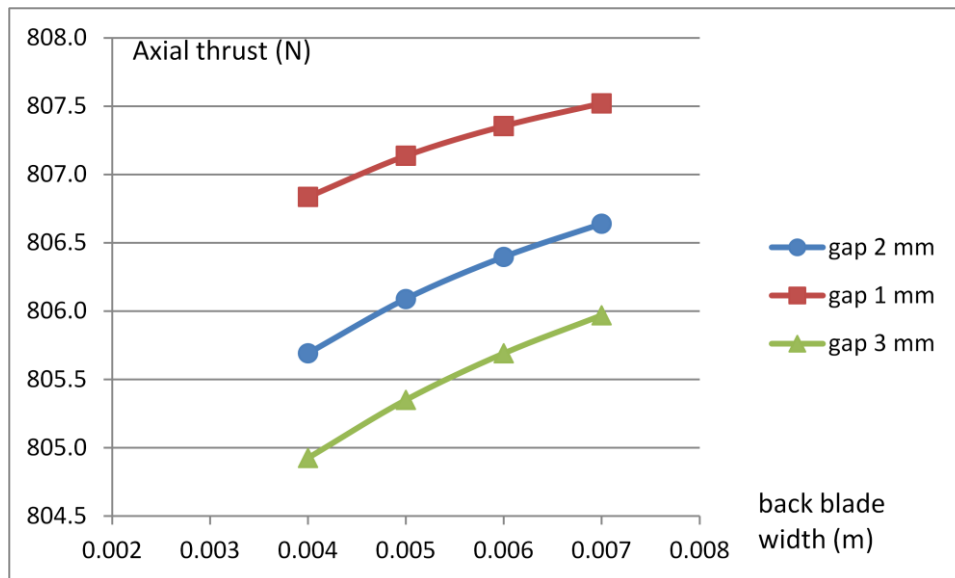


Fig.8. Axial thrust balanced with dorsal blades vs width of the blades and gap between impeller and casing

The article presents the procedures to calculate axial forces, particularized for these two methods of balancing. Calculations are exemplified for a multistage pump with 2-7 stages.

Balancing with front and back labyrinths to the same diameter is a good way and often applied, but for many stages lengthens more the shaft and the pump. It is also important the suction pressure. Article shows the pressure that cancels or changes the sense of axial thrust.

Balancing with dorsal vanes provides a more compact impeller, but the geometry is more complex, increasing the impeller's weight. It must be taking into account the dorsal vanes diameter and the gap / clearance between impeller and casing. Article presents the variation of axial thrust with the dorsal vane diameter, indicating the sense change of axial thrust. Also, paper presents the variation of axial thrust with the gap between impeller and casing and with vanes width variation.

In conclusion the balancing method with back labyrinth and wearing is more efficient and more convenient for small number of stages. The method with dorsal vanes is the best for balancing a great number of stages, but with a more complex geometry.

Notation

F_p, F_1, F_2 – pressure forces (N)

F_{ax} – axial thrust (N)

C_0 – inlet speed (m/s)

Q – flow rate (m^3/s)

q – flow losses through the discharge holes (m^3/s)

n_g – number of discharge holes

d_g – holes diameter (m)

$p_p, \Delta p$ – pressure variation (Pa)

p_1, p_2 – inlet, outlet pressure (Pa)

p_a – suction pressure (Pa)

n – rotational speed (rpm)

ω – angular rotational speed (s^{-1})

ω_1, ω_2 – idem for fluid rotation on disk, respectively back blade (s^{-1})

D_2 – outlet diameter of the impeller (m)

D_{la}, D_{le} – diameter at suction labyrinth, respectively back labirinth

D_{pd} – diameter of dorsal blades (m)

D_b – diameter of the impeller hub (m)

γ - fluid specific weight (N/m³)

ρ - fluid density (kg/m³)

B – back blade width

J – gap / clearance impeller casing

References

- [1] Igor J. Karassik, Joseph Messina, Paul Cooper, Charles Heald, “Pump Handbook”, the 3-rd edition, McGRAW-HILL, pp 2.124-2.126
- [2] Stepanoff A.J. “Centrifugal and Axial flow pumps - Theory, Design & Application”, John Wiley and Sons – 2nd edition – 1953. pp. 182-223.
- [3] Kovats A., Desmur G., “Pompes, ventilateurs, compresseurs centrifuges and axiaux”, Editure Dunod, Paris, 1962.
- [4] Val S. Lobanoff & Robert R. Ross, “Centrifugal Pumps design and application”, Jaico publishing house – 2nd edition 1995. pp. 333-353.
- [5] Pavel Dorin, “Masini Hidraulice”, Editura Energetica de stat, Bucuresti, 1955, pag 235-249.
- [6] Budea Sanda, “Ghid de proiectare al pompelor centrifuge – proceduri si programme de calcul”, Ed. Printech, Bucuresti, 2006, pag. 35-43.
- [7] Majan Gantar, Dr. Dussn Florjancic, Dr. Brane Sirok, “Hydraulic Axial Thrust in Multistage Pumps - Origins and Solutions”, Proceedings of ASME FEDSM’01, May 29 -June1.2001, pag. 1-8.
- [8] “Centrifugal pumps for petroleum, heavy duty chemical and gas industry services”, American Petroleum institute – 610 10th edition-October 2004.
- [9] Vasant Godbole, Rajashri Patil, Gavade S.S. – Axial thrust in Centrifugal Pumps – Experimental analysis, 15th International Conference on Experimental Mechanics, Porto/Portugal, 22-27 July 2012.
- [10] DELLA GATTA Stefania, SALVADORI Simone, ADAMI Paolo, BERTOLAZZI Laura, “CFD Study for Assesment of Axial Thrust Balance in Centrifugal multistage pumps”, Conference on Modelling Fluid Flow (CMFF’06), The 13th International Conference on Fluid Flow Technologies Budapest, Hungary, September 6-9, 2006.

Considerations Regarding the Behavior to Cavitation Erosion of Two Carbon Alloy Stainless Steels Used in the Manufacturing of Hydraulic Equipment Drawers of Command, Adjustment and Distribution

PhD.stud. eng. Cristian GHERA¹, Prof. PhD. eng. Ilare BORDEASU²,
PhD.stud. eng. Laura SALCIANU³, Lecturer PhD. eng. Sebastian Titus DUMA⁴,
PhD.stud. eng. Ștefan-Eusebiu KATONA⁵, Assoc. Prof. PhD. eng. Adrian PUGNA⁶,
PhD.stud. eng. Lavinia Madalina MICU⁷, 3rd rank SR PhD. eng. Luoana Florentina PASCU⁸

¹ Politehnica University of Timisoara, cghera2000@yahoo.com

² Politehnica University of Timisoara, ilarica59@gmail.com

³ Politehnica University of Timisoara, salcianu.laura@yahoo.com

⁴ Politehnica University of Timisoara, sduma_titus@yahoo.com

⁵ Politehnica University of Timisoara, keusebiu@yahoo.com

⁶ Politehnica University of Timisoara, adrian.pugna@upt.ro

⁷ Politehnica University of Timisoara, lavimicu@yahoo.com

⁸ INCD ECOIND Bucharest, luoanapascu@yahoo.com

Abstract: *The performances of hydraulically driven systems are dependent on the developed forces and execution speed. However, increasing the speed of execution makes that inside of the command, adjustment and distribution equipment, when using low viscosity fluids, to appear hidromatic phenoms of the cavitation type. Modern methods of flow modeling shows that the areas where pressure oscillations leads to the appearance of cavitation, are the flow slots created between the mobile elements (drawers) and body/seat of the hydraulic equipment. Although the literature contains more information about the behavior/cavitation resistance of materials of components that run within the range of cavitation, an investigation of their behavior to cavitation erosion is required. Filling the data with cavitation erosion elements is beneficial, since it occurs simultaneously with cavitation erosion and abrasive erosion, cumulative effects that can affect the performance and work accuracy of the equipment. Therefore, this paper contains the result of research and analysis of the behavior to vibratory erosion of two low alloy steels (16MnCr5 and 34CrNiMo6), in annealed condition, used in the manufacturing of mobile elements of hydraulic equipment. Qualitative assessment of resistance to cavitation is done by comparing the carbon steel alloy 41Cr4, standard in the cavitation laboratory of the Polytechnic University of Timisoara, for steels in this category. The comparison based on curves and cavitation erosion specific parameters show that the investigated steels have lower resistance to the standard, but can be improved by applying surface hardening technologies and increasing the mechanical properties of the surface exposed to cavitation.*

Keywords: *cavitation erosion, carbon steel alloy, cavitation resistance, mechanical properties, chemical composition, average penetration depth of erosion, erosion rate, cumulative erosion rate*

1. Introduction

The speciality literature presents the cavitation as a complex hydrodynamic phenomena, specific to the flowing of liquids, which is manifested by reducing the energy and functional parameters, the appearance of noises and vibrations, and worst of all, by erosion of solid borders which guide the flow [1], [5].

How the phenomenon can only be diminished, hydromechanical equipment, which is always present, will work, almost always in the so-called "industrial admitted cavitation", that cost in maintaining the current energy parameters, low level noise and vibration and acceptable cavitation erosion, requiring repairs and replacements of equipment after long periods of operation.

Most cavitation erosion studies are made on hydraulic machines, pumps and marine propellers,

because they are the most affected and involves high costs of manufacturing and repairing [9]. From the bibliographic documentation [1], [2], [3], [4] results that the hydraulic equipment from the actuating schemes are, also, subject to cavitation, with all it's effects.

Observations made at the current and maintenance works, on the crossing zone between drawers and command equipment slots, distribution and control, as well as numerical modeling, have highlighted cavitation and abrasive erosions of drawer shoulders and equipment bodies.

Therefore, the performance of the equipment is subject to the judicious selection of the material, respectively of the application of heat treatments, thermo-chemical and mechanical for the increase of their resistance to the destructive effects of cavitation erosion, taking into account the economic effects of such measures [6], [9].

So, along with the basic problem concerning a compromise between the mechanical strength and plasticity characteristics, the cavitation erosion behavior must also be studied.

The research accomplished in this paper provides important data on cavitation erosion behavior of two low alloy carbon steels (*16MnCr5 and 34CrNiMo6 in annealed condition*), commonly used at manufacturing of mobile elements of the hydraulic systems equipment [10].

2. Research material. Apparatus and research method

From the analysis of the hydraulic equipment manufacturers, coupled with the analysis of the properties of materials and supply costs of materials [2], [7], from which these elements are made, results the fact that the most suitable for the hydraulic equipment drawers, are the low alloy steels.

To investigate the effects of cavitation erosion, there were chosen two alloy steels 16MnCr5 and 34CrNiMo6, used in the manufacturing of control device drawers, distribution and control of hydraulic system actuators.

The chemical compositions of the two steels (according to the quality certificate released by S.C. MECHEL-TARGOVISTE S.A., Romania) are displayed in Table 1, and the values of the main mechanical characteristics, determined in the Strength of Materials laboratory of the Polytechnic University of Timisoara, are summarized in Table 2.

In Tables 1 and 2 are given the chemical composition and values of the mechanical properties of the 41Cr4 steel, standard for alloy steels and used in the manufacturing of hydraulic equipment components exposed to the cavitation erosion [2].

TABLE 1: Chemical composition of the examined steel

Brand	Accompanying and alloying elements, %										
	C	Si	Mn	Cr	S	P	Al	Ti	Mo	Cu	Ni
16MnCr5	0,21	0,32	0,97	1,00	0,03	0,09	0,0175	0,035	0,018	0,2	0,1
34CrNiMo6	0.34	0.25	0.50	1.5	0.035	0.025	-	-	0.25		1.55
41Cr4	0.42	0.25	0.70	1.05	0.03	0.025	-	-	-	-	-

The mechanical characteristics, determined in Strength of Materials laboratory of the Polytechnic University of Timisoara, have the values shown in Table 2.

TABLE 2: Mechanical characteristics

Material	Rm N/mm ²	Rp0,2 N/mm ²	A5% %	Z% %	HB daN/mm ²	Bibliography
16MnCr5	1174	1059	12	51	207	[12]
34CrNiMo6	1200	900	10	45	250	[13]
41Cr4	1000	660	12	35	255	[2], [14]

The researches have been accomplished in the Cavitation laboratory of the Polytechnic University of Timisoara, on the performant crystal piezoelectric vibrator device, with modern facilities, that ensures process control and computer management, accomplished by international standards ASTM G32-2010 [11].

The functional parameters of the device, kept constant throughout the whole research duration, are: power 500 W, vibration frequency 20000 ± 2% Hz, amplitude of vibration 50 µm, sample diameter 15,9 ± 0,05 mm, supply voltage 220 V/50 Hz, working fluid double distilled, working fluid temperature 22±1°C [4], [8].

In accordance with the requirements of the standards ASTM G 32-2010, the search procedure [2], [6], [10], from both steels were exposed three samples to cavitation erosion. The total duration of the cavitation attack, according to custom laboratory is 165 minutes, divided into a period of 5 and 10 minutes and 10 of 15 minutes each.

In the diagrams contained in the paper, the analysis underlying the cavitation behavior, are shown the curves obtained from the mediation of experimental results recorded on the three samples.

3. Experimental results. Analysis and discussions

In Figures 1 and 2 are presented measured values for the eroded mass and the corresponding velocity, of different periods of attack.

The mass of material, lost by the sample through cavitation erosion, was obtained by weighing the analytical balance type Zatkłady, which allows the reading of five decimals places. To assess the distant mass, the reading was performed at the beginning and end of the final period of attack ; between periods, the samples were stored in a dessicator, in order to avoid oxidation affecting real loss by cavitation erosion.

Erosion rates, expressed in points, corresponding to the 12 periods of attack, were calculated according to the ratio:

$$v_i = \Delta M_i / \Delta t_i \quad (1)$$

where Δm - represents the mass of material lost through cavitation erosion in the period Δt

Δt – represents the duration of the “i” period of attack (of 5, 10 and 15 minutes)

In Figure 1 are shown images of degradation produced by the vibratory cavitation in the 165 minute attack. Images of the eroded structure are recorded at the scanning electron microscope (magnification of 2500 x), and the degraded surfaces of the samples were photographed with the photo camera, at a magnification of 8 x.

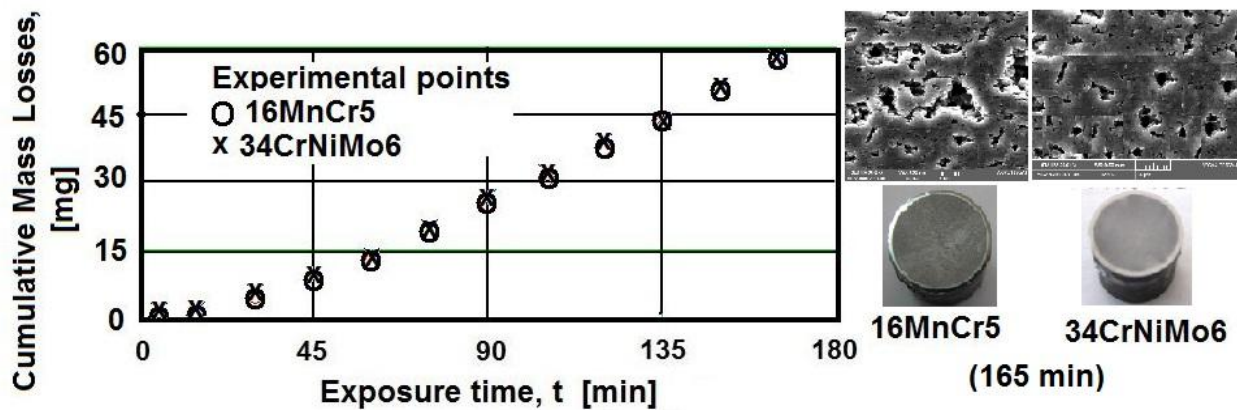


Fig. 1. Evolution of the weigh loss (cumulative) with the duration of the cavitation attack

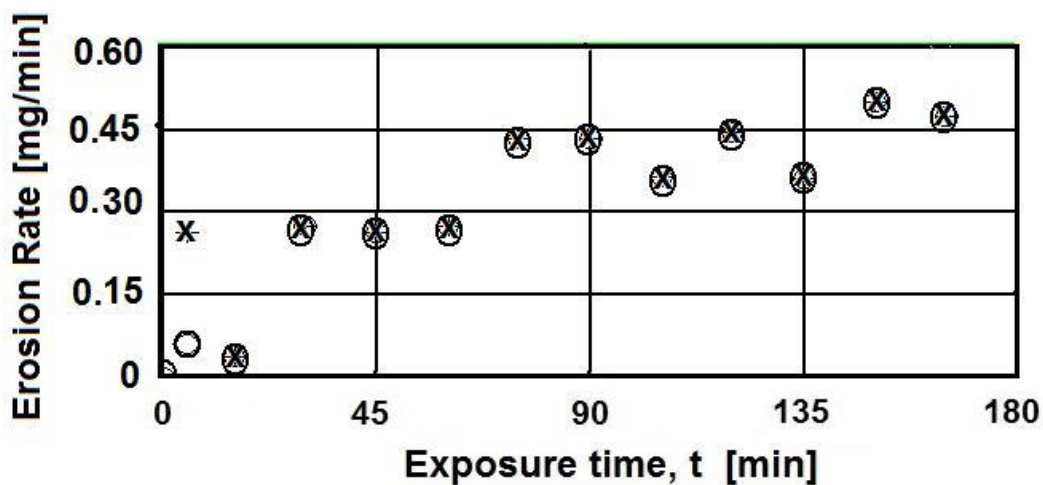


Fig. 2. Dispersion of the erosion rates during the periods of cavitation attack

The developments of the experimental points (1 and 2), show that the two steels, in the annealed condition, behave identically to the erosion generated by the vibratory cavitation. This kind of behavior, rare met, even in materials from the same quality class (as in the case of the two steels), shows the cumulative influence of all factors that determine the type of material (chemical constitution, respectively structure type, level of the mechanical properties). The only behavior difference is the one of the 5 minute period, in which the 34CrNiMo6 steel leaves the impression that it has greater losses (the phenomenon is very well visible in Figure 2). Our experience and all researches show that the losses from the first 15 minutes are not a real reflection of the sample mass loss by cavitation. They are strongly influenced by the abrasive dust and the tip of the roughness, remaining after processing the surface exposed to the attack, regardless the washing type before subjecting to the test [2]. Also, images of the degraded surface and of the cavitated microstructure, attached to the diagram of mass loss (Figure 1), are a confirmation of the identity of the two steels throughout the whole duration of the attack. The caverns left after the expulsion of grains and the level of pitting, highlighted by the pictures taken with the scanning electron microscope shows that in the annealed condition, the two steels (16MnCr5 and 34CrNiMo6) have the same resistance to cavitation erosion generated by the vibrator unit of the Polytechnic University of Timisoara's laboratory. Given that the device is accomplished by the ASTM G32-2010 standards, we estimate that even in the testing conditions at cavity vibration generated by the devices with different functional parameters (electric power, amplitude and frequency of vibration) the behavior would be similar to the one recorded by us.

In Figure 3 are shown the mean depth losses cumulated by the penetration of erosion and in Figure 4 penetration rates of erosion. The two parameters were calculated using the equation (2):

-mean depth erosion (MDE), corresponding to a period of attack:

$$MDE_i = \frac{4 \cdot M_i}{\rho \cdot \pi \cdot d_p^2} \text{ [mm]} \tag{2}$$

respectively the cumulative one

$$MDE_i = \sum_{i=1}^{12} \Delta MDE_i \text{ [mm]} \tag{3}$$

-mean depth erosion rate (MDER), corresponding to a period of attack:

$$MDER_i = \Delta MDE_i / \Delta t_i \tag{4}$$

The physical significance of the measurements from the ratio (2) is:

ρ - steel density, ($\cong 7.85 \text{ g/cm}^3$ for the 16MnCr5 steel [12] and $\cong 7.84 \text{ g/cm}^3$ for the 34CrNiMo6 steel [13])

d_p - sample diameter (= 15.9 mm).

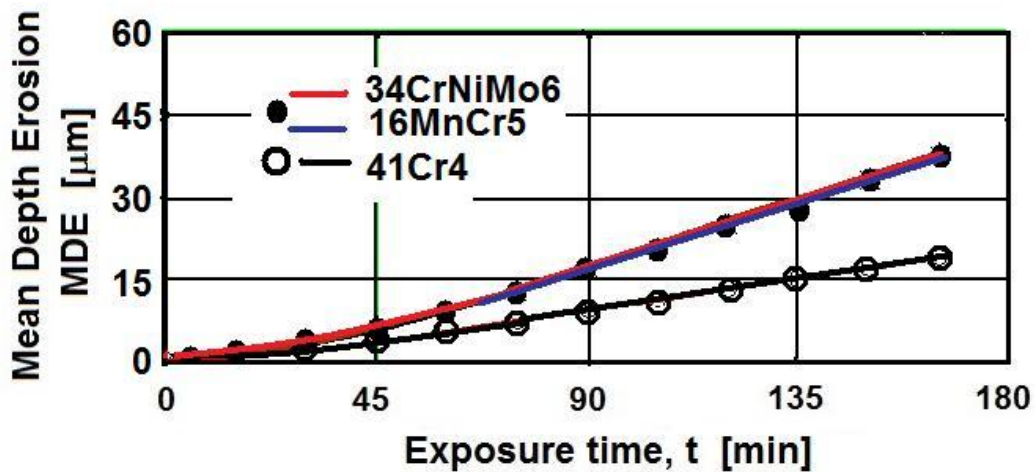


Fig. 3. Mean depth erosion with the duration of cavitation attack

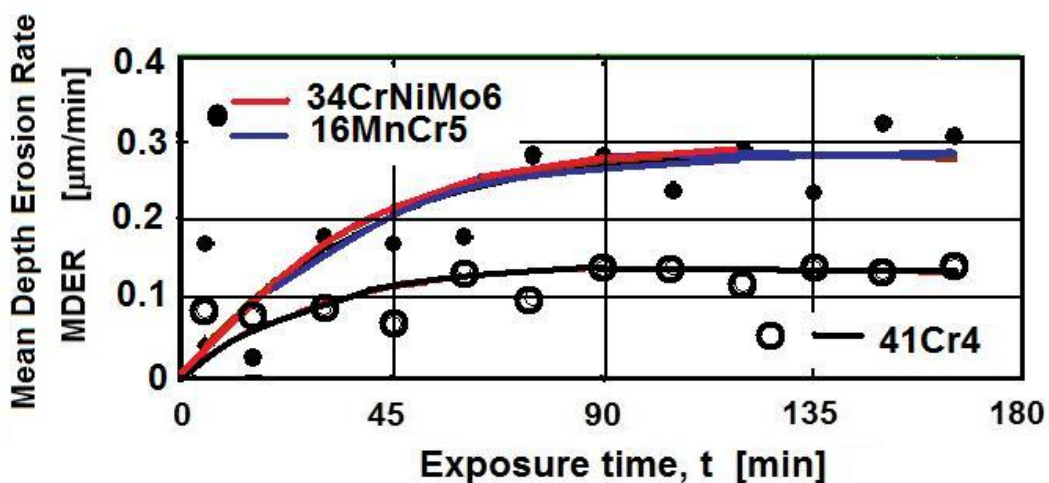


Fig. 4. Mean depth erosion rate with the duration of cavitation attack

In these diagrams, the experimental values are mediated by analytical curves constructed with ratios developed in the laboratory by Bordeasu and a.o. [2], [3], [4].

And the analytical mediation curves show that the two steels have identical behaviors and resistances at the vibratory cavitation intensity. The flattening tendency of the analytical curves at maximum values, according to the results obtained by specialists in the cavitation behavior of the materials, show that the two steels are categorized as those with good resistance to cavitation. The comparison with the 41Cr4, standard steel in our laboratory, for this type of material, shows that in annealed condition, both investigated steels have lower resistance.

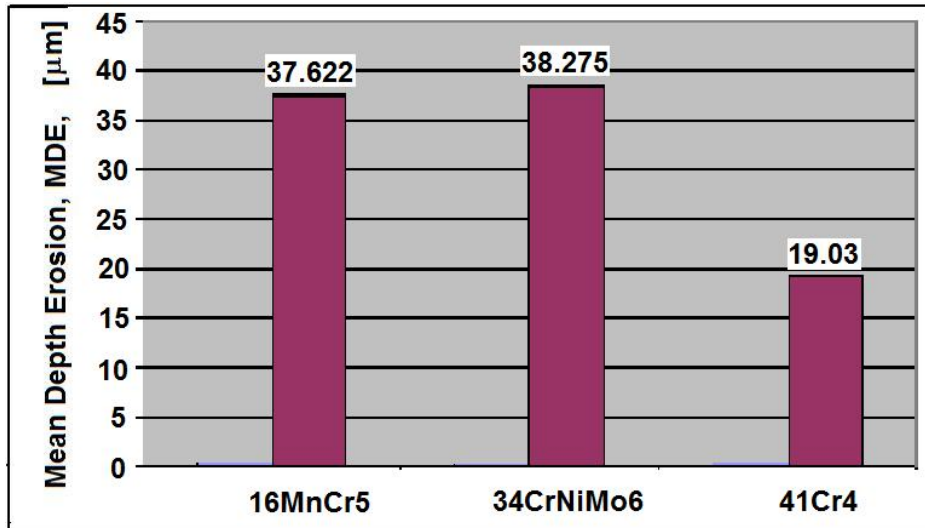


Fig. 5. Comparison of the mean depth of erosion recorded at the end of the test

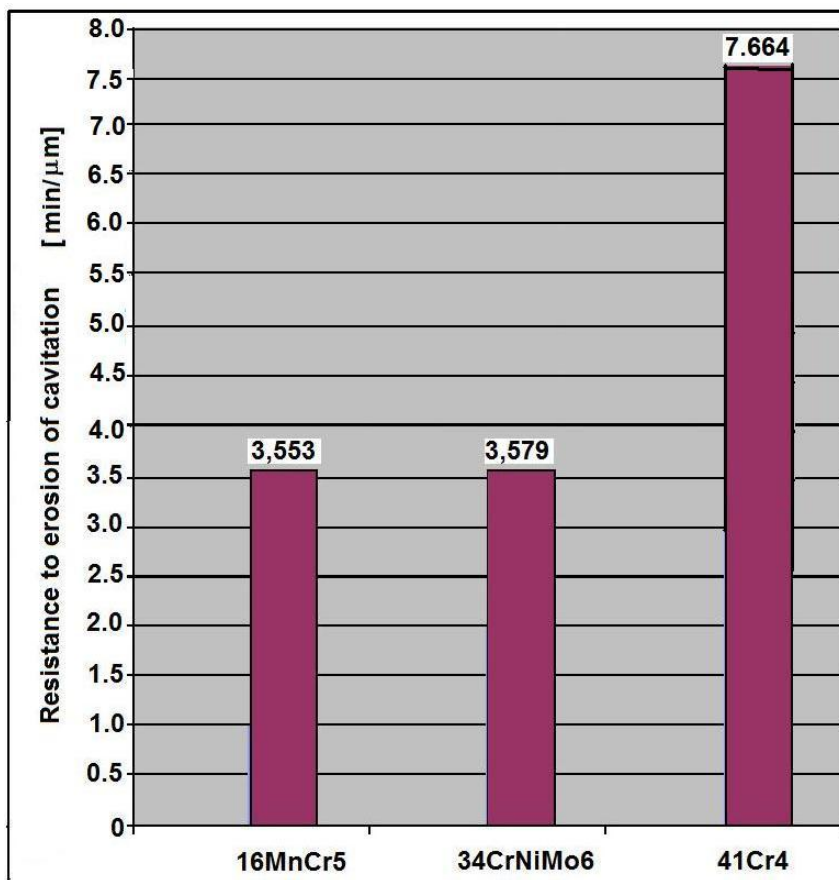


Fig. 6. Comparison of the resistance to erosion of cavitation

The histograms from Figure 5 and 6, built on the final values of the MDE parameter and the stabilizing parameter MDER, allow an approximate evaluation of the resistance of both investigated steels. Thus, compared to the standard steel 41Cr4, the depth of penetration increases by about 97,7% to 16MnCr5 and doubles (about 101%) at the 34CrNiMo6 steel. The about 3% difference between the two steels is in the specific of differences obtained for specimens taken from the same material and the same charge [2].

In terms of resistance to cavitation, expressed by the parameter $1/MDER$, Figure 6, there is a decrease by about 115 % for the 16MnCr5 steel and about 114% at the 34CrNiMo6 steel. And the difference between the values of the parameter $1/MDER$, of the two investigated steels is insignificant and falls within the specified deviation of samples from the same material and charge.

4. Conclusions

The 16MnCr5 and 34CrNiMo6 steels, in annealed condition, degrade similar to the microjet impact and shock waves generated by the implosion of cavitation bubbles produced by vibrating. The behavior and resistance, to this type of attack, are identical.

From the comparison with the standard steel 41Cr4, results a decrease of resistance at the cavitation attack, but based on the tendency of stabilization at maximum value of the MDER parameter curve, is estimated to be a good one. Also, the comparison with the standard steel, for components of the hydraulic equipment of command, distribution and adjustment, which works in areas with cavitation currents, shows the need of treatment/hardening of the exposed surface, in order to improve it's resistance characteristics to cavitation erosion.

References

- [1] Anton I, Cavitatia, Vol.I, Editura Academiei RSR, 1984;
- [2] Bordeasu I., Eroziunea cavitaionala a materialelor, Editura Politehnica Timioara, ISBN: (10)973-625-278-7; (13)978-973-625-278-5, 2006;
- [3] Bordeasu I., Popoviciu, M., Improving cavitation erosion resistance through surface and structural hardening, Machine Design, PP. ISSN ISSN 1821-1259, 2012;
- [4] Bordeasu I., Mitelea I., Cavitation Erosion Behavior for some Stainless Steels with Constant Nickel and variable Chromium Content, MP Materiall Testing, Issue 01, ISSN: 0025-530, pp. 53-58, 2012;
- [5] Frank J.P., Michel J.M., Fundamentals of cavitation. Kluwer Academic Publishers- Dordrecht/Boston/London, 2004;
- [6] Micu Lavinia Mdalina, Bordeasu I., Mitelea I., Ghera C., Slcianu Laura, Cercetarea eroziunii cavitaionale asupra oelului inoxidabil X2CrNiMn22-5-3 tratat termic, tiina i Inginerie, an XIV, vol.26/2014, Sebe – Alba, ISSN: 2067-7138, Editura AGIR, Bucureti, 2014, p.425-430;
- [7] Mitelea, I., tiina materialelor, vol.I, Editura Politehnica, ISBN 978-973-625-826-8, 2009;
- [8] Slcianu L., Bordeasu I., Micu L, M., Ghera Cr.,Rezistenta la eroziunea cavitatiei a doua oeluri inoxidabile diferite structural si supuse aceluiasi tratament termic volumic, Conferinta Nationala Multidiciplinara „Profesorul Ion D Lazarescu” fondatorul scolii romanesti de teoria aschierii, Editia I Cugir, 2014, pp.675-682;
- [9] Truculescu M, Ieremia A.,(1983), *Oeluri inoxidabile i refractare*, Editura Facla, Timioara;
- [10] Bloiu. V., Bordeasu, I., Popoviciu, M. O., Ghiban, B., Gombos, R.Raszga, C., Upon cavitation effects in hydraulic driving devices, Metalurgia International, vol. XIV (2009), special issue, no.11, ISSN 1582-2214, pp.48-51;
- [11] *** Standard method of vibratory cavitation erosion test, ASTM, Standard G32, 2010;
- [12] *** <http://www.upsteel.com/index.php?c=index&a=show&catid=20&id=9604>
- [13] *** <http://www.upsteel.com/index.php?c=index&a=show&catid=20&id=9595>
- [14]***http://www.saarstahl.com/fileadmin/saarstahl_extranet/images/04_produkte/walzstahlsorten/english/7035_7039_41Cr4_41CrS4.pdf

Pneumatic Tracking System for Photovoltaic Panel

Dr. Eng. Ionel Laurentiu ALBOTEANU¹

¹ University of Craiova, Faculty of Electrical Engineering, lalboteanu@em.ucv.ro

Abstract: Applications that use photovoltaic systems are continuously growing, in recent years, according to EU policies that foster the renewable energy sources. The current trend is to optimizing these systems by ensuring functionality with maximum efficiency. One of the methods of optimization refers to the capture of large quantities of solar energy using tracking systems for photovoltaic panels. The most of photovoltaic tracking systems uses the electric drive. This paper presents another type of tracking system based on a pneumatic drive. Of the existing tracking systems in literature, the pseudo-equatorial system was adopted. This tracking system was particularized for Craiova location.

Keywords: tracking system, photovoltaic (PV) panel, pneumatic drive, sun position

1. Introduction

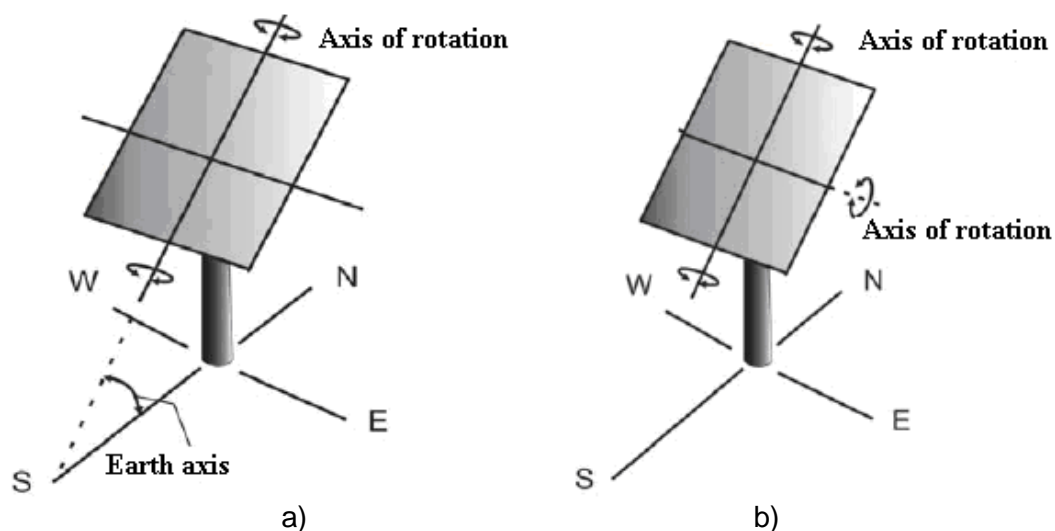
Photovoltaic conversion of solar energy is one of the most attractive and dynamic options to use renewable energy to produce electricity. In order to compete with conventional sources of electricity generation have found solutions to increase the efficiency and decrease the cost price of photovoltaic modules.

Ideally, a PV panel should follow the sun so that the sun rays fall perpendicular to its surface, thus maximizing solar energy capture and thus we obtain the maximum output power. The tracking systems using controlled mechanisms that allow maximization of direct normal radiation received on PV panel [7].

2. Photovoltaic tracking systems

Electricity production of a PV system depends largely on solar radiation absorbed by the photovoltaic panels. As the sun changes with the seasons and over a day, the amount of radiation available for the conversion process depends on the panel tracking [3, 5, 6, 7].

In practice are two kinds of tracking systems: single axis and double axes tracking systems (Fig. 1). In the case where the two orientation axes 3 types of systems can be distinguished, depending on how the axes are placed and how the two movements are entered into the system [7]: the azimuthally systems, the equatorial systems and the pseudo-equatorial systems. In this paper was considered the pseudo-equatorial system.



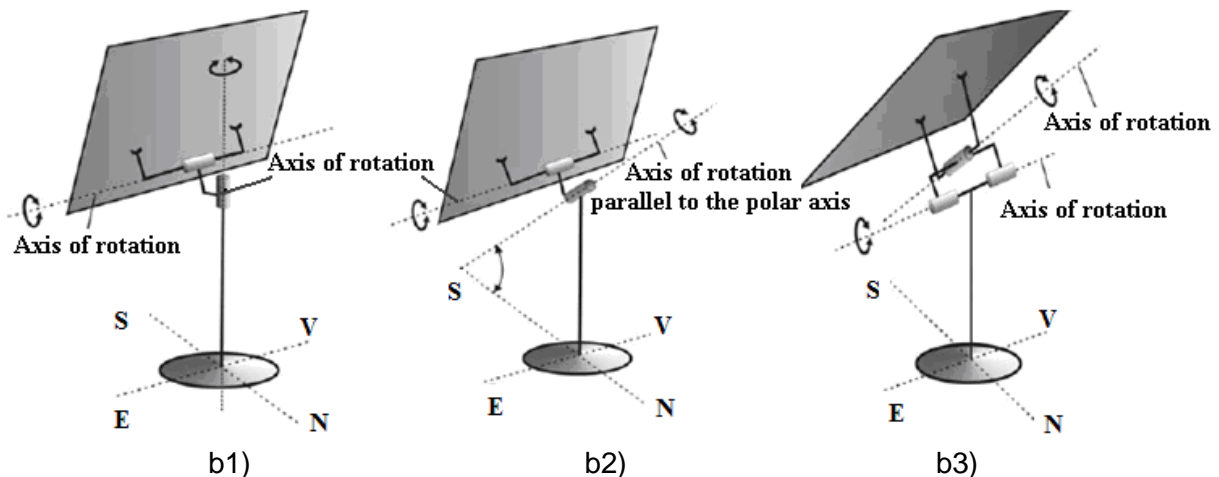


Fig. 1. Tracking systems of PV panels: a) - single axis, b) - double axes, b1) - azimuthal, b2) - equatorial, b3) - pseudo-equatorial

The tracking systems presented above is based on two methods of orientation:

- method based on going through a predetermined trajectory;
- method based on the search of maximum illumination.

In this paper we present a method based on going through prescribed tracks.

3. Determination of PV panel position

It is known that the Earth behaves a complete rotation in a year, around the Sun in an elliptical orbit and a complete rotation around its own axis during 24 hours. Earth's rotation axis has a fixed direction in space and inclined angle $\delta_0 = 23.5^\circ$ to the perpendicular plane of the orbit (Fig. 2). The angle between the direction to the Sun and the equatorial plane, δ is named declination and varies during the year from 23.5° , at the moment of the summer solstice (June 21) to -23.5° , at the winter solstice (December 21st).

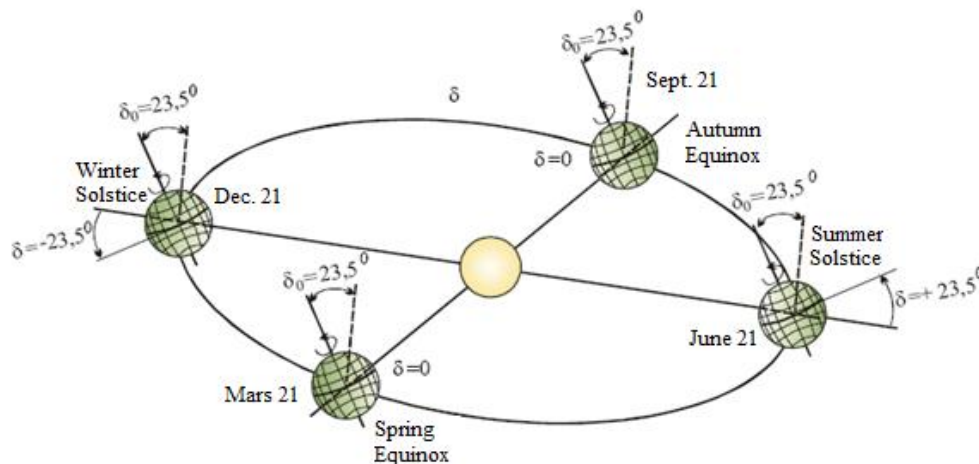


Fig. 2. Earth's orbit and the angle of declination, δ

On 21 March, respectively - September 21 declination $\delta = 0$ and the length of day and night are equal.

Declination can be calculated with the Copper formula [6]:

$$\delta = 23,45 \cdot \sin\left(360^\circ \frac{284 + n}{365}\right) \quad (1)$$

where n - is the number of days in a year, the first day considering January 1. Using monthly average of 'n' values can be calculating the declination of Earth during a year.

Geometric relations between an arbitrarily oriented plane to the horizontal and direct sunlight that falls on the plan at any point of time, the position of the sun to this plan can be described in terms of several angles.

Latitude, φ - angle measured from the equator to the point of interest on the earth's surface, is considered positive for the northern hemisphere and negative - to the south.

The inclination angle of plane β - the angle between the plane and the horizontal surface; $0 \leq \beta \leq 180$, (Fig. 3). For normal solar installations, maximum angle does not exceed 90° .

Azimuthally angle, γ - the angle between the projection on the horizontal plane perpendicular to the surface of the plan and the local meridian (Fig. 3); equal to zero for that plan south facing; negative - to east, positive - to west; $-180 \leq \gamma \leq 180$.

Solar azimuthally angle, γ_s , - the angle between the south and the projection on the horizontal direct radiation (sunlight) (Fig. 3 b); angles measured from south east direction are negative, the measured westward - positive.

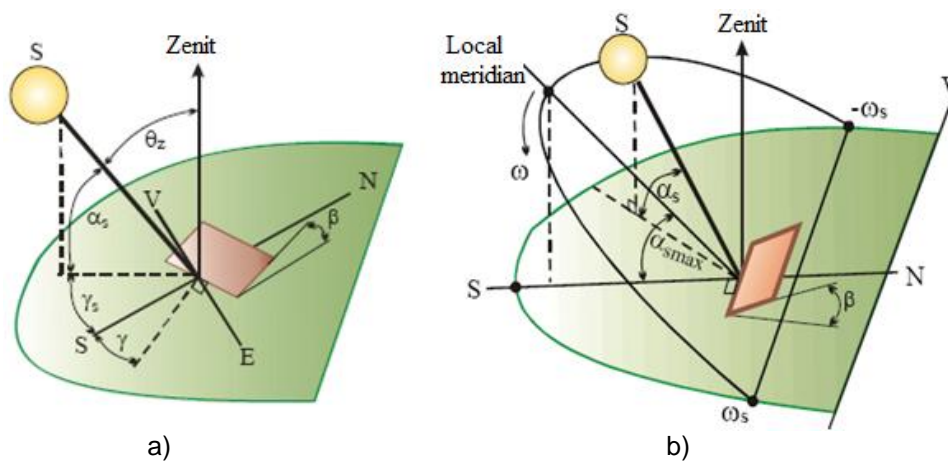


Fig. 3. Explanation regarding to sun's angles

The angle of elevation of the sun, α_s , - the angle between the horizon and the sun line linking point of interest, or the incident solar beam at the point of interest (Fig. 3).

Zenith angle, θ_z , - the angle between the vertical and the line connecting the sun and the point of interest, or α_s complementary angle (Fig. 3).

Hour angle, ω , - determines the position of the sun in the sky at a given moment. Equals zero when crossing the local meridian sun, ie when midday positive and negative east - west (Fig. 3 b). Accordingly, ω_s corresponds to the angle of sunrise, and $(-\omega_s)$, the angle of the sun dusk.

It is obvious that in an hour the sun across the sky at an angle equal to 15° , and his position at any time T is determined by the expression:

$$\omega = 15 \cdot (12 - T) \quad (2)$$

If you know the angles δ , φ and ω , then easily determine the position of the sun in the sky for the point of interest for any time, any day, using the expressions [6]:

$$\sin \alpha_s = \sin \delta \sin \varphi + \cos \delta \cos \varphi \cos \omega = \cos \theta_z \quad (3)$$

$$\cos \gamma_s = \frac{\sin \alpha_s \sin \varphi - \sin \delta}{\cos \alpha_s \cos \varphi} \quad (4)$$

In equation (3) by imposing the condition, calculate east respectively west angle hourly of the sun from the relationship:

$$\omega_s = \pm \cos^{-1}(-\tan \varphi \cdot \tan \delta) \quad (5)$$

For every day of the year in (4) with declination δ previously determined from (1) for a time T is determined the hour angle ω and knowing the latitude φ is determined the sun elevation angle α_s .

In figure 4 is presented photovoltaic panel, P directed to the South. Surface of panel P is inclined to the horizontal with β angle.

Solar radiation on the PV panel will be highest when the afternoon when the sun elevation angle, α_s is the maximum distance panel and sunlight will be minimal time and angle $\omega = 0$. This situation will occur where direct radiation is perpendicular to the surface of the PV panel, P.

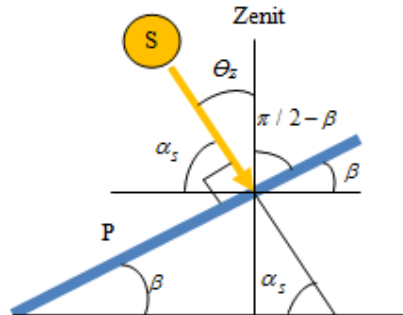


Fig. 4. Direct solar radiation on an inclined plane in midday: $\omega=0$; $\gamma=0$;

Figure 4 shows that $\theta_z = \beta$, and angle of the panel on S-N direction (elevation), from the horizontal plane is determined by the relationship:

$$\cos \theta_z = \sin \delta \sin \varphi + \cos \delta \cos \varphi = \cos(\varphi - \delta) \tag{6}$$

$$\beta = 2\pi - (\pi + \alpha_s) \tag{7}$$

Based on present relationships above, customizing for city of Craiova was obtained graphical representation of specific angles describing the position of the sun in the sky and the PV panel position (Fig. 5, Fig. 6, Fig. 7).

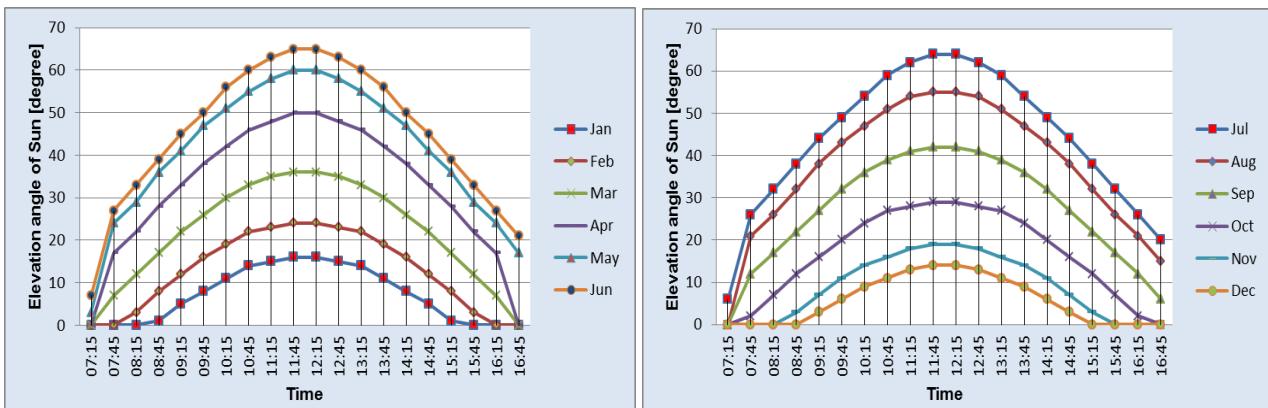


Fig. 5. Elevation angle of sun for each month of year

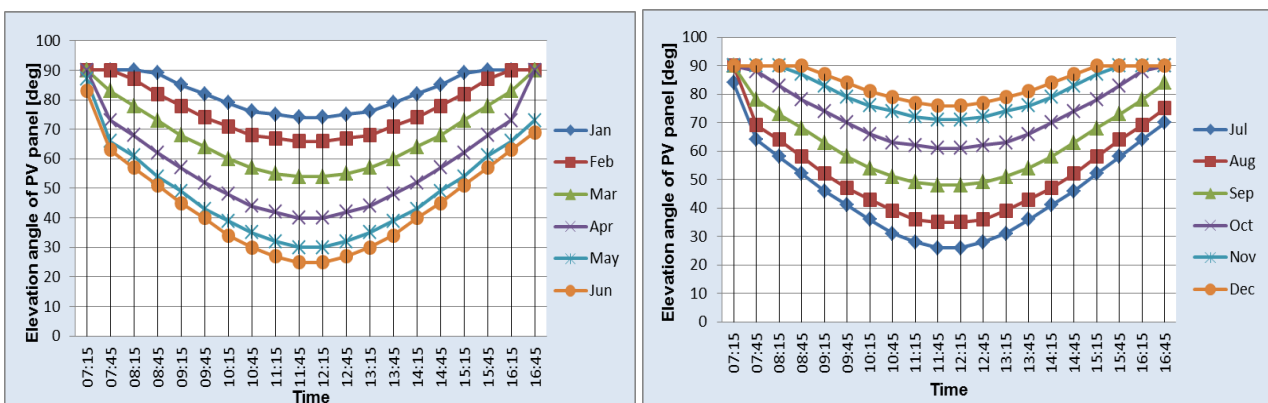


Fig. 6. Elevation angle of PV panel for each month of year

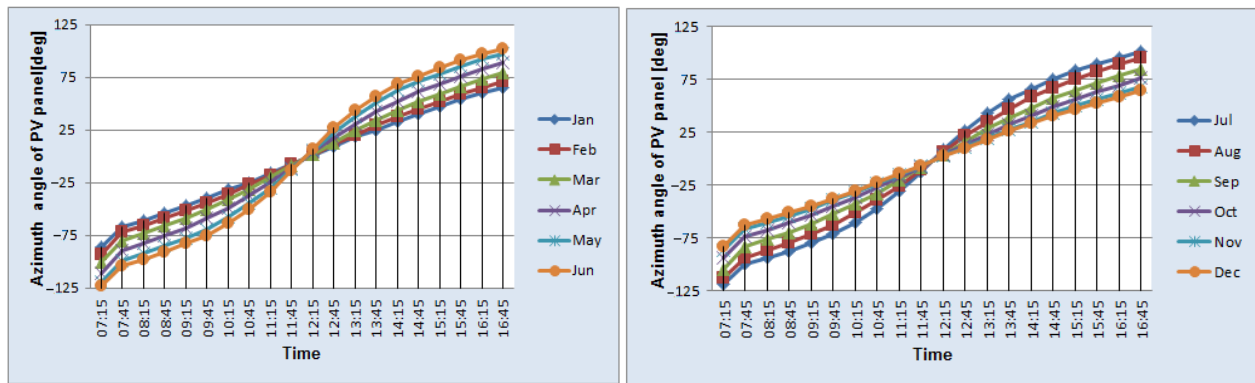


Fig. 7. Azimuth angle of PV panel for each month of year

The graphs above reveals PV panel position every 30 minutes throughout the day. Knowing the position of the panel can develop the control algorithm of pneumatic tracking system.

4. Simulation of pneumatic tracking system

The most of PV tracking systems uses the electric motors. In this paper is proposes another type of tracking system that uses a pneumatic drive (Fig. 8). Were considered the following advantages:

- the forces, moments and engine speeds can be adjusted easily using simple devices;
- pneumatic motor overload does not introduce risk of damage;
- pneumatic transmissions allow starts, stops, frequent and sudden changes of direction without risk of damage;
- compressed air is relatively easy to produce and transport networks is environmentally friendly non-flammable;
- can be stored in high quantity;
- risk of injury is reduced;
- easy maintenance.

For achieving the structure and pneumatic control of system and also, to simulate the operation has been used dedicated software named FluidSim [16], (Fig. 9, Fig.10).

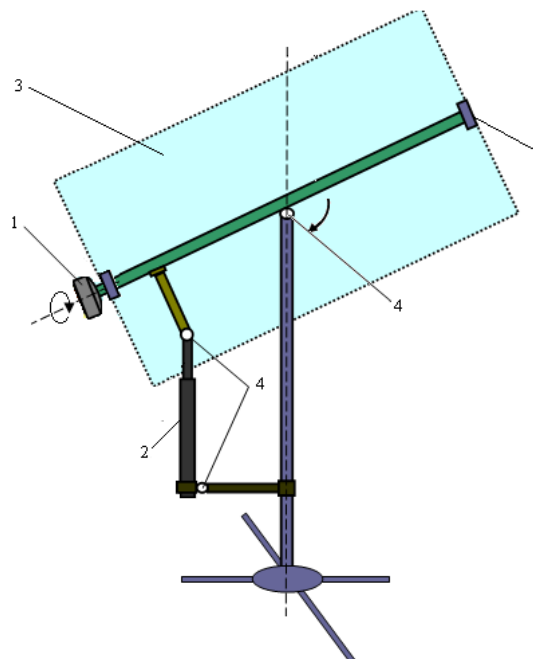


Fig. 8. Structure of pneumatic tracking system

1- Semi-rotary actuator; 2- linear cylinder; 3- PV panel; 4- joints; 5- fixture for PV panel

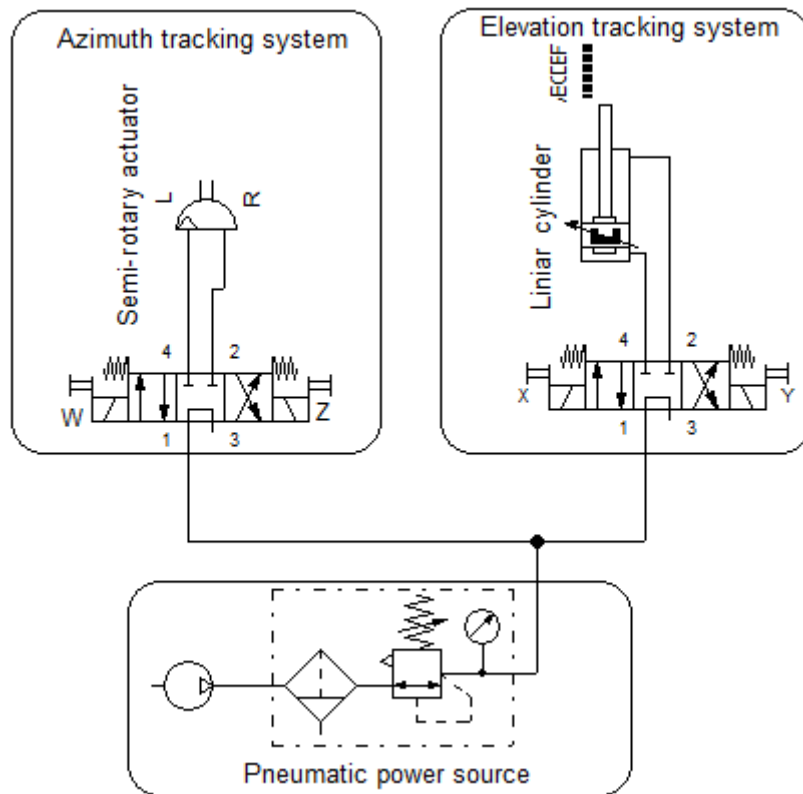


Fig. 9. Structure of pneumatic drive

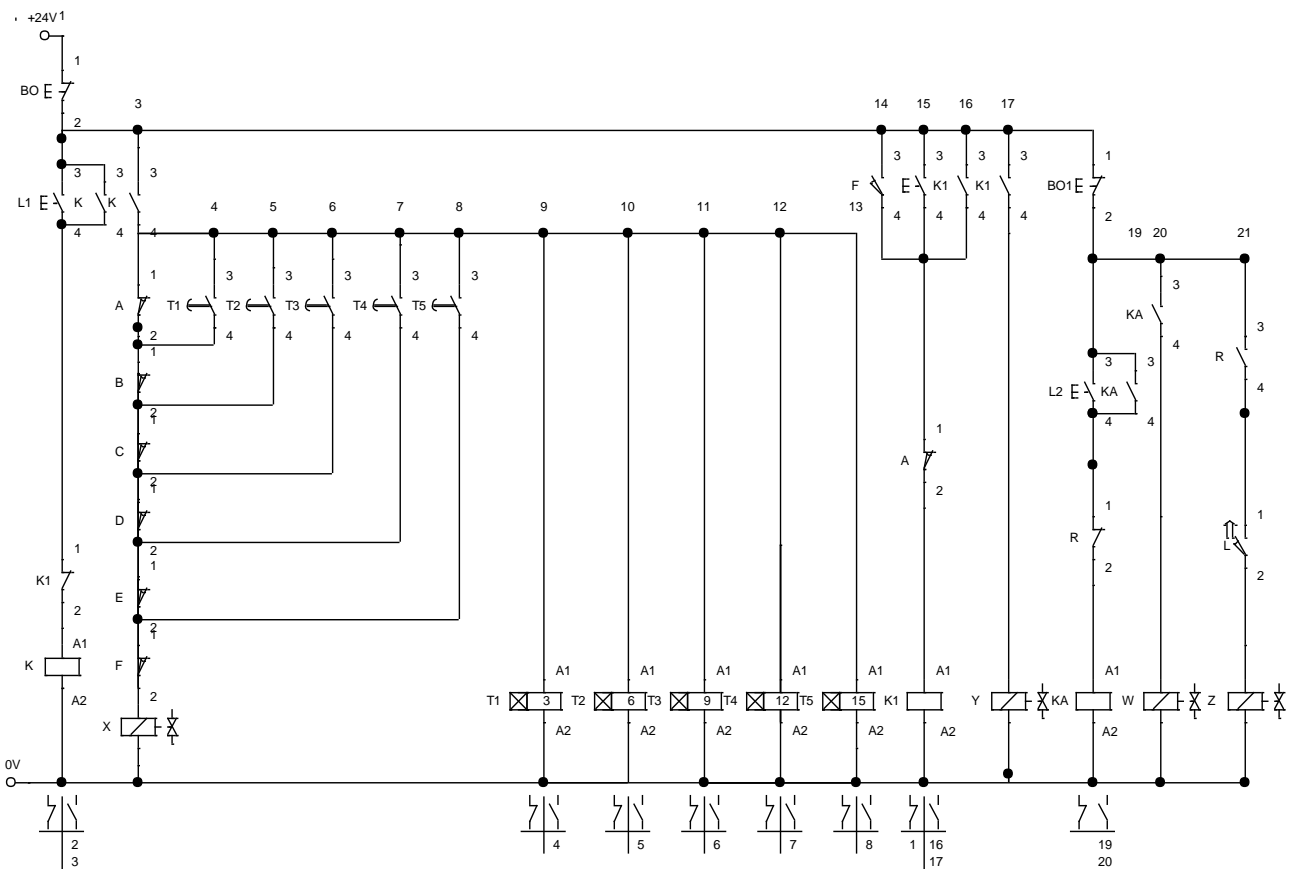


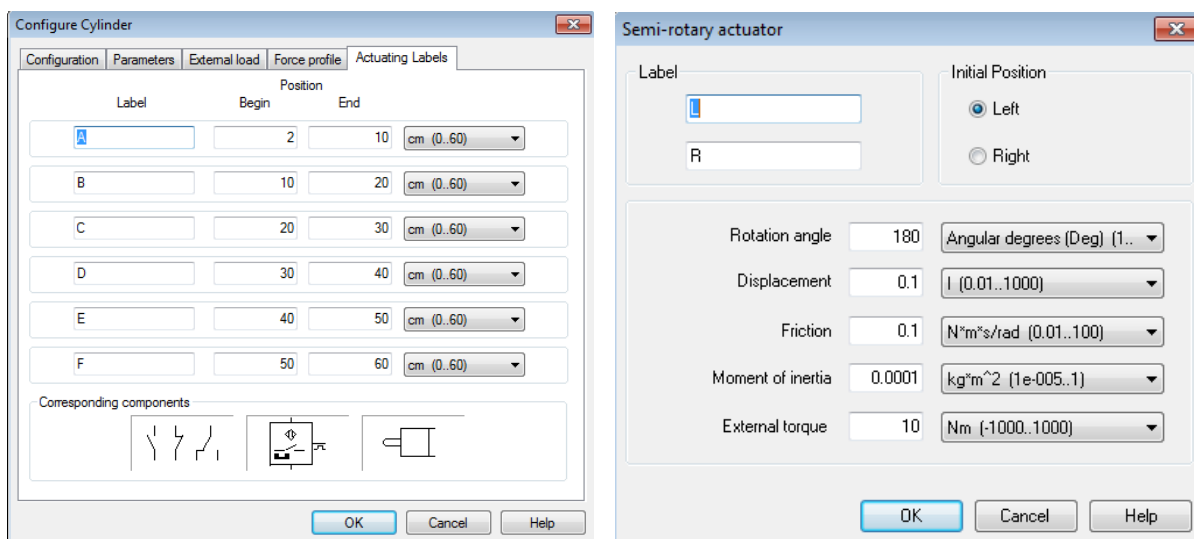
Fig. 10. Electrical circuit for control of pneumatic drive

Positioning of the PV panel on elevation is made by a linear cylinder and on azimuth by a semi-rotary pneumatic motor (Fig. 9). The position of linear cylinder is controlled by limit switch (A, B, C, D, E, F) and timer relays (T1, T2, T3, T4, T5), (see Fig. 10).

Figure 11a) reveals position of limit switches according to the cylinder rod. The first limit switch activating (A) lead to interrupt the power supply to X solenoid valve. After timing generated by a time relay the X solenoid valve is again activated and cylinder is put in motion until reaching another limit switch. (see Fig.10). The sequences are repeated until reaching the ultimate limit switch (F). Now the valve is commanded by a Y solenoid, and the piston of cylinder is returned to initial position.

The movement of semi-rotary pneumatic motor is controlled by pneumatic valve provided with the solenoids W and Z respectively. The semi-rotary pneumatic motor performs a rotating motion between R and L limits at an angle of 180°.

The FluidSim dedicated software allows viewing the characteristic parameters of pneumatic drive. Figure 12 presents the results of simulation for linear cylinder.



a)

b)

Fig. 11. Configuration of pneumatic actuators: a) linear cylinder; b) Semi-rotary actuator

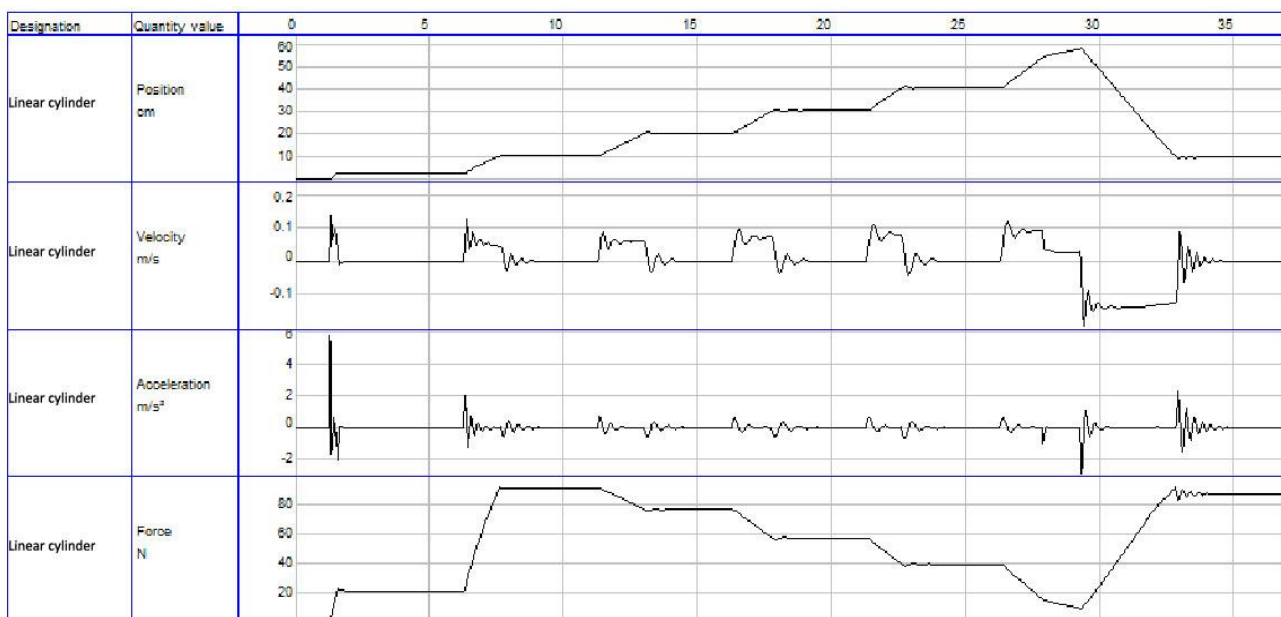


Fig. 12. Results of simulation for linear cylinder

5. Conclusions

In this paper were presented aspects of tracking systems for PV panels. Particularly was presented a pseudo-equatorial tracking system type based on a pneumatic drive. Simulation of automatic drive system was performed with dedicated software named FluidSim. Simulation results showed the evolution of the typical parameters of pneumatic drive. The practical and experimental aspects will be presented in a future work.

Acknowledgments

This work was partially supported by the grant number 29C/2014, awarded in the internal grant competition of the University of Craiova.

References

- [1] I. L. Alboteanu, “Advanced stand-alone photovoltaic system”, Universitaria Publishing House, Craiova, 2013;
- [2] I. L. Alboteanu, F. Ravigan, and A. Novac, “Automation of a Sun Tracking System for Photovoltaic Panel with Low Concentration of Solar Radiation”, “Annals of the University of Craiova: Engineering series”, No. 38/2014, ISBN 1842-4805, pp. 157-163.
- [3] I. L. Alboteanu, F. Ravigan, and S. Degeratu, “Methods for Increasing Energy Efficiency of Photovoltaic Systems”, “International Journal of Power and Renewable Energy Systems”, No.1/2014, ISBN: 2374-376X, pp. 51-61;
- [4] I. L. Alboteanu, Gh. Manolea, F. Ravigan, and A. Nour, “Strategy Of control For Solar Panels Positioning Systems”, “Annals of the University of Petrosani, Electrical Engineering”, vol. 9, 2007, ISSN: 1343-8418, pp. 347-363;
- [5] I. L. Alboteanu, F. Ravigan, S. Degeratu, C. Sulea, “Aspects of designing the tracking systems for photovoltaic panels with low concentration of solar radiation”, “Computational problems in Engineering”, 2015, Springer-Verlag Publishing House, in press;
- [6] I. Bostan, V. Dulgheru, I. Sobor, V. Bostan, and A. Sochirean, “Renewable energy conversion systems”, Tehnica-Info Publishing House, Chisinau, 2007;
- [7] M. Comșit, “Specific orientation mechanisms of solar energy conversion systems”, PhD thesis, Transilvania University of Brasov, 2007;
- [8] D. Diaconescu, et al., “The Incidence Angles of the Trackers Used for the PV Panels’ Orientation. Part I: Equatorial Trackers”. In: ICEEMS – International Conference on Economic Engineering and Manufacturing Systems, Jurnalul RECENT, Vol. 8, nr. 3a (21a), Brasov, Romania, October 2007, p. 281-286;
- [9] I. Hermenean, I. Vișa, D. Diaconescu, “On The Geometric Modelling of a Concentrating PV-Mirror System”, “Bulletin of the Transilvania University of Brașov Vol. 2 (51) – 2009 Series I: Engineering Sciences”, pg. 73-80;
- [10] F. Ravigan, I. L. Alboteanu, “Reducing Shocks due to Wind on the Photovoltaic Trackers Using the Magnetorheological Fluid Dampers”, HERVEX-2014, Calimanesti, Romania, November 5-7, 2014, “Proceedings - International Conference of Hydraulics and Pneumatics”, ISSN: 1454 8003, pp. 241-248;
- [11] F. Ravigan, N. Boteanu, I. L. Alboteanu, and E. Subtirelu, “Remote control of a positioning system”, 2nd International Conference on Systems, Control and Informatics (SCI 2014), Athens, Greece, November 28-30, 2014, “Recent Advances in Electrical Engineering and Educational Technologies”, 2014, ISBN: 978-1-61804-254-5, pp.175-179;
- [12] B. Robert, van Varseveld and G. M. Bone, “Accurate Position Control of a Pneumatic Actuator Using On/Off Solenoid Valves”, “IEEE/ASME TRANSACTIONS ON MECHATRONICS”, VOL. 2, NO. 3, SEPTEMBER, 1997, pp. 195-204;
- [13] O. Stalter, B. Burger, S. Bacha, and D. Roje, “Integrated Solar Tracker Positioning Unit in Distributed Grid-Feeding Inverters for CPV Power Plants”, ICIT 2009, Australia;
- [14] J. Tang and G. Walker, “Variable structure control of a pneumatic actuator”, “ASME J. Dynamic Syst., Measur., Contr.”, vol. 117, Mar. 1995, pp. 88–92;
- [15] I. Vișa, D. Diaconescu, V. Popa, B. Burduhos, “On the Incidence Angle Optimization of the Dual-Axis Solar Trackers”, 11th International Research/Expert Conference TMT - “Trends in the Development of Machinery and Associated Technology”, Hamammet, Tunisia, 04-09 Septembrie 2007, ISBN 994861733-X, pg. 1111-1113;
- [16] <http://www.festo.com/net/startpage/>

Process Study on the Work of a Dough Kneader with a Planetary Motion of the Kneading Arm

PhD. Eng. Dorel STOICA¹, PhD. Eng. Gheorghe CONSTANTIN¹

¹ University POLITEHNICA of Bucharest, Faculty of Biotechnical Engineering, dorelstc@yahoo.com

Abstract: For choosing the best working arrangements for the movement of machinery and processing the kneading of the dough, technological flux on the bread, it is necessary to gain greater knowledge of physical characteristics of the raw materials used, as well as rheological behavior and knowledge of the mixtures obtained. The mathematical formula shown in work and the results obtained may be of assistance to specialists working in connection with the design, construction and use of planetary mixers.

Keywords: kneading machine, planetary mixers, hypocycloid

1. Introduction

Planetary kneading machines belong to the category of operating kneading machines with discontinuous, with the kneading tanks cylindrical flat-bottomed or ball-and-bottomed, being provided with the kneading arms spiral type, cage or an anchor, single or dual.

The kneading arms have planetary movement because all dough from the tank to be driven on-the-move, and all the particles of flour hydrated forms to participate in the process of mixing. The kneading area snapshots is restricted with a diameter approximately equal to the outer diameter non sheathed spiral arm or the kneading.

In the process of working flour particles hydrated form agglomerations which join in the end between them forming dough.

Each point of the kneading arm describes hypocycloid trajectories so that the batter beside the wall basin is driven by the center of it and vice versa so that all the components of the tank are well mixed and thoroughly kneaded.

2. Materials and methods

In the case of the bread dough, the process will continue until it is formed the network of gluten which gives consistency and which constitutes the matrix which holds dough linked to and incorporates the fermentation gases (1,2).

Planetary mixers have, in general, the variable speed operation, in such a way that kneading and mixtures oxygenation should be carried out at an optimum level.

The kneading arm speed can be changed even during operation without feeling shocks when switching from a speed to another.

The mixer Dito Sama BE5 (Fig.1), used to experimental determinations is a three speed ranges in ten steps, the first two steps are used to knead crusts with normal consistency (baked goods) with the arm spiral kneading; another six steps used for mixing creams with the arm type anchor and two more steps very quickly foams used to tapping the egg or in the preparation of the cream, with transition from one gear to another during operation.

The mixer has been used for kneading the dough of wheat flour for the manufacture of fine bakery using the kneading arm spiral.

Tank capacity is 5 liters, but the capacity of work of the mixer is 1.5 kg flour at the ability of solvation (water absorption) and 1 kg stiff dough.

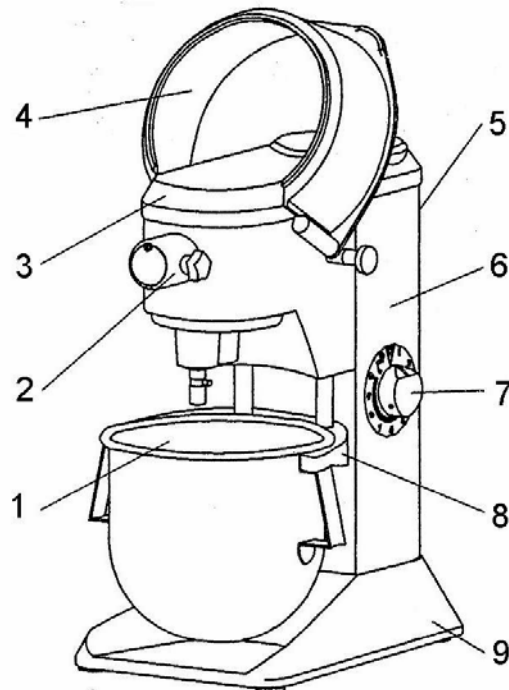


Fig.1. Planetary mixers with three bodies of work [155] 1.vat; 2.capable fixing optional accessories; 3.cover; 4. removable screen; 5. housing; 6.column; 7. on / off switch and speed control; 8.support tank; 9. frame

The kneading arm drive is done with an electric single phase motor via a transmission belt with serrated and a hypocycloidal mechanism through which the mixing arm forms a planetary movement.

In figure 2 is illustrated the hypocycloidal mechanism drive and the kneading arm mixer planetary drive will be analyzed.

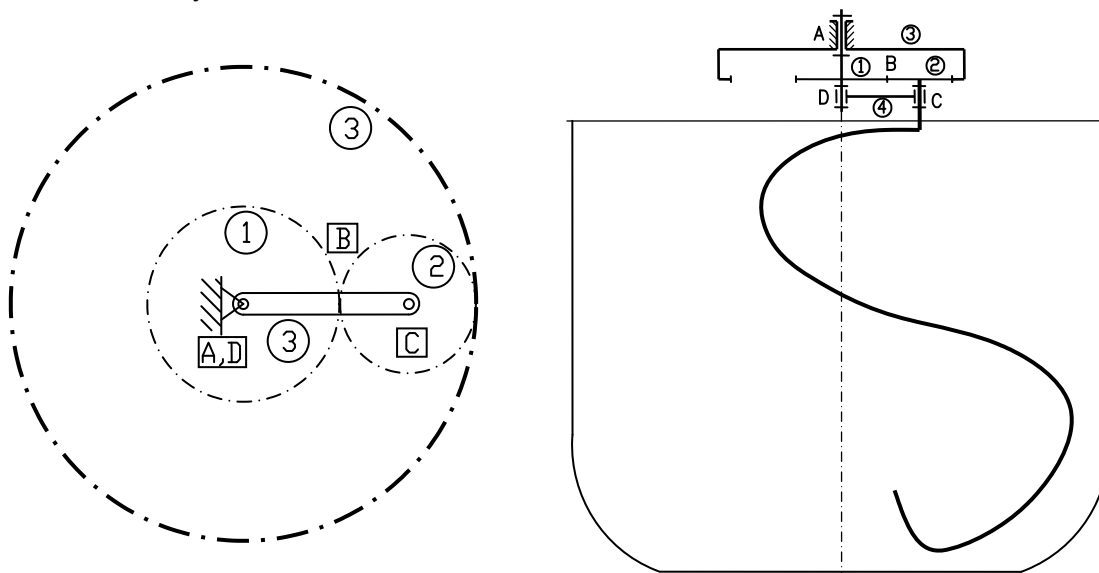


Fig.2. The hypocycloidal mechanism of planetary mixers and computing notations, (2): 1.main drive pinion; 2.driving gear arm with planetary motion; 3.the ring gear fixed; 4.leverage and the kneading arm pick-up; A,B,C,D characteristic points

Determining the equations of the hypocycloid, in Cartesian coordinates is shown in Fig.3. For the purpose of determining the equations of the hypocycloid in Cartesian coordinates is used vector equation

$$\overline{O_1T} = \overline{O_1O} + \overline{OT}. \tag{1}$$

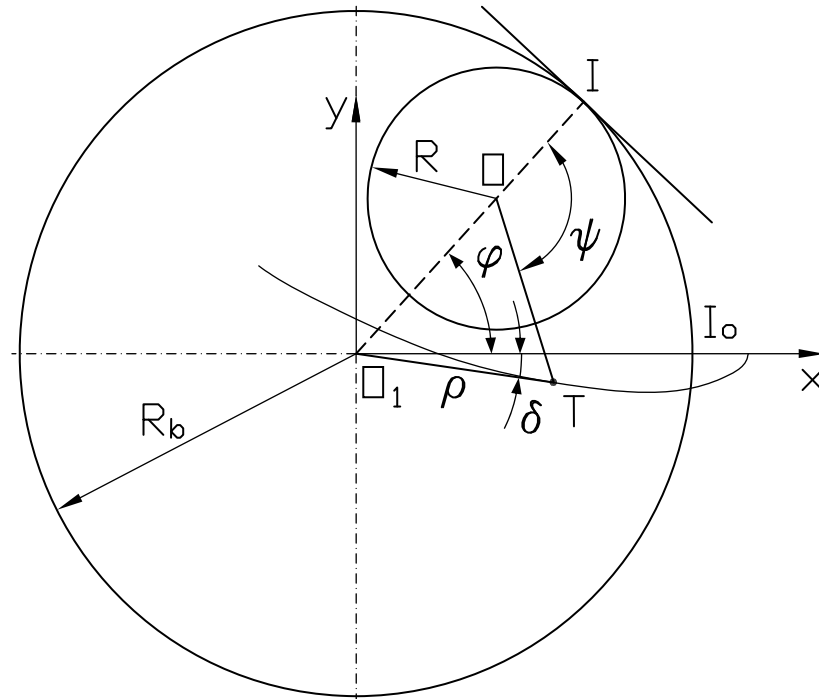


Fig.3. Layout for the calculation of the trajectory points on the kneading arm (1)

Projection vector of equation (4.5), to the axis coordinate system xOy there are obtained two equations scale, as follows (3, 4, 5):

$$\begin{aligned} x_T &= (R_b - R) \cos(\varphi) + OT \cdot \cos(\varphi - \psi) \\ y_T &= (R_b - R) \sin(\varphi) + OT \cdot \sin(\varphi - \psi) \end{aligned} \tag{2}$$

where: R_b is radius ring gear; R - radius of drive sprocket of the kneading arm; φ - the rotation angle at the center of the crown planetary gears in motion.

In view of the fact that tape measure radius R rolls out smoothly on the circle, the radius, it can be written the relationship

$$R \cdot \psi = R_b \cdot \varphi, \tag{3}$$

It results:

$$\psi = \frac{R_b}{R} \cdot \varphi. \tag{4}$$

Using the relation (4), the equations (2) becomes:

$$\begin{aligned} x_T &= (R_b - R) \cos(\varphi) + OT \cdot \cos \left[\left(1 - \frac{R_b}{R}\right) \varphi \right]; \\ y_T &= (R_b - R) \sin(\varphi) + OT \cdot \sin \left[\left(1 - \frac{R_b}{R}\right) \varphi \right]. \end{aligned} \tag{5}$$

which means the equations of the hypocycloid, in Cartesian coordinates.

Depending on the position of the front point T circumference circle, following conditions occur:

- OT = R, hypocycloidal normal;
- OT > R, hypocycloidal lengthened;
- OT < R, hypocycloidal shortened.

Kinematic analysis of the planetary drive. The planetary drive gear, for the operation of the kneading arm mixer, consists of:

Sun gear (center) 1, with external teeth, which receives the rotating movement of the electric motor, by means of a belt transmission with serrated; sun gear 3, with internal teeth which is fixed at the frame; satellite wheel 2, with external teeth; carrier 4, which forms a link between sun gear 1 and satellite 2.

Between the components of the rotation speed planetary drive, it is possible to write the following relations, taking into account the configuration mechanism (Fig.2).

So, using his relationship Willis (7, 8), between rotation speeds of items 1, 2 and 4 shall be written the relationship:

$$i_{12}^4 = \frac{\omega_1 - \omega_4}{\omega_2 - \omega_4} = -\frac{z_2}{z_1}. \quad (6)$$

From the relation (1) results:

$$\omega_2 = -\omega_1 \frac{z_1}{z_2} + \omega_4 \left(1 + \frac{z_1}{z_2}\right). \quad (7)$$

Between rotation speeds of items 1, 3 and 4 there is no relationship:

$$i_{13}^4 = i_{12}^4 \cdot i_{23}^4 = \frac{\omega_1 - \omega_4}{\omega_3 - \omega_4} = \left(-\frac{z_2}{z_1}\right) \left(\frac{z_3}{z_2}\right) = -\frac{z_3}{z_1} \quad (8)$$

In view of that fact, from the relation (8) results:

$$\omega_4 = \frac{\omega_1}{1 + \frac{z_3}{z_1}} \quad (9)$$

In cinematic diagram of the planetary drive, it is to be noted that:

$$z_3 = z_1 + 2z_2, \quad (10)$$

So that:

$$\omega_4 = \frac{\omega_1}{2 \left(1 + \frac{z_2}{z_1}\right)}. \quad (11)$$

The gears of the planetary drive have the following numbers of teeth: $z_1 = 25$; $z_2 = 19$; $z_3 = 63$ teeth. The module gears being $m=1.5$ mm, it follows that they have the diameters of division: $d_1=37,5$ mm, $d_2 = 28.5$ mm and $d_3 = 94.5$ mm. Using relations (7) and (11), results from: $\omega_4=0.28409 \cdot \omega_1$ (rad/s), and $\omega_2 = -0.65789 \cdot \omega_1$ (rad/s).

Using the model of calculation presented there have been drawn graph trajectories of the kneading arm to the lowest point of the arm, that is for the point that is the furthest away from the center ($r=60$ mm). The graphs are shown in Figures 4, 5 and 6.

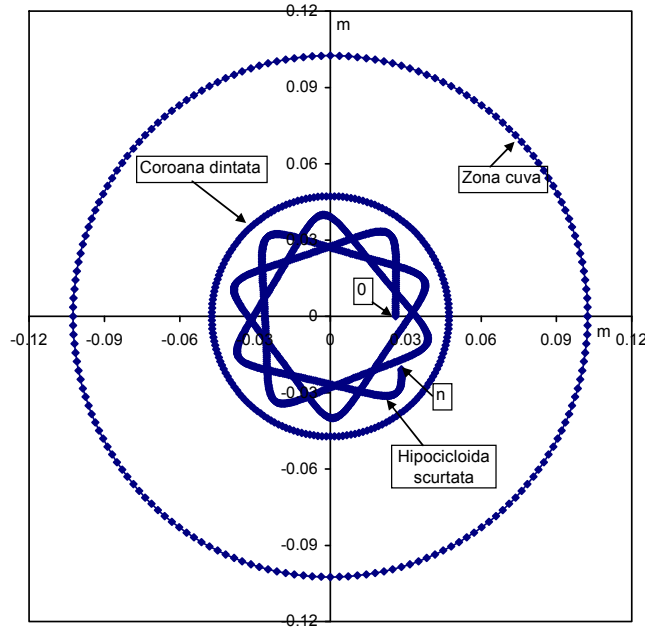


Fig.4. Hypocycloidal lower point of the kneading arm, (1)

Having regard that the number of teeth for the two sprockets located in mesh, 1, 2 respectively, is different, after a cycle of operation (i.e., a complete rotation of the item 4) the trajectory any point on the kneading arm spiral will move from the first electronic stability program, which is beneficial for the flow of the process of work because all areas in cross-section of the tank will also be covered.

The actuators of planetary mixers are, in general, hypocycloidal mechanisms with two main gear trains connected to each other by means of a lever, the drive pinion of the kneading arm while remaining in constant contact and with a ring gear which ensures fixed planetary movement in cross-section of the tank.

The kneading zone instant the area is small compared to the tank of the kneading, but by planetary movement of the kneading arm it is ensured that they will cover the entire surface area of the tank. The kneading arm has also a rotating movement that provides a main process of mixing properly.

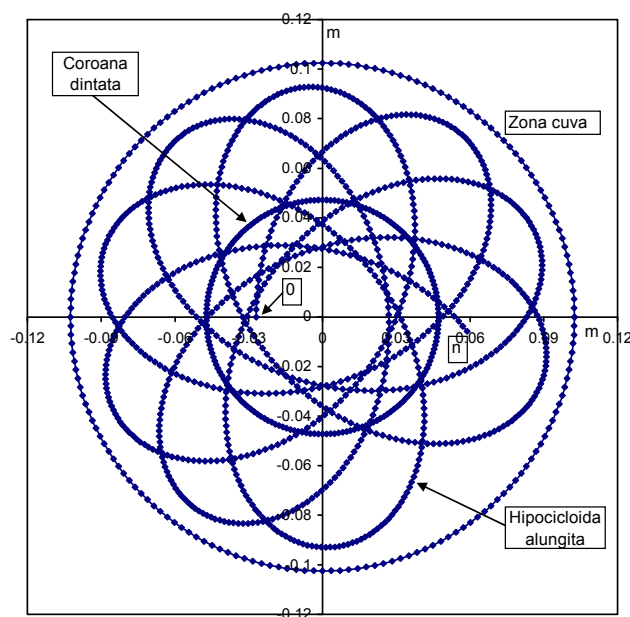


Fig.5. The trajectory of the point hypocycloid exterior to spiral kneading arm for a complete cycle, (1)

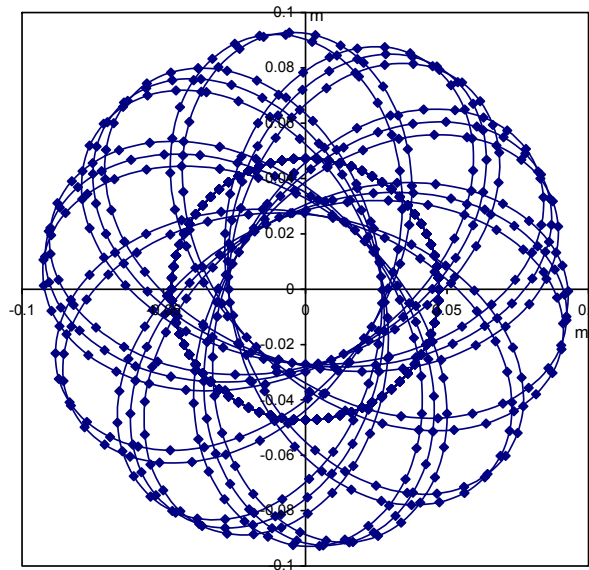


Fig.6. The trajectory of the point hypocycloid exterior to the kneading arm spiral for three cycles, (1)

The mathematical formula shown in this paper work, as well as the results obtained may be of assistance to specialists working in connection with the design, construction and use of planetary mixers.

CONCLUSIONS

1. The process of mixing operation is extremely significant in baking industry; by this wheat flour, water and additional ingredients are modified by the flow of mechanical energy for kneading inconsistent. Dough properties are strongly influenced by the way of their mixing;
2. Knowing the physical and rheological parameters of bread and mixtures is useful to specialists and workers in the field for the evaluation of process parameters of functional machinery which processes pie crusts, as well as for the establishment of process quality parameters of bread-making;
3. Use of models in complex rheological behavior modeling dough at molding and machining is also cumbersome relations because of the complexity involved in mathematical models, but also because of the high degree of difficulty for the verification of models in experimental determinations.

References

- [1] Gh. Voicu, Gh. Constantin, V. Moise, N. Ungureanu, P. Voicu, Analysis of the working process of a dough-kneading machine with planetary motion arm, Third International Conference Research people and actual tasks on multidisciplinary science, Lozenec, Bulgaria, vol.2, 2011, pp.24-28;
- [2] Gh. Voicu, Procese și utilaje pentru panificație, Bren Publishing House, Bucharest, 1999;
- [3] I.I. Artobolevski, Theorie des mecanismes et des machines, Mir Publishing House, Moscow, 1977;
- [4] S.A. Mohsen, N. Phan-Thien, Stress relaxation and oscillatory tests the distinguish between doughs prepared from wheat flours of different varietal origin, Cereal Chemistry, 75(1), 1998, pp.80-84;
- [5] Chr. Pelecudi, D. Maroș, V. Merticaru, N. Pandrea, I. Simionescu, Mecanisme, Didactic and Pedagogical Publishing House, Bucharest, 1985;
- [6] V. Moise, I. Simionescu, M. Ene, M. Neacșa, I. A. Tabără, Analiza mecanismelor aplicate, Printech Publishing House, Bucharest, 2007;
- [7] Gh. Constantin, Cercetări privind comportarea reologică a aluaturilor din făină de grâu pentru panificație și aplicații, PhD thesis, Bucharest, 2011.

Determining the Response of a Pneumatic System with Medium and High Pressure Actuators to Step Signal

PhD. eng. Gheorghe SOVAIALA¹, PhD. eng. Radu RADOI¹,
PhD. eng. Gabriela MATACHE¹, Tech. Ioan PAVEL¹

¹INOE 2000-IHP, Bucharest, sovaiala.ihp@fluidas.ro

Abstract: This paper presents the research concerns of Hydraulics and Pneumatics Research Institute in Bucharest in gaining knowledge about the specific phenomena and processes related to the operation of medium and high pressure actuators, in order to increase energy efficiency of pneumatic drive systems. At INOE 2000-IHP, in the Laboratory of Pneumatics have been conducted tests on the EM of a pneumatic system with medium and high pressure actuators. The following tests have been carried out upon it: the response of the pneumatic drive system with medium pressure actuator to step signal, for various values of the PID controller and controlled load, and there have been developed the next graphs: attenuation vs. frequency and phase vs. frequency (Bode plot).

Keywords: pneumatic drive system, pressure actuator, medium and high pressure, step signal, Bode plot

1. Introduction

The conditions under which tests have been conducted

The tests have been conducted at the premises of INOE 2000-IHP Bucharest, 14 Cutitul de Argint Street, district 4 – the Laboratory of Pneumatics.

Ambient temperature 20-28°C

The tests have been carried out in dynamic conditions on a specially designed pneumatic system, according to the testing methodology.

Description of the system under tests

The pneumatic system with medium pressure actuators which has been under tests consists of mechanical assembly of two linear actuators, a drive actuator and a load actuator, and is equipped with pressure transducers on the chambers of the drive actuator, force transducer between the rods of the two actuators and incremental displacement transducer (see Figure 1).

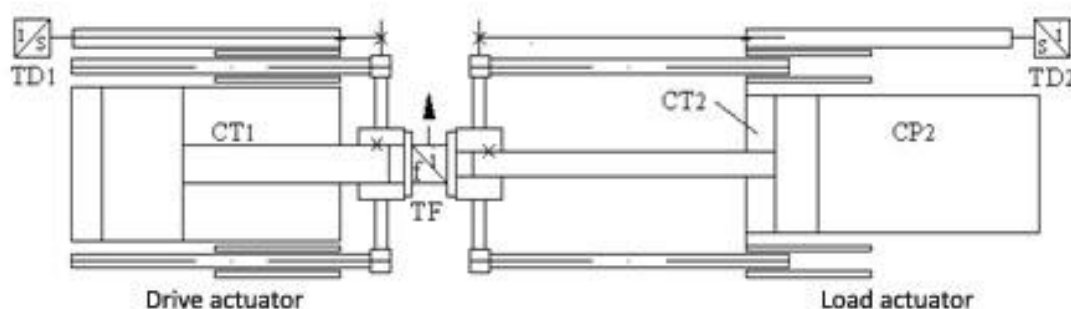


Fig. 1. Structure of the pneumatic system under tests

The signals from the transducers are taken over from an acquisition board (DAQ) which is connected, as shown in Figure 2, to a PC equipped with data acquisition and processing software developed in LabVIEW.

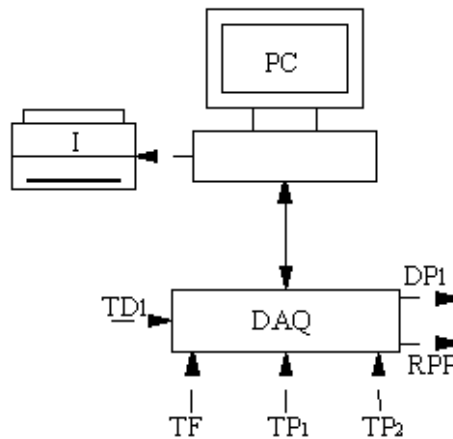


Fig. 2. Diagram of the pneumatic system under tests

Technical characteristics of the pneumatic system with actuators are shown in Table 1:

TABLE 1: Technical characteristics of the pneumatic system

Input pressure	8 bar;
Load adjustable pressure	0-6 bar;
Maximum working flow rate	50 Nm ³ /h
Control current	0-10mA;
Pneumatic coupling	3/8"
Working voltage	24V DC
Drive and load linear actuators FESTO type DNCI 32	Ø32x Ø16x 300
USB-6218 data acquisition board	6 inputs, 2 outputs

2. Targets of the tests conducted

Conducting tests on the EM of the pneumatic system with medium and high pressure actuators targets:

- **The response of the pneumatic drive system with medium pressure actuator to step signal, for various values of the PID controller and pneumatic spring type load**

There has been observed the evolution of the positioning accuracy (error) at various values of the PID controller with pneumatic spring type load. There have been changed in turns the compliance parameters of the automatic controller with various values for P ($k_c=6000-11000$, $T_i=5000-7000$, $T_d=0.001-0.003$), and the goal was that the positioning error to be at the minimum and the system to be steady. There have also been recorded on the diagram the evolution of force and stroke of the cylinder rod, and also the pressure rates in the cylinder chambers.

- **Drafting the attenuation vs. frequency graph and the phase vs. frequency graph (Bode plot)**

It was intended data acquisition in dynamic mode, plotting the attenuation vs. frequency graph (the response to sine wave signal), the phase shift vs. frequency graph, and also drafting the Bode plot.

3. The results obtained

The system which was under tests is a pneumatic axis with medium pressure actuators, servo actuator with incremental displacement transducer and proportional drive and control instrumentation.

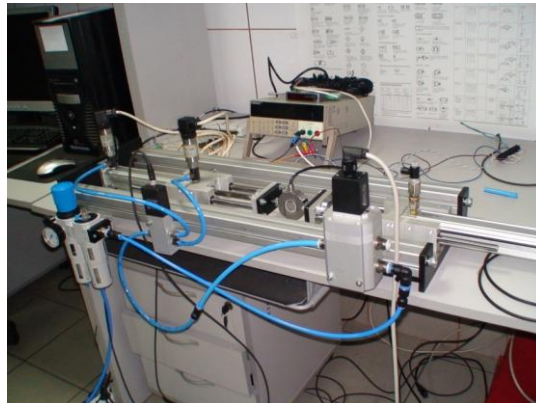


Fig. 3. Pneumatic drive system with medium and high pressure actuators, with pneumatic spring type load

During tests there was observed the behaviour of the drive system with medium pressure servo actuator and pneumatic spring type load to step signal, respectively triangular signal, with various frequencies, applied to the proportional flow directional control valve at the signal generator of LabVIEW application. System response to the applied step/ramp signal is an electrical type signal (voltage), with the same rate of curve, received from the incremental displacement transducer of the system drive actuator.

The load type pneumatic spring has been generated by means of the bypass valve throttles mounted on the fittings of the pneumatic load actuator chambers.

Values of the automatic PID controller parameters influence the system stability, as it follows:

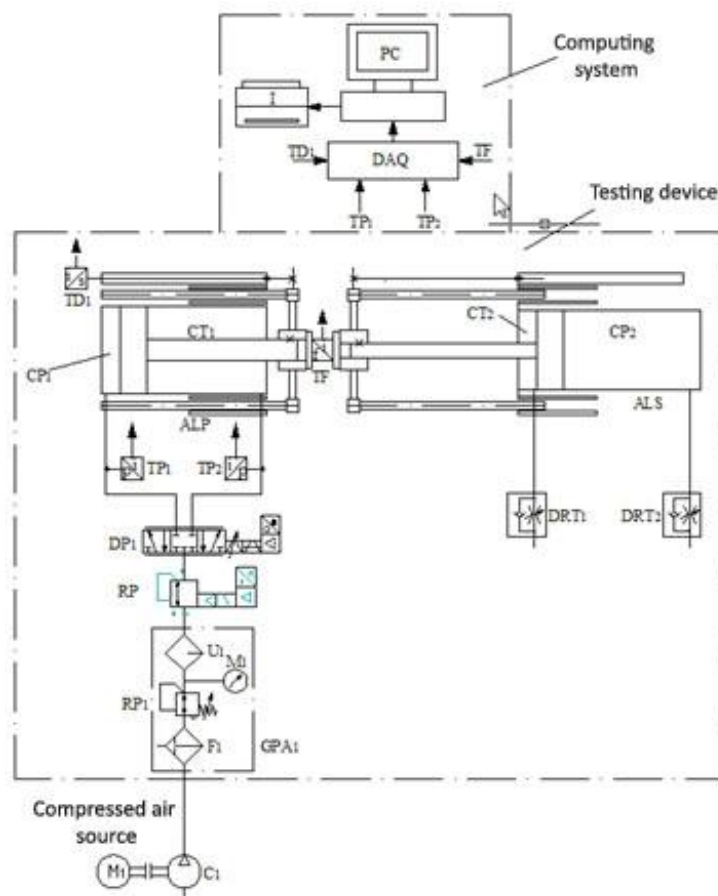


Fig. 4. Testing diagram of the pneumatic drive system with medium pressure actuators and pneumatic spring type load

Step signal

In Figures 5 and 6 it can be noticed that for a working pressure of the system drive actuator equal to 6 bar, amplification factor $k_c=6000$, integration constant T_i [min]=5000, derivation constant T_d [min]=0.001, frequency $f=0.07$ Hz, the system has steady functioning, without override. The error in positioning accuracy (difference between rated and achieved) is 10%.

By increasing the amplification factor ($k_c=9000$), integration constant (T_i [min]=6000) and frequency ($f=0.5$ Hz), see Figures 7 and 8, the positioning error goes up to 16.6%. The system has almost steady functioning, with speed oscillations. It can also be noticed that the pneumatic spring type load, with fully closed throttles, limits the possibility of achieving the prescribed position, significant differences occurring between the position control and the achieved position. This is because at stroke ends the piston can move until the pneumatic spring force, generated by reducing the volume of air in the load actuator chamber, reaches the limit equal to the force inside the rod of the drive actuator.

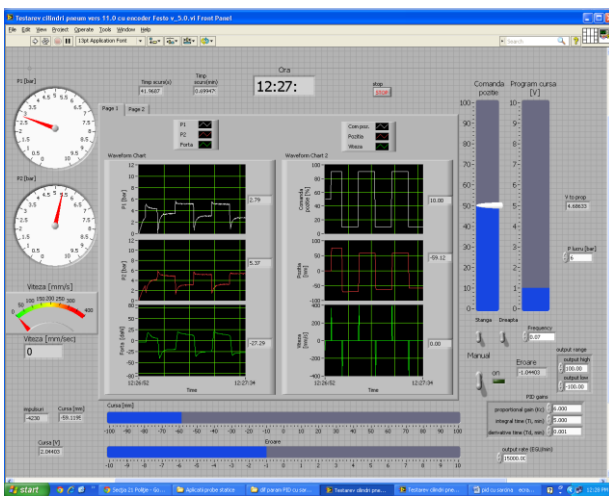


Fig. 5

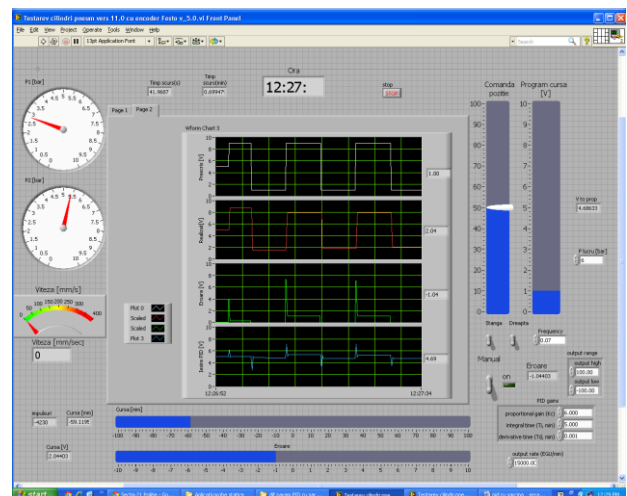


Fig. 6

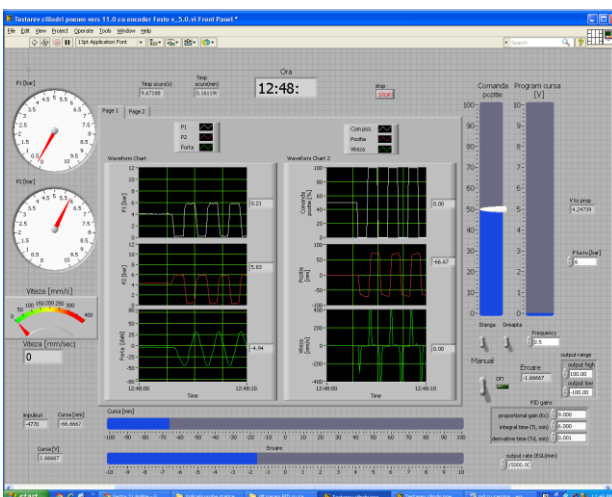


Fig. 7

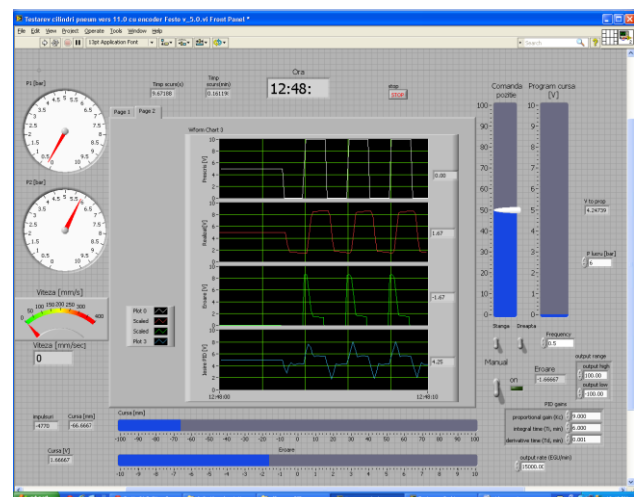


Fig. 8

Ramp signal

In Figures 9, 10, 11 and 12 is revealed the system behavior to triangular signal (increasing and decreasing ramp).

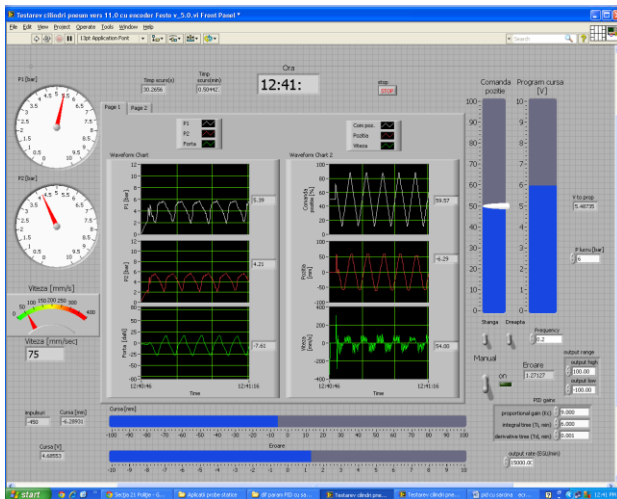


Fig. 9

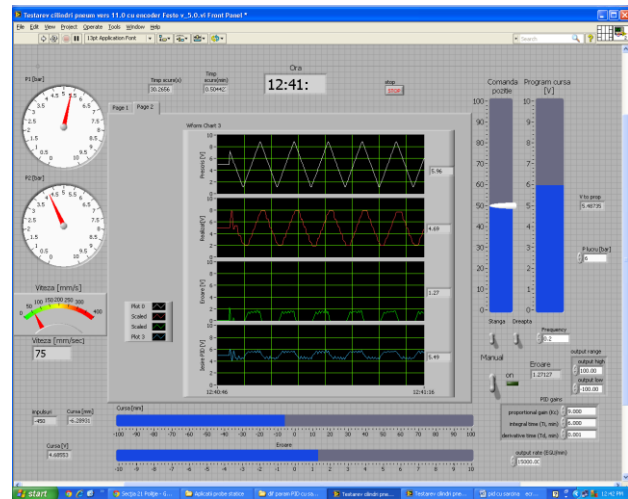


Fig.10

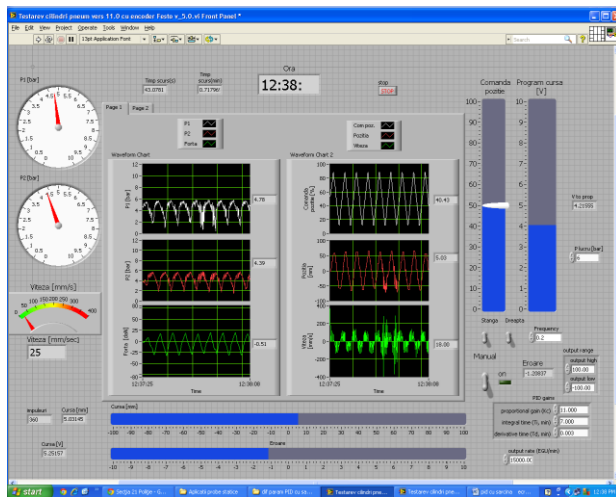


Fig. 11

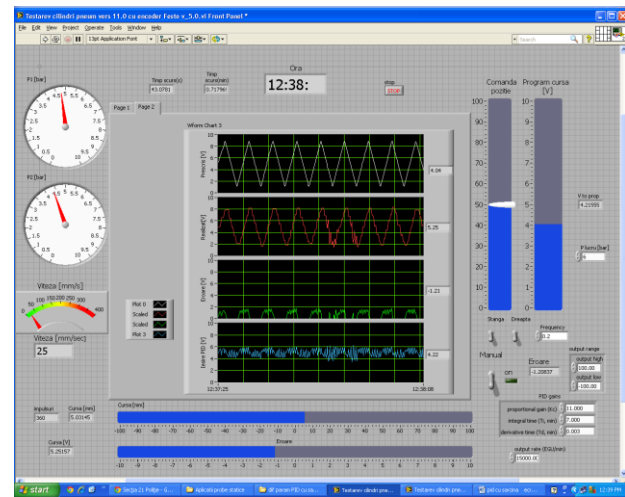


Fig. 12

It can be noticed that for a working pressure of the system drive actuator equal to 6 bar, amplification factor $k_c=9000$, integration constant T_i [min]=6000, derivation constant T_d [min]=0.001, frequency $f=0.2$ Hz, the system has unsteady functioning, with speed oscillations along the piston rod in both displacement directions. The error in positioning accuracy goes up to 12.7%. It can be considered that **the system has critical behaviour in speed**.

When increasing the value of the PID controller parameters: amplification factor $k_c=11000$, integration constant T_i [min]=7000, derivation constant T_d [min]=0.003, frequency $f=0.2$ Hz, system unsteadiness gets worse, it showing strong oscillations mainly in speed, error and the PID automatic controller output signal. It can also be noticed that slight oscillations occur in position, it nevertheless remaining within acceptable limits. The positioning error is 12%. As in the previous case, it can be considered that **the system has critical behaviour in speed**.

4. Conclusions

Following the tests conducted on the product **Pneumatic drive system with medium pressure actuators, with pneumatic spring type load**, we reached the following conclusions:

- General conclusions: the characteristics of the system components comply with those presented in the manufacturer catalogue, FESTO SA – Germany;
- The results of tests on this application refer exclusively to tests carried under laboratory conditions, using simplifying assumptions (T =steady; error of 2.5 % included in measurements);

c) The results of tests reveal system behavior for various values of the PID automatic controller parameters:

- the type P controller significantly reduces override, leads to a short transient period, but introduces a high stationary error ε_{st} ;
- by introducing the component I , the type PI controller cancels the stationary error at step input, but leads to a higher override compared with the one at the P controller and to a long duration of the response time;
- by introducing the component D , the type PD controller improves the dynamic behavior (override σ and duration of the transient mode are low), but maintains a high stationary error;
- the PID type controller, combining the effects P , I and D , gives higher performance both in steady and transient mode.

The tested system had steady behaviour for values of the PID controller parameters between the limits: $k_c=4000-6000$; $T_i=5000-6000$; $T_d=0.001$.

References

- [1]. M. Avram, “Acționări hidraulice și pneumatice - Echipamente și sisteme clasice și mecatronice”, University Publishing House, Bucharest, 2005;
- [2]. Belforte, Bertetto, Mazza, “Pneumatico - curso completo”, Techniche nuove Publishing House, Milano, 2004;
- [3]. V. Banu, T. Demian, “Motoare pneumatice liniare si rotative”, Technical Publishing House, Bucharest, 1994;
- [4]. Banu, Stanescu, Atodiroaiei, Gaburici, “Sisteme de automatizare pneumatice”, Technical Publishing House, Bucharest, 1997;
- [5]. SMC Romania, “SMC International Training-Introducere in pneumatica”, SMC Romania 2004;
- [6]. E. Diaconescu, “Controlul pozitiei cu Labview”, Publishing House of Pitesti University, 2006.

Kinematic and Dynamic Irregularities of Roller Pumps

Part I. Modeling of Kinematic and Dynamic Irregularities

Prof. MSc. Gencho POPOV PhD¹, MSc. Yuliyán ANGELOV PhD¹

¹University of Ruse “Angel Kanchev”, Bulgaria, gspopov@uni-ruse.bg, julian@uni-ruse.bg

Abstract: In this work generalized models for the determination of some typical irregularities in roller pumps, mainly used to work with water and water solutions, have been presented. It is concluded that when for the investigation of the kinematic characteristics of this type of pumps, the approximate equation for estimating the relative move of the rolls in the rotor’s canals is used, the occurred deviation will be negligible. Some equations, which can be used for the determination of: the change of a given working camera’s flow rate; the pump’s total momentary flow rate; the loading of rolls, have been established. The equations describing the rotation of a given roll, has also been found.

Keywords: Roller pump, models of kinematic and dynamic irregularities.

1. Introduction

The roller pumps are volumetric hydraulic machines, finding a wide range of application in crop-protective machines, used in agriculture, bio-technics, etc. They are mainly considered to work with relatively low pressures (up to 2 MPa) and specialized into the transportation of low-oil liquids, such as water and water solutions. This is the main reason for the rolls to be produced by nonmetallic antifriction materials (Teflon, naylor, different modifications of solid rubber, etc.), while both, the stator and rotor, are cast-iron details. The principle scheme of this kind of a pump is given in fig. 1.

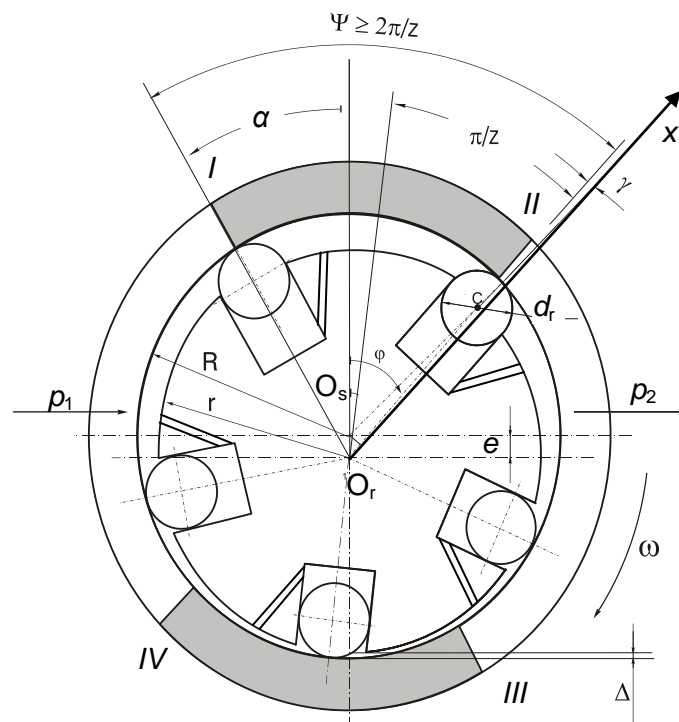


Fig.1 A scheme of a roller pump

The principle of work of this kind of machines, including different irregularities, according to their type and grade, which are determined by the processes, concerning the liquid transportation from the sucking (low pressure) zone to the zone of high pressure, as well as the features of the

kinematic and dynamic pump's working elements (the rolls). The main parameters, characterizing these processes, respectively are: the geometric volume of the pump's working cameras and its change in the range of one full rotation of the pump's shaft; the theoretical (geometric) flow rate and the grade of the flow rate's kinematic irregularity; the geometry of the liquid's distribution in the transitional sections, dividing each other the pump low and high pressure zones; the force loading of the pump's main working elements, etc.

In this work some theoretical equations, found by the authors and used for the determination of the roller pump's parameters, mentioned in the above paragraph, are being generalized.

The implemented parameters and their symbols are given in Table 1:

TABLE 1. Used parameters

Radius (diameter) of the stator's directive cylindrical surface	$R(D)$
Radius (diameter) of the rotor	$r(d)$
Radius (diameter) of the roll	$r_r(d_r)$
Roll's relative radius	$\bar{r}_r = r_r / R$
Number of rolls	z
Eccentricity of the stator with respect to the rotor	e
Relative eccentricity	$\lambda = e/R$
Rotor's width (length)	b
Relative rotor's width (length)	$\bar{b} = b/R$
Angular, determining the beginning of the transitional sections	α
Angular, determining the length of the sealing sections	ψ
Angular between two adjacent rolls	$\beta = 2\pi/z$
Angular between the radiuses of the pump's rotor and stator	$\gamma = \arcsin(\lambda \sin\varphi)$
Minimal gap between the rotor and stator	Δ
Roll's mass	m
Mass inertia torque of a roll	J
Gravity acceleration	g
Rotor's angular velocity	ω
Roll's angular velocity and acceleration	ω_r and ε_r
Slipping coefficients of friction	μ_1 and μ_2
Coefficient of resistance, when viscosity friction between the roll and working surface, is indicated	k
Force of pressure, acting on the pump's rolls	F
Force of gravity of the rolls	G
Inertia force of the transitional and relative roll's acceleration	Φ
Coriolis inertia force	F_k
Torque, occurred as a result of the resistance against the roll's (auxiliary-rotation) rotation	M_s
Roll's inertia torque	$M^{(\Phi)}$
Normal reactions, occurred in the zone of contact between the stator's directive surface and the rotor's canal's wall	N_1 and N_2
Forces of friction between the stator's directive surface and the rotor's canal's wall	T_1 and T_2

2. Kinematic irregularities modeling

The kinematic irregularity of a roller pump is due to the existing of the irregular relative roll's move, with respect to the rotor's canals, occurred in the range of one full pump shaft's rotation. The physical law, describing the roll's move into the canal, can be presented as a function of the rotor's angular of rotation - φ . As a preliminary base, used for the determination of these kinematic parameters, the equation, estimating the radius-vector of the stator's cylindrical directive surface, in respect to the axis of rotation, can be selected. This equation is equal to the equation, valid for one-acting radial-piston pumps and vane pumps, having same type of directive surfaces:

$$\rho_{\varphi} = R \left(\sqrt{1 - \lambda^2 \sin^2 \varphi} + \lambda \cos \varphi \right). \quad (1)$$

By using equation (1), the physical law, determining the relative roll's move, in respect to the rotor's canal, when its angular of rotation is φ , can be found (fig. 1):

$$x = R + e - \rho_{\varphi} = R \left(1 + \lambda - \lambda \cos \varphi - \sqrt{1 - \lambda^2 \sin^2 \varphi} \right). \quad (2)$$

For the simplification of equation (2), different methods can be used. It is a well-known fact, that best results can be achieved in case that the radical, given in brackets, is being presented according to the Newton's binomial theorem, by taking the first two articles - $\sqrt{1 - \lambda^2 \sin^2 \varphi} \approx 1 - 0,5\lambda^2 \sin^2 \varphi$. With this approximation the physical law, describing the relative roll's move in the canal x^* , can be given by the following equation:

$$x^* = R \left(\lambda - \lambda \cos \varphi + 0,5\lambda^2 \sin^2 \varphi \right). \quad (3)$$

The relative percentage deviation, between the results found by using the approximate equation (3), instead of the precise equation (2), can be evaluated by the following equation:

$$\delta = \frac{x - x^*}{x} 100, \%. \quad (4)$$

The equation, used for the estimation of the relative deviation δ , given as a function of the angular of rotation φ , for pumps having different eccentricity λ , is given in fig. 2. It can be seen that, when for the investigation of the kinematic parameters of the roll's move in the rotor's canals, the approximate equation (3) is used, the relative deviation is negligible (its value is less than 0.6 % for the high eccentricity pumps).

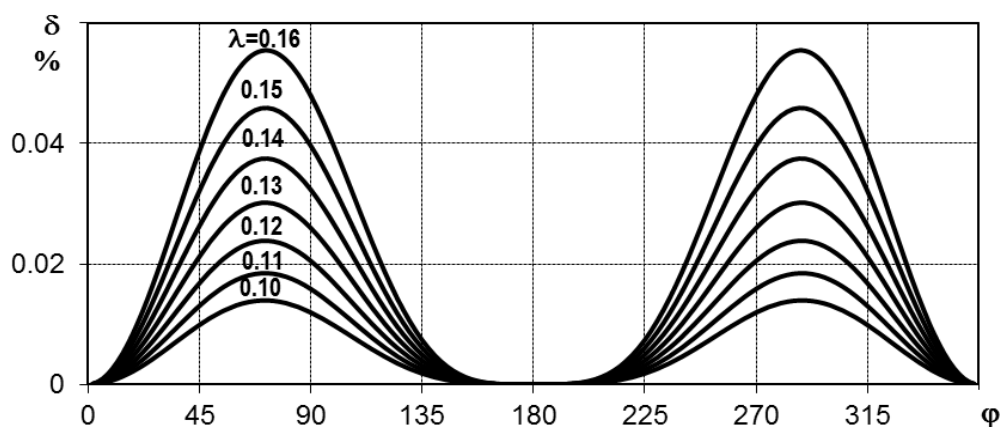


Fig. 2. Change of the relative deviation, when for the determination of the roll's move the approximate equation is used

The relative velocity and relative acceleration of the roll's move, in the radial canal of the rotor, can be determined by using the approximate equation (3):

$$v = \frac{dx}{dt} = \frac{dx}{d\varphi} \frac{d\varphi}{dt} = \omega R^3 \bar{r}_r \bar{b} \lambda (\sin\varphi + 0,5\lambda \sin 2\varphi), \quad (4)$$

$$a = \frac{dv}{dt} = \frac{dv}{d\varphi} \frac{d\varphi}{dt} = -\omega^2 R^3 \bar{r}_r \bar{b} \lambda (\cos\varphi + \lambda \cos 2\varphi). \quad (5)$$

The kinematic irregularity of the pump's flow rate is due to the irregular move of the rolls in the rotor's canals. To investigate this irregularity, first it is necessary for the change of the volume of the pump's working cameras, given as a function of the angular of rotation [5], to be determined. The equation, used for the estimation of the volume of a working camera, is given in a dimensionless order:

$$\begin{aligned} \bar{V}_\varphi = \frac{V_\varphi}{\bar{b}R^3} = & 0,5 \left\{ \lambda \left[\sin(\varphi + \beta) \sqrt{1 - \lambda^2 \sin^2(\varphi + \beta)} - \sin\varphi \sqrt{1 - \lambda^2 \sin^2\varphi} \right] + \right. \\ & + \arcsin\lambda \sin(\varphi + \beta) - \arcsin\lambda \sin\varphi + 0,5\lambda^2 [\sin 2(\varphi + \beta) - \sin 2\varphi] - \\ & \left. - 2\bar{r}_r \left[\sqrt{1 - \lambda^2 \sin^2(\varphi + \beta)} - \sqrt{1 - \lambda^2 \sin^2\varphi} \right] - 2\lambda\bar{r}_r [\cos(\varphi + \beta) - \cos\varphi] \right\} + A, \end{aligned} \quad (6)$$

where A has a constant value, independent by φ .

The flow rate - $Q_{1,\varphi}$, ensured by a working camera, can be estimated by the following equation [4]:

$$Q_{\varphi,1} = \frac{dV}{dt} = \omega \frac{dV}{d\varphi}$$

Using the equation of estimation the flow rate $Q_{1,\varphi}$, given in [4], the dimensionless value of the flow rate for a given pump's working camera, can be determinate by the following equation:

$$\begin{aligned} \bar{Q}_{1,\varphi} = \frac{Q_{1,\varphi}}{\omega\bar{b}R^3} = & \lambda \left\{ \cos\varphi \sqrt{1 - \lambda^2 \sin^2\varphi} - \cos(\varphi + \beta) \sqrt{1 - \lambda^2 \sin^2(\varphi + \beta)} + \lambda [\cos^2\varphi - \cos^2(\varphi + \beta)] + \right. \\ & \left. + \bar{r}_r [\sin\varphi - \sin(\varphi + \beta)] + 0,5\bar{r}_r \lambda \left[\frac{\sin 2\varphi}{\sqrt{1 - \lambda^2 \sin^2\varphi}} - \frac{\sin 2(\varphi + \beta)}{\sqrt{1 - \lambda^2 \sin^2(\varphi + \beta)}} \right] \right\}. \end{aligned} \quad (7)$$

Equation (7) indicates that the flow rate, ensured by a working camera, changes according to a complicate trigonometric mathematical function, which can be recognized as a typical feature, concerning all hydraulic machines with similar kinematic of driving to their main working elements. The momentary pump's flow rate can be determined by summing of all the separate flow rates, ensured by each of the working cameras, which are connected to the high pressure canal:

$$Q_\varphi = \sum_{m=1}^{k-1} Q_{1,\varphi},$$

where k is the number of the same time connected to the pump's high pressure zone cameras.

By using equation (9), indicating the fact that (usually) for the roller pumps $\lambda \leq 0,1$ and assuming that $\sqrt{1 - \lambda^2 \sin^2\varphi} \approx \sqrt{1 - \lambda^2 \sin^2(\varphi + \beta)} \approx 1$, some simplifications can be accomplished. In this case the value of the dimensionless momentary flow rate can be estimated by the following equation:

$$\begin{aligned} \bar{Q}_\varphi = \frac{Q_\varphi}{\omega\bar{b}R^3} = & \lambda \left\{ \sum_{m=0}^{k-1} [\cos(\varphi + m\beta) - \cos(\varphi + \beta + m\beta)] + \lambda \sum_{m=0}^{k-1} [\cos^2(\varphi + m\beta) - \cos^2(\varphi + \beta + m\beta)] + \right. \\ & \left. + \bar{r}_r \sum_{m=0}^{k-1} [\sin(\varphi + m\beta) - \sin(\varphi + \beta + m\beta)] + 0,5\bar{r}_r \lambda \sum_{m=0}^{k-1} [\sin 2(\varphi + \beta) - \sin 2(\varphi + \beta + m\beta)] \right\}, \end{aligned} \quad (8)$$

where after the above equation is being mathematically transformed, it can be given in the following way:

$$\begin{aligned} \bar{Q}_\varphi = & \lambda \left\{ \cos\varphi - \cos(\varphi + k\beta) + \lambda [\cos^2\varphi - \cos^2(\varphi + k\beta)] + \right. \\ & \left. + \bar{r}_r [\sin\varphi - \sin(\varphi + k\beta)] + 0,5 \bar{r}_r \lambda [\sin 2\varphi - \sin 2(\varphi + k\beta)] \right\}. \end{aligned} \quad (9)$$

It is well-known that for pumps with an even number of rolls $k = z/2$ and respectively - $k\beta = \pi$. For those with an odd number of rolls, the number of cameras k , belonging to the pump's high pressure zone at the same time, depends on the angular of the rotor's rotation - φ . Within the range of an angular step ($\beta = 2\pi/z$) it changes from $k = (z+1)/2$, in the first half of the rotation, to $k = (z-1)/2$ - during the second half of it.

To evaluate the pump's flow rate irregularity, it is recommended for the coefficient of the flow rate's irregularity to be used:

$$\delta = \frac{Q_{\max} - Q_{\min}}{Q_T} 100, \quad \% , \quad (10)$$

where Q_{\max} and Q_{\min} are the maximal and minimal values of the pump's momentary flow rate and Q_T is the average value of the theoretical flow rate, which can be estimated by the following equation:

$$Q_T = 2eDb \left(\pi k_z - \bar{r}_r z \cos \frac{\pi}{z} \right) n \quad (11)$$

where $k_z = \frac{\sin \pi/z}{\pi/z}$ is a coefficient, indicating the number of rolls.

For an even number of rolls the coefficient of the flow rate's irregularity can be estimated by the following equation:

$$\delta = \frac{1}{k_z} \left[\frac{1 - \cos(\alpha + \arctg \bar{r}_r)}{\cos(\alpha + \arctg \bar{r}_r - \frac{\pi}{z})} \right] \cdot 100, \quad \% . \quad (12)$$

The estimation of the angular α (fig. 1), determining the beginning of the transitional sections, located between the low and high pressure zones, can be done by using the following equation [5]:

$$\alpha = \frac{\pi}{z} - 2\lambda \frac{r_r}{r_{r,\min}} . \quad (13)$$

Using the condition of non-allowing any blocking, the minimal value of the roll's radius - $r_{r,\min}$, can be determined by the following equation:

$$r_{r,\min} = R \left(\frac{1+\lambda}{2} - \sqrt{\left(\frac{1-\lambda}{2} \right)^2 - \lambda(1-\bar{\Delta}) - \bar{\Delta}} \right), \quad (14)$$

where $\bar{\Delta} = \Delta/R$ is the relative minimal value of the gap between the rotor and stator.

Equation (9), used to estimate the pump's momentary flow rate in case of an odd number of rolls, has no exact solution in respect to its minimum and maximum. This is the main reason for the irregularity δ to be found by using an empirical equation, indicating the impact of the main geometric parameters on the flow rate's irregularity:

$$\delta = \frac{125}{z^2} \left(1 + 2,55 \cdot z^{0,87} \cdot \lambda^{z^{0,15}} \right), \quad \% . \quad (15)$$

The established equations, presented in the above paragraphs, ensuring for the impact of some of the main geometric and constructive parameters on the kinematic irregularities in roller pumps, in respect to their: change of the flow rate of the working cameras; momentary and theoretical flow

rates and their irregularities, etc., to be investigated and analyzed.

3. Dynamic irregularities modeling

Theoretical deterministic models, described by equations referred to Mathematics and Mechanics, of the given object, are mainly used to investigate the existing unsteady processes. Based on this, in [1, 2 and 3] a method for the determination of the force loading on the rolls and a generalized model for the investigation of the periodical dynamic processes of these rolls, are being presented. In [4 and 5] it is paid attention to other irregularities, typical for these machines, concerning the geometry of the liquid’s distribution and the pump’s flow rate. As a source of excitation for the existing dynamic processes, having different characteristics, the forces, occurred in the main pump’s working elements, can be considered. The forces acting on the rolls are respectively: the force F , which is a result from the difference between the pressures in the low and high pressure zones - $\Delta p = p_2 - p_1$ (fig. 1); the force of gravity of the rolls - G ; the forces of reaction, occurred in the zones of contact between the roll and stator - N_1 and T_1 , and between the rolls and the surfaces of the rotor canals - N_2 and T_2 ; the inertia forces, occurred as a result of the existing roll’s transmission and relative accelerations - Φ , as well as the Coriolis inertia force - F_k ; the torque - M_s , which is a result of the viscosity resistance, occurred because of the roll’s rotation (with $M^{(\phi)}$ it is indicated the roll’s inertia torque).

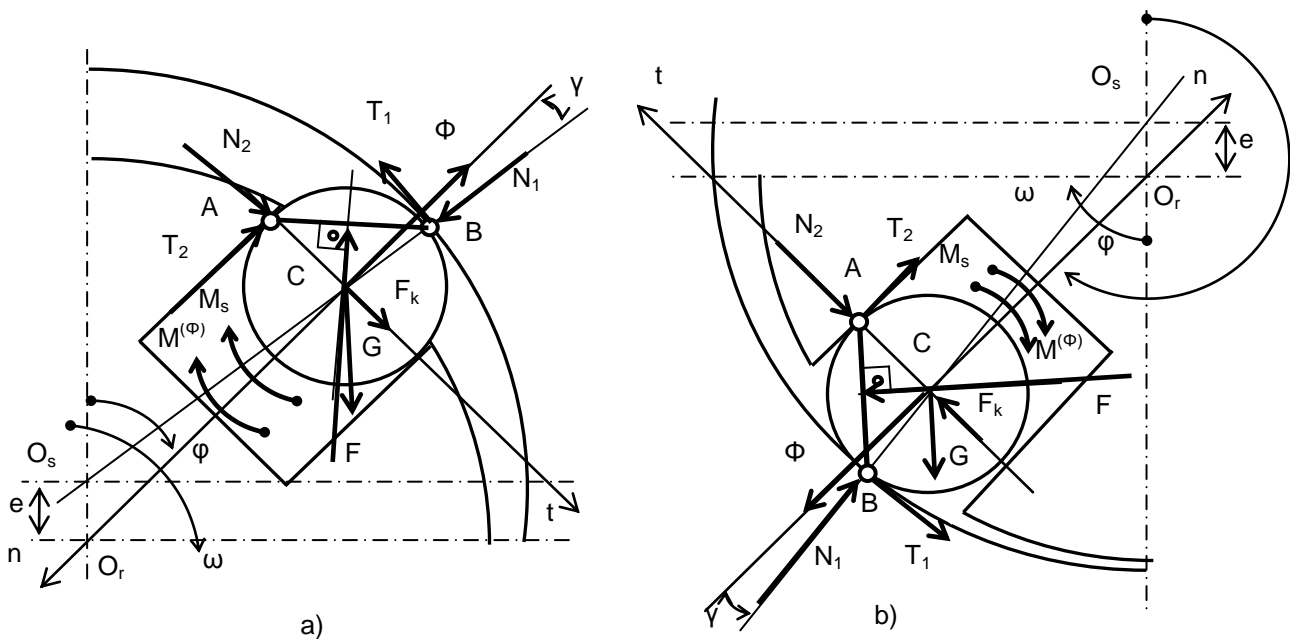


Fig.3 A scheme of roll's loading in the sealing sections:
 a) in the high pressure zone;
 b) in the low pressure zone.

The boundaries of the sealing sections – high pressure „I-II” and low pressure „III-IV”, can be defined by the following intervals:

$$\varphi_{I,II} \in [-\alpha \div (\beta - \alpha)] \text{ and } \varphi_{III,IV} \in [(\pi - \alpha) \div (\pi + \beta - \alpha)]. \tag{16}$$

The angular α (fig. 1), determining the beginning of the transitional sections – between the low and high pressure pump zones, can be estimated by (13) and (14).

The length of the sealing sections can be determined by implementing the condition, indicating the necessity for at least one roll to belong them incessantly, so that the low and high pressure zones to be permanently separated each other (fig. 1). This can be formalized by the following inequality: $\psi \geq \beta$, where β is the angular between any two adjacent rolls.

The acting of the force of pressure F on the rolls is valid only for the intervals (1) and its magnitude depends of the roll surface's size (the part of the total surface, where the pressure difference Δp is acting), and it is known that the force will be directed from the high to the low pressure zone (fig. 3):

$$F = \Delta p b \overline{AB} = 2\Delta p b r_r \sin\left(\frac{\gamma + \beta}{2}\right), \quad (17)$$

where: $\overline{AB} = 2r_r \sin(\pi/4 + \gamma/2)$ is the chorda's length, determining this part of the roll's surface, where the pressure difference is acting.

The rolls belonging to the high and low pressure cameras, determined by the intervals:

$$\varphi \in [(\beta - \alpha) \div (\pi - \alpha)] \text{ and } \varphi \in [(\pi + \beta - \alpha) \div (2\pi - \alpha)], \quad (18)$$

get into isobaric environment, as a result of which $F = 0$. For a given correct interpretation of these processes (fig. 3) different schemes of calculation, consistent with the following intervals:

$$\varphi_a \in [-\alpha \div (\pi - \alpha)] \text{ and } \varphi_b \in [(\pi - \alpha) \div (2\pi - \alpha)], \quad (19)$$

are being formulated.

For each of these schemes it has been applied the principle of d'Alambert, as well as the relevant kineto-static equations, in respect to the axes of the flat rolling movable coordinate system – Cnt , are established. For the scheme, given in fig. 3a, it can be given the following equations:

$$\vec{F}_n^{(e)} + \vec{\Phi}_n = \vec{0}; \quad G \cos \varphi - F \cos(\pi/4 - \gamma/2) + N_1 \cos \gamma - T_1 \sin \gamma - T_2 - \Phi = 0,$$

$$\vec{F}_t^{(e)} + \vec{\Phi}_t = \vec{0}; \quad G \sin \varphi - F \sin(\pi/4 - \gamma/2) - N_1 \sin \gamma - T_1 \cos \gamma + N_2 + F_k = 0,$$

and for the scheme in fig. 3b:

$$\vec{F}_n^{(e)} + \vec{\Phi}_n = \vec{0}; \quad -G \cos(\pi + \varphi) - F \cos(\pi/4 - \gamma/2) + N_1 \cos \gamma + T_1 \sin \gamma + T_2 - \Phi = 0,$$

$$\vec{F}_t^{(e)} + \vec{\Phi}_t = \vec{0}; \quad -G \sin(\pi - \varphi) + F \sin(\pi/4 - \gamma/2) + N_1 \sin \gamma - T_1 \cos \gamma - N_2 + F_k = 0.$$

Indicating the restrictions, given in (17), (18) and (19), and transforming them in respect to the normal reactions N_1 and N_2 , the following equations, valid only for the intervals (20) and (21), can be given:

- for $\varphi_a \in [-\alpha \div (\pi - \alpha)]$:

$$N_1 = \frac{F[\cos(\pi/4 - \gamma/2) + \mu_2 \sin(\pi/4 - \gamma/2)] - G(\cos \varphi + \mu_2 \sin \varphi) - \mu_2 F_k + \Phi}{\cos \gamma (1 - \mu_1 \mu_2) - \sin \gamma (\mu_1 + \mu_2)},$$

$$N_2 = F \sin(\pi/4 - \gamma/2) + N_1 (\sin \gamma + \mu_1 \cos \gamma) - G \sin \varphi - F_k,$$

$$F = 0 \text{ for } \varphi \in [(\beta - \alpha) \div (\pi - \alpha)]; \quad (20)$$

- for $\varphi_b \in [(\pi - \alpha) \div (2\pi - \alpha)]$:

$$N_1 = \frac{F[\cos(\pi/4 - \gamma/2) - \mu_2 \sin(\pi/4 - \gamma/2)] - G(\cos \varphi + \mu_2 \sin \varphi) - \mu_2 F_k + \Phi}{\cos \gamma (1 - \mu_1 \mu_2) + \sin \gamma (\mu_1 + \mu_2)},$$

$$N_2 = F \sin(\pi/4 - \gamma/2) + N_1 (\sin \gamma - \mu_1 \cos \gamma) + G \sin \varphi + F_k,$$

$$F = 0, \text{ for } \varphi \in [(\pi + \beta - \alpha) \div (2\pi - \alpha)]. \quad (21)$$

For the structuring of the model, representing the forces and torques, acting on the rolls, it is also necessary for the equations, given in [1], to be applied:

$$\Phi = m \omega^2 R [1 - r_1/2R - \lambda^2/4 + 2\lambda \cos \varphi + 5\lambda^2 \cos(2\varphi)/4],$$

$$F_k = 2m\lambda\omega^2 R [\sin \varphi + \lambda \sin(2\varphi)/2], \quad (22)$$

$$G = mg, \quad T_1 = \mu_1 N_1, \quad T_2 = \mu_2 N_2, \quad M_s = k\omega_r, \quad M^{(\Phi)} = J\varepsilon_r,$$

For the interval - $\varphi \in [-\alpha \div (2\pi - \alpha)]$, using the torque kineto-static equation, in respect to the axis

of the roll's rotation:

$$\vec{M}_c^{(e)} + \vec{M}_c^{(\phi)} = \vec{0}; \quad T_1 r_p - T_2 r_p - M^{(\phi)} - M_c = 0$$

its acceleration can be estimated:

$$\varepsilon_r = \frac{2(\mu_1 N_1 r_r - \mu_2 N_2 r_r - k \omega_r)}{m r_r^2}. \quad (23)$$

Equation (23) is a second order linear inhomogeneous differential equation, having constant values of its coefficients. Finding a solution of this equation, when its zero initial conditions have been selected, ensuring for the physical law of its rotation and speed of rotation to be found:

$$\varphi_r = (T_1 - T_2) \frac{J r_r}{k^2} \left(e^{-\frac{k}{J} t} + \frac{k}{J} - 1 \right), \quad (24)$$

$$\omega_r = (T_1 - T_2) \frac{r_r}{k} \left(1 - e^{-\frac{k}{J} t} \right), \quad (25)$$

where $t = \varphi / \omega$ is the current time.

Conclusions

Analyzing the presented generalized models, used to determine the typical irregularities in roller pumps, the following more important conclusions can be given:

- Comparing the results found by using the approximate equation (3) for estimating the relative roll's rotation in the rotor's canals, instead of the precise equation – (2), it can be seen that the occurred deviation is negligible (less than 0,06%);
- The established equations, describing the change of the pump's volume (6) and the flow rate of a given working camera (7), as well as the total momentary theoretical flow rate (8) or (9), ensuring good possibilities for the investigation of the kinematic irregularities of roller pumps;
- The established model of force loading of a pump's rolls and its intervals of validation (20) and (21), have been strictly defined.
- The physical law (24), describing the rotation of a given roll, which also can be used for the investigation of the phase characteristics of the roll's rotation, is found.

References

- [1] Angelov Y., G. Popov Dynamics of the rollers of a roller pump, Part I. Modeling of force load. PROCEEDINGS of the UNIVERSITY OF RUSE “Angel Kanchev” Volume 53, book 2 Mechanics, Mechanical and Manufacturing Engineering, ISBN 1311-3321, Ruse, 2014, 111-115 p.
- [2] Angelov Y., I. Nikolaev Dynamics of the rolls of a roller pump, Part II. Numerical study of the dynamics of rolls. PROCEEDINGS of the UNIVERSITY OF RUSE “Angel Kanchev” Volume 53, book 2 Mechanics, Mechanical and Manufacturing Engineering, ISBN 1311-3321, Ruse, 2014, 116-120 p.
- [3] Batsov T, G. Popov, Y. Angelov A model for forces racting upon rollers of a roller pump investigation. *Mechanika na mashinite*, year XIII, book 1, Varna, 2005.
- [4] Popov G., P. Russev. Irregularities in a roller pump's flow rate. PROCEEDINGS of the UNIVERSITY OF RUSE “Angel Kanchev” Volume 37, ser. 9, ISBN 1311-3321, Ruse, 1999, 102-105 p.
- [5] Popov G., P. Russev. About the geometry of the flow rate's distribution in roller pumps. PROCEEDINGS of the UNIVERSITY OF RUSE “Angel Kanchev” Volume 37, ser. 9, ISBN 1311-3321, Ruse, 1999, 106-110 p.
- [6] Popov G., P. Russev, Iv. Nikolaev. Investigation of the force loading on the vanes and determination of the mechanical loses in one-acting vane pumps. *Mechanika na mashinite* 39, book 1, Varna, 2002, pp. 50-53.

Hydrostatic Transmissions Used to Drive Electric Generators in Wind Power Plants

Ph.D. eng. Corneliu CRISTESCU¹, Ph.D. eng. Catalin DUMITRESCU¹,
Ph.D. stud.eng. Ioana ILIE¹, Dipl. eng. Liliana DUMITRESCU¹

¹ INOE 2000-IHP, Bucharest, cristescu.ihp@fluidas.ro

Abstract: *The article presents the new trend of massive use of wind energy by its conversion into electrical energy, this being clean and sustainable energy; it also presents the wind power potential in Romania, as well as the evolution of this industry in our country and abroad. It presents some aspects of wind energy conversion into electricity and highlights the role and advantages of hydrostatic transmissions. In the end, it presents some achievements at global level, and also some research concerns in Romania regarding the promotion of hydrostatic transmissions in wind power plants.*

Keywords: *wind power, hydrostatic transmission, adaptive hydraulic transmission, fluid power transmission, renewable energy, power hydraulics, wind industry*

1. Introduction

Wind energy is a form of solar energy and that's because at the basis of its generation is the sun.

Wind energy is the energy of wind, a form of renewable energy [1]. In the current context, characterized by the alarming rise in pollution because of energy production by burning fossil fuels, is becoming increasingly important to reduce dependence on these fuels. Wind energy has already proven to be a very good solution to the global energy problem. Using renewable resources addresses not only energy production, but also, by particular way of production, it restates the development model, by decentralizing the electrical energy sources.

Yearly wind power potential amounts to about 260.000 TWh worldwide. Theoretically this potential exceeds by far the yearly global consumption of electricity [2]. This potential is **15 times higher than the world's current energy consumption** and 40 times higher than the world's current electricity consumption. Exploiting this potential of energy is limited by certain constraints or disadvantages.

Disadvantages of wind power are: relatively small energy concentration; energy concentration in a very limited timeframe; unpredictability.

The unpredictability of wind can make 20-25% of the total installed capacity to appear or disappear suddenly, which raises serious problems of management.

Advantages of wind power are: Does not generate greenhouse gases; Does not results in concentrated toxic and radioactive wastes; Does not consume fossil fuel; The cost comes down to return on investment and the maintenance; It is widespread geographically; Land immobilized by wind turbine is insignificant; Wind farms can vitalize rural economies by renting land and royalty fees.

In the last decade, a significant development had the onshore wind farms, Figure 1, and also the offshore ones, Figure 2.

Total installed wind capacity has increased by 2010, according to the diagram in Figure 3, and will increase until 2020 as in the diagram in Figure 4.

Demand for renewable energy sources has led to major technological breakthroughs in wind energy development. Therefore, a large number of new wind turbines installed worldwide in the past 20 years now offer new ways of generating electricity.

According to a report of **Wind Energy Association** cited by Reuters Agency, on June 11, 2011, China surpassed the USA, and, at global level, the largest producers of wind energy are: China (44.733 MW), USA (40.180 MW), Germany (27.215 MW), Spain (20.776 MW), India (13.065 MW), Italy (5.797 MW), France (5.560 MW), UK (5.203 MW), Canada (4.008 MW), Danmark (3.734 MW).



Fig. 1. Onshore wind farms



Fig. 2. Offshore wind farms

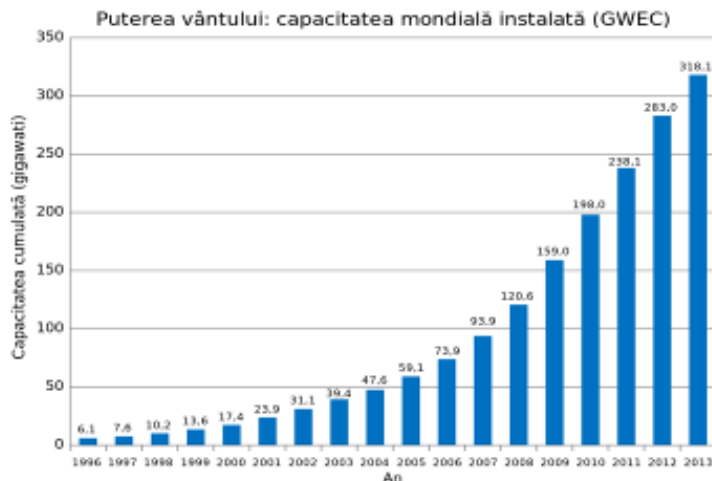


Fig. 3. Total installed wind capacity by 2010

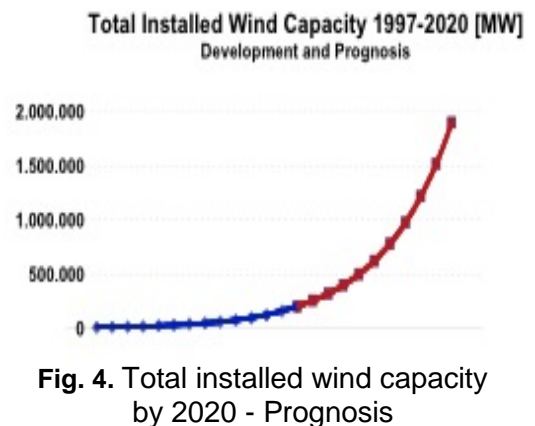


Fig. 4. Total installed wind capacity by 2020 - Prognosis

In Romania, wind turbines in the area of Constanta and Tulcea, Figure 5, have surpassed the capacity of **the Nuclear Power Pant** in Cernavoda, peaking at number 10 in the world, depending on the capacity of the wind farms commissioned, as shown by statistics published by the European Wind Energy Association. Currently Romania has installed wind farms of about 2100 MW, following investments of over 3 billion euro. [2]. In total, at this moment in Romania there are 25 large wind farms with a total capacity of nearly 1.900 MW. In addition to these large projects, there are a number of small size farms, which do not fall under the control of the national power dispatcher, their capacity being more than 200 MW, according to the data released by Transelectrica on 01.04.2013. The map of wind potential in Romania, with winds at 50 m height, is shown in Figure 5, while the map of usable wind speeds is shown in Figure 6.

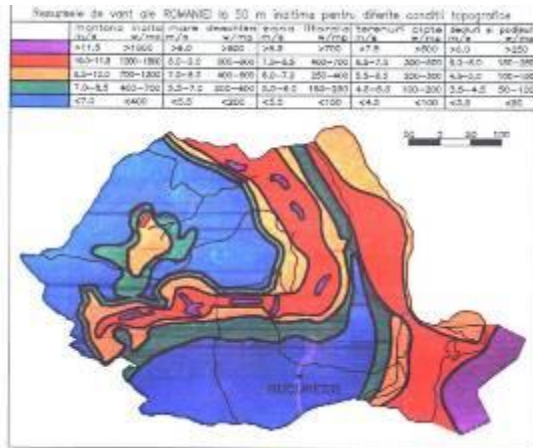


Fig. 5. The map of wind potential in Romania

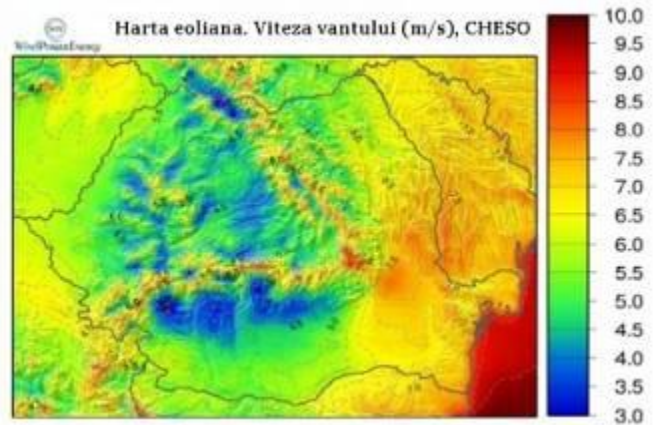


Fig. 6. The map of usable wind speeds

To produce enough electricity for a lot of people, power companies build "wind farms" with dozens of huge wind turbines. The wind farms are built in open plain areas, where the wind blows at minimum 14 miles per hour, Figure 7, but also in mountain areas, Figure 8.



Fig. 7. Wind farms in plain areas



Fig. 8. Wind farms in mountain areas

Wind potential is generally operated in areas with intense and constant wind, as the coastal areas of northwest Europe. Thus, large-scale wind turbines (500-1000 kW) have made remarkable progress in the last decade. A complementary orientation, with great expectations, is returning to small power wind turbines (<100 kW) integrated in decentralized/distributed applications, especially for rural areas with moderate winds. Compared with large wind turbines, small power wind turbines (SPWT) are more versatile and have a considerably higher technological development potential. In addition, SPWT, through its direct placement in areas of consumption, reduce energy losses due to energy transport from place of production to the user. [3]

Taking into consideration the wind power potential in Romania, the perspective for further development of great investments, and also of small-size wind power plants, special attention should be paid to rendering efficient the operation of these wind power plants.

To this goal research themes have been initiated, both in our country and abroad, which deepen and optimize various aspects of converting wind energy into electricity.

2. Aspects of converting wind energy into electrical energy

The kinetic energy of the wind is used to rotate some wind turbines which, through special mechanical transmission, actuate the electric generators, which are capable of converting the mechanical energy of the wind into electrical energy.

Conversion chain elements are of several types. However, some elements are always found in the conversion chain, such as a wind turbine, Figure 9, an electric generator, an interlocking device which achieves connecting the generator to the distribution network or to a remote load, Figure 10.

A major problem with these models is that variable rotational speed of the turbine requires a frequency converter to connect each turbine to the grid. Other issues include reliability problems with mechanical gearbox and with the weight of electric generator, due to increasing turbine size.



Fig. 9. A wind turbine

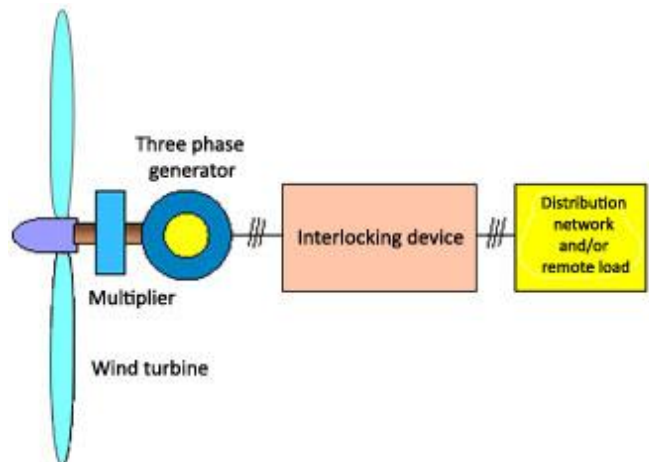


Fig. 10. Schematic wind power plant

Generally, for wind energy conversion into electrical energy there is used a mechanical transmission between the wind turbine and the electric generator; the common solutions consist in using one mechanical speed multiplier, with a high multiplying ratio, because these transmissions are difficult to manufacture, contain expensive components and generate high maintenance costs. Essentially, for small power wind plants, to become profitable it is necessary to increase the rate of extraction of basic energy and conversion of it into electrical energy, even to the low speed of the wind, which is frequently in a large period of the year.

An important role in increasing the energy efficiency of the wind power plants is played by the type and performance of the transmissions used to allow mechanical energy from the wind turbine to reach, with appropriate parameters, at the electric generator, which, in turn, generates electricity with the desired frequency constant, regardless of the wind velocity in the range accepted to be good.

3. Hydrostatic transmissions used in wind power plants

One of the ways to increase the energy efficiency and also flexibility and elasticity in functioning, in the sense of increasing possibilities to adapt to variation in wind speed, or variation of rotation speed of the wind turbine, is the use of **hydrostatic transmissions**, which offers a number of advantages, as it will be seen below.

In principle, a hydrostatic transmission consists of a pump, which is driven by wind turbine, and a hydrostatic motor, which drives the generator, Figure 11. In reality, aiming at a maximum efficiency of energy capture is more complex because the wind speed is variable in a very wide range, Figure 12.

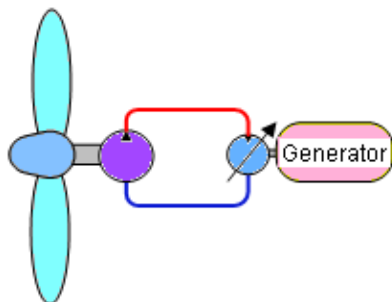


Fig 11. Principle hydrostatic transmission

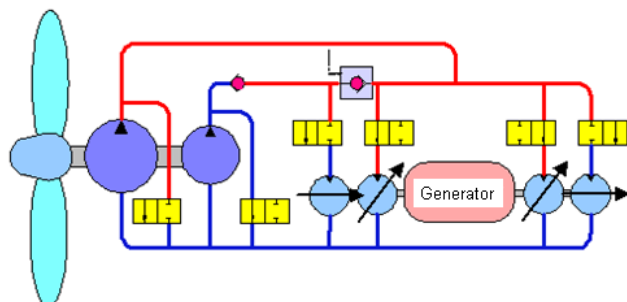


Fig. 12. Real hydrostatic transmission

Hydraulic transmission of wind energy to the ground is a research direction that we found in R-D programs related to renewable energy. Hydraulic transmission and driving included in the wind plant has all the advantages of hydraulic driving. Small power horizontal-axis wind turbines equipped with adaptive hydraulic transmissions can operate at variable speed. The adaptive hydraulic transmission allows adjustment of the outlet to the consumer demands (power or constant speed), without affecting the performance of the turbine. Adaptive hydraulic transmission requires a constant speed of the electric motor shaft during variations in pump speed at the hydraulic motor shaft. For the cases analyzed, it was found that the adaptive hydraulic transmission behaves like a stable system of damped oscillatory type with good dynamic performance [3].

Generally, for energy conversion and transmission, solutions with mechanical speed multiplier or the direct coupling between the turbine and the slow electric generator are adopted. These transmissions contain difficult to manufacture or expensive components: slow electric generator, gear transmissions, frequency converters etc.

Replacing the mechanical speed multiplier with a hydraulic transmission can lead to a more robust behaviour and competitive cost prices. If hydraulic transmission takes over also the speed multiplier function, the system can use series AC motors as electric generator.

In case of hydraulic transmission, the speed control can be achieved by adjusting the displacement of pump from hydrostatic transmission. The wide range of variation of power and speed impose the use of positive displacement hydraulic machines, respectively adjustable volume pumps. Hydraulic transmissions have a reduced gauge, a high power density, they allow a continuous and widely adjustment of the output mechanical parameters (are flexible) and offer the possibility to attach rotation speed and/or torque adaptive control systems into conversion subsystem [3].

At the designing of the hydraulic transmission, it is necessary to obtain a good dynamic behaviour, with a good safety and stability of the system in functioning.

4. Hydrostatic transmissions intended for wind power plants investigated worldwide

In the last period, a new concept, transferring the power via a hydrostatic drive train is supposed to combine good efficiency and grid stability with high reliability and low costs.

Institute for Fluid Power Drives and Controls (IFAS) of RWTH Aachen University, has developed a prototype of a hydrostatic transmission for wind energy plants of the 1-MW power class which is intended to replace the commonly used gearbox and the frequency converter. The idea is to use a slow turning pump that is directly connected to the turbine shaft to transfer the power into a high pressure oil flow and to use a hydrostatic motor that can convert this oil flow back into mechanical power to drive the generator. The high transmission ratio that is needed in a turbine can easily be achieved by the displacement ratio of pump and motor. By using a variable displacement motor the transmission ratio can be varied so that the generator can run at constant speed directly connected to the grid. [4]

The authors tell that one of the main requirements when dimensioning a transmission is a good efficiency at rated power as well as in partial load, where the turbine is operating most of the time. At the same time the rotor also influences the total power output, since the energy captured from the wind can be optimised by adjusting the rotation speed of the turbine to the actual wind situation.

Figure 13 shows a power and a torque plot of a three bladed rotor over wind speed and over rotation speed. It can be seen that to each wind speed a specific rotation speed maximises the captured power. At the same time these points of operation are not at maximum torque.

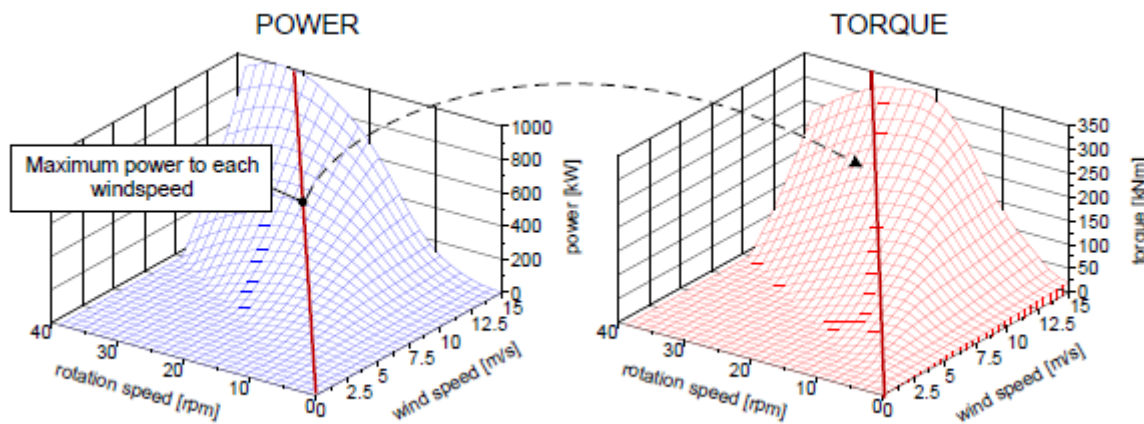


Fig. 13. Power and torque of a three bladed wind turbine

Optimal power production of a wind turbine is achieved by optimizing the drive train to the important points of operation and simultaneously using a control strategy leading to an operation in these points.

In order to optimize the efficiency, the authors have developed a great theoretical and experimental research. [5]

The authors have analyzed and evaluated different drive train concepts. Figure 4 summarizes the four main categories. The first concept consists of one pump directly driven by the turbine and one variable displacement motor mounted on the generator. Due to the wide power range such a transmission has to operate within, concept 2 uses two pumps and motors and thus can switch off single components in partial load. On the pump side this is done by connecting the high and low pressure side of one pump via a switching valve and thus setting this unit into idle mode. On the motor side, a single unit can be swiveled to zero displacement and cut off from high pressure to prevent leakage. In addition the affected generator can be switched off to prevent turning losses. Concept three also uses switchable pumps and motors but in a different way. To reduce the required pump displacement a spur gear is installed between the turbine shaft and the pump. Thus it is also simpler to connect multiple pumps to one single shaft. In contrast to concept two this configuration uses only one generator for both motors. Consequently all motors are rotating all the time even when a single motor is switched off. The fourth configuration is a power split transmission with one mechanical and one hydraulic path [5].

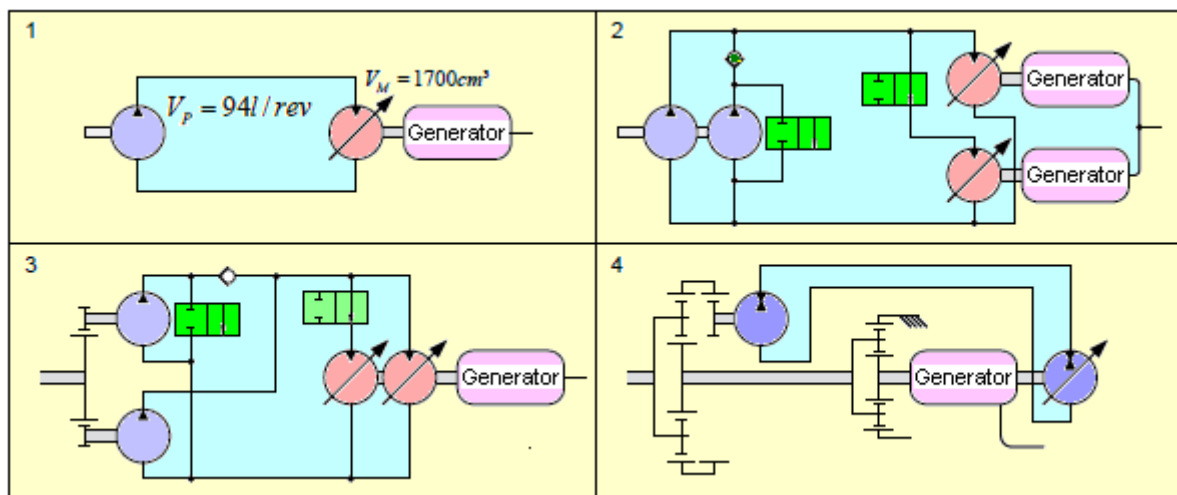


Fig. 14. Layout of four different concepts

In the Figure 15 is presented and compared the simulated overall efficiency of the four concepts. These values have been generated in simulations. At rated power (12 m/s wind speed) the full hydraulic concepts have nearly the same overall efficiency, since in this point of operation all components are activated and the total displacement of pumps and motors is the same. The power split concept 4 has a higher efficiency at full power because only about 45% of the rated power is transferred through the hydraulic path at this point. But, at the partial load the concepts differ substantially. [5]

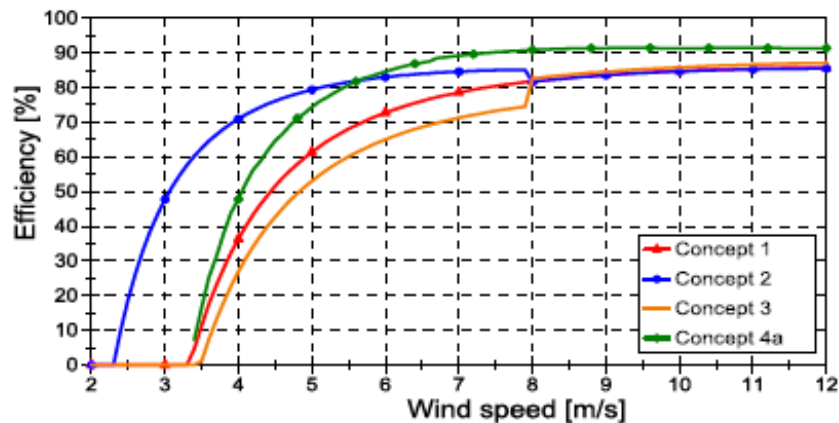


Fig.15. Overall efficiency of concept 1-4

In the following, the authors have studied different variants for the concept 4: Simple power split transmission (4a); Power split transmission with switchable hydraulic path (4b); Power split with two generators (4c) and Power split with reduced share of hydraulic power (4d). Finally, there are presented the results and is made a comparison of presented concepts.

There have been compared the various new concepts using split path technology with previous results of fully hydrostatic transmissions from which it can be seen that the overall efficiency could be improved especially at partial load. Compared to a fully hydrostatic drive train the split path concepts are beneficial but at the same time have a much higher complexity. In addition, the drive train is not completely decoupled as in a fully hydrostatic system. Before selecting a drive train for a wind turbine at a specific site two additional aspects have to be considered. First of all, each concept needs to be evaluated not only for the optimal point of the turbine but in all possible points of operation. Secondly dynamic loads have to be included since the transition between different points of operation is also relevant for the total power output.

5. Hydrostatic transmissions investigated in Netherlands

A very interesting solution for a hydrostatic transmission used in wind plant has been developed in Netherlands, in Delft University of Technology, Offshore Engineering Section, for the drive train of offshore wind turbines. The Delft Offshore Turbine (DOT) concept for the drive train of offshore wind turbines is to have the rotor shaft directly coupled to an oil-hydraulic pump in the nacelle. The hydraulic motor is located at the base of the turbine tower, where it is coupled to a seawater-hydraulic pump. The pressurized flow of seawater from each turbine converges to a hydro-power-like generator station where it is converted to electricity using Pelton turbines. All related studies and experiments until now have confirmed the technical feasibility and economic potential of this technology. [6]

The approach is to re-evaluate the way in which wind energy offshore is converted to electricity onshore. The project's defining research line is the re-assessment of the power conversion and wind energy power conversion & transmission technology is complex, heavy, and expensive and requires frequent maintenance. In any industry where robust machinery is required to handle large torques, the hydraulic drive systems are a common choice. It is therefore almost the obvious

solution for wind turbines. The design of the DOT power transmission system consists of two hydraulic circuits: a closed oil circuit and an open seawater circuit. The first runs from the shaft of the aerodynamic rotor to the base of the turbine. From here, the second circuit runs to the generator station.

The goal of the DOT demonstrator is to show-case this hydraulic power transmission system in a real turbine offshore using off-the-shelf components.

The focus of the project so far is on the power transmission system. An overview of the DOT transmission concept is given in Figure 16.

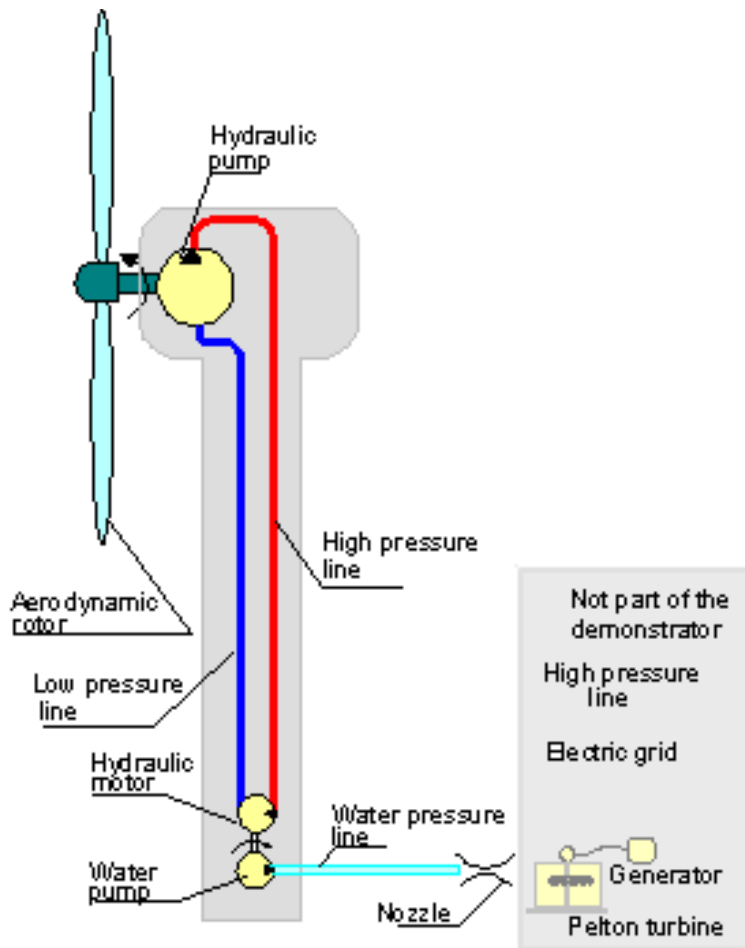


Fig. 16. DOT transmission concept

The energy conversion process from wind to electricity is radically different from conventional techniques. Recognizing the potential of fluid power transmission for wind turbines, the DOT pushes this idea one step further to fluid power transmission for offshore wind farms, with centralized electricity production and seawater as hydraulic fluid.

The energy in the seawater from multiple turbines is thus relayed to one station where it is converted to electricity, see Figure 17, where is presented the Artist impression of the DOT transmission concept.

This idea was invented and patented by Jan van der Tempel. (Van der Tempel, J. Energy extraction system, has water pump attached to rotor, windmill for pumping water from sea, water system connected to water pump, for passing water pumped from sea, and generator connected to water system, December 2009.), [6].

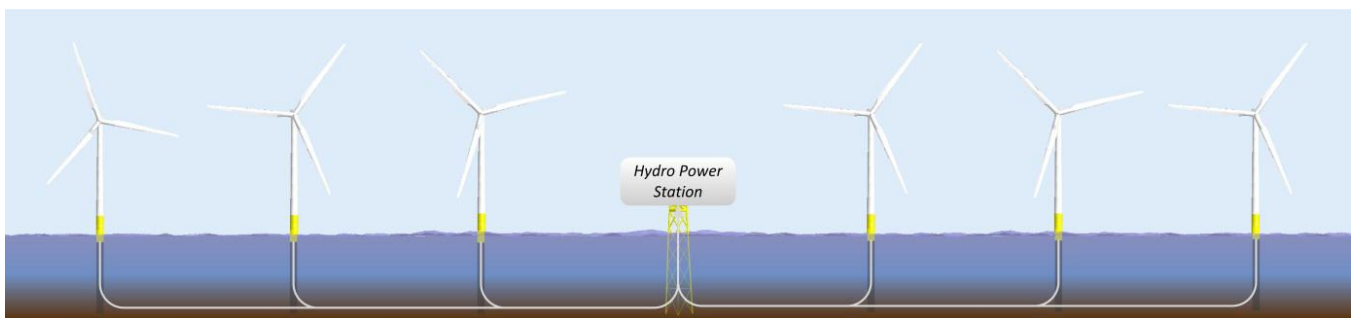


Fig.17. Farm of seawater turbines

The simplified hydraulic diagram of the DOT demonstrator is presented in Figure 18.

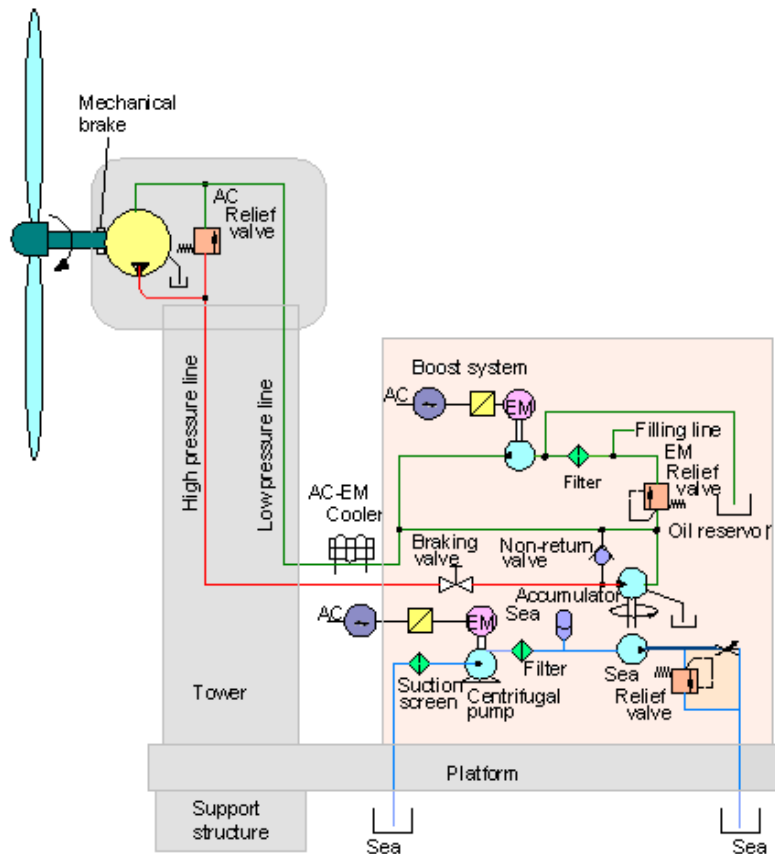


Fig. 18. Simplified hydraulic diagram of the DOT demonstrator

The only drive train component located in the nacelle is a directly driven positive displacement pump. A single pipe will transport seawater from each turbine to the generator platform. This gives the wind farm an open-circuit seawater-based power transmission system.

The goal is to use as few components and as little software as possible in order to simplify assembly and functionality, and reduce installation and maintenance requirements. In recent years mathematical models of fluid power transmission systems in wind turbines were developed and validated at the TU Delft.

Laboratory experiments were successfully carried out at scales of 600W (validation of control method with water hydraulics & rotor in wind tunnel) and 10kW (coupled oil and water circuits). Another set of experiments was carried out using the 1MW test rig (oil) at the Institute for Fluid Power Drives and Controls (IFAS) at RWTH Aachen University. **The main idea** of a variable speed wind turbine is that in order to operate at maximum aerodynamic performance, the rotor should be able to operate with a constant tip speed ratio where the maximum power coefficient is achieved for the required range of wind speeds. [6]

The main functional requirements of the Power Transmission System of a Single DOT were defined for the rotor & transmission:

- The aerodynamic rotor should operate at or close to max aero efficiency below rated wind speed.
- The fluid power transmission system should operate with energy efficiency of > 70% between the rotor shaft and the jet.
- Peaks detected in the aerodynamic torque due to tower shadow or turbulence should not be visible from readings at the nozzle.
- Safety: redundancy in shutting down capabilities.

Long lines of pipes allow the heat to dissipate via convection and radiation. By using the intake of the open seawater circuit as a source of cooling, the required capacity is decreased.

The seawater hydraulic pump is not self-priming. Thus the pressure needs to be boosted to secure the flow to the pump. The foreseen method to be applied for this is to have an integrated boost and filter system. An electrically driven German centrifugal pump sucks in seawater through an initial filter known as a suction screen. The flow then enters a filter system, after which it reaches the pump.

In Figure 18 can be seen: the Container TowerNacelle; AC Relief valve platform; Oil reservoir; Filling line; Sea Relief valve; Boost system; EM Relief valve; Non-return valve; Suction screen; Sea accumulator; Mechanical brake; Spear valve; Centrifugal pump; Braking valve high pressure line; low pressure line filter; AC EM cooler filter; Support structure.

The design constraints are based on properties of state-of-the-art off-the-shelf components. The properties that define the design values are 1. the maximum allowable tip speed of the blades (70 m/s), which sets the limit for the rotation speed of the aerodynamic rotor (25 rev/min), (2) the nominal pressure in the oil (350 bar) and water hydraulic circuits (415 bar), (3) the nominal rotation speed of the hydraulic motor (1800 rpm).

The relevant dimensions of the main components of the power transmission system, for the 500kW demonstrator, are given in Table 1.

TABLE 1: Design parameters for the 500kW demonstrator

Parameter	Value	Unit	Note
Radial pump volumetric displacement	52.8	L/rev	based on Hägglunds CBP 840
Hydraulic motor volumetric displacement	0.625	L/rev	based on Bosch-Rexroth hydraulic motors (500cc+125cc)
Seawater high-pressure pump volumetric displacement	0.489	L/rev	based on Hydrowatt pump R250/250
Nozzle diameter	7.7	mm	Adjustable nozzle through the spear valve

All properties of the radial piston pump are taken from the Hägglunds CBP840 hydraulic motor. A charge pressure of 15 bar is used for both oil pump and motor.

The operational envelope of the hydraulic transmission from rotor to nozzle is obtained as a function of the pump rotational speed, see Figure 19 and Figure 20. The possible operational area is shown as a shaded area based on the minimum and maximum nozzle diameter which allows staying within the design limits of power, pressure and speed. In terms of **power transmission efficiency** it is observed in Figure 20 that a significant part of the operational envelope has efficiencies above 60% and around 82% at rated conditions. For lower rotational speeds the efficiency is relatively low, however the selection of a rotor should be done in a way in which the lower rotational speeds correspond to the wind speeds with lower energy content and probability of occurrence.

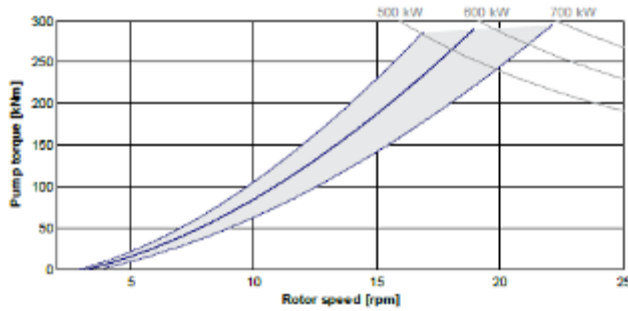


Fig. 19. Torque-speed envelope of the fluid power transmission

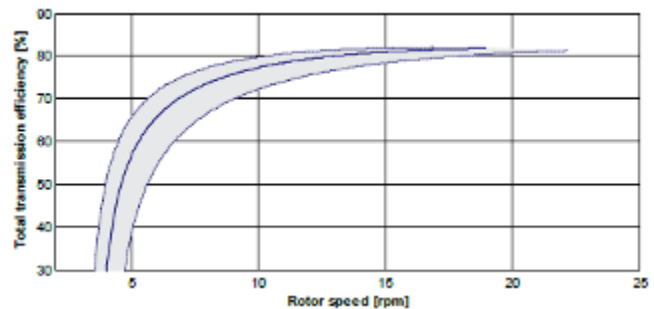


Fig. 20. Operational efficiency of the power transmission

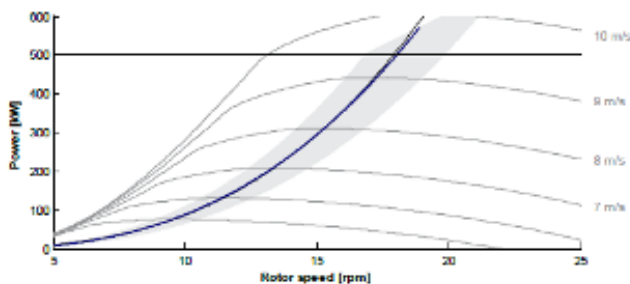


Fig. 21. Power speed curve for a rotor of 30m radius

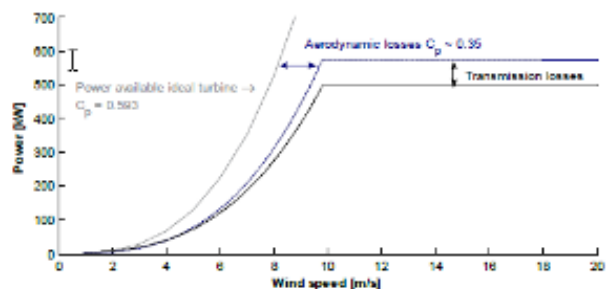


Fig. 22. Power curve example for the 500kW DOT demonstrator

In order to illustrate the overall performance of the DOT demonstrator, it is assumed that a three bladed rotor with a radius of 30m is available and coupled to the transmission. The rotor is assumed to have an optimal tip speed ratio of 6 with a resulting power coefficient of 0.35. The result of matching the rotor and power transmission envelope is seen in Figure 21. The power curve shows the effective power transmitted via the nozzle for different operational wind speeds, see Figure 22.

The power transmission efficiency is dependent on the properties of the main transmission components which are derived from current state-of-the art components.

Based on simulation results, it is shown that a hydraulic transmission provides a damped response of torque and transmitted power while keeping operational parameters within design limits.

The power transmission efficiency is dependent on the properties of the main transmission components which are derived from current state-of-the art components.

Based on simulation results, it is shown that a hydraulic transmission provides a damped response of torque and transmitted power while keeping operational parameters within design limits [6].

5. Hydrostatic transmissions investigated in ROMANIA

In our country, have been developed several technical solutions for wind turbines, under various national research programmes. [3]

Some of these wind concepts, were investigated both theoretically, through mathematical modeling and numerical simulation on the computer, and experimentally, through conducting laboratory tests, where have been performed physical measurements done by acquiring data, subsequently stored and processed by computer.

Such research activities has been conducted in technical universities of Bucharest, Iasi, Cluj-Napoca, Timisoara, Craiova and Constanta.

5.1. Adaptive hydraulic transmission for small wind power plant

The Department of Fluid Mechanics of „Gheorghe Asachi” Technical University in Iasi together with Hydraulics and Pneumatics Research Institute INOE2000-IHP in Bucharest have developed a concept for an adaptive hydraulic transmission for small wind power turbine, and also a test stand [3].

The adaptive hydraulic transmission is based on specific operation elements of a wind turbine under variable wind speed and variable load at user. The realized experimental stand allows the testing of hydraulic transmission behaviour at turbine shaft speed variation (due to changes in wind speed) and at hydraulic motor shaft load variation.

5.1.1. The concept of adaptive hydraulic transmission for small wind power plant

The block diagram for the adaptive hydraulic transmission designed for low power horizontal-axis wind turbines is shown in Figure 23.

Wind turbine **WT** transforms aerodynamic power (wind speed v) in mechanical power with parameters ω_1 (angular velocity) and M_1 (moment). The pump with adjustable unit volume **PAV** transforms mechanical power into hydraulic power with parameters Q (flow) and p (pressure). The hydraulic motor **HM** transforms hydraulic power into mechanical power transmitted to load **L**. The feedback loop includes speed transducer **ST** which gives signal $U\omega$. This is compared with reference value U_r . At the outlet of the regulator **R** results the command value c . The servomechanism **SVM** transforms the command value into an execution value m , which acts on the pump flow control elements **PAV**. In the absence of the feedback loop, changes in wind speed v will increase pump speed, pump flow and therefore the drive speed of load **S** as well. Similarly, load variation leads to a decrease in motor speed.

The feedback loop, which depends on the value of the engine speed MHR , allows maintaining a constant speed imposed by the reference value U_r on the hydraulic motor shaft, under variations of

both the wind speed and the load S . The adaptive system allows adjustment of two disruptive values: wind speed v and load S variation on the engine.

5.1.2. The test stand

In order to simulate the working conditions of an adaptive hydraulic transmission designed for small wind power, we have developed a test stand with the configuration shown in Figure 23. A general view of test stand can be seen in Figure 24, where are presented the load module, the closed circuit module, the control panel and the frequency converter.

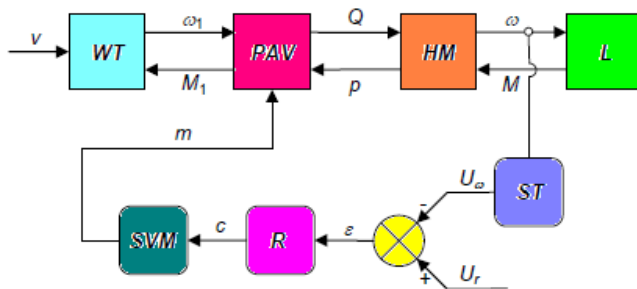


Figure 23. Block diagram of the adaptive hydraulic transmission system

Fig. 24. General view of test stand

The transmission module includes the pump with adjustable unit volume /flow **PAV** and the hydraulic motor **HM**, connected in closed circuit. **PAV** is a double pump unit and is composed of a main unit with adjustable volume (flow) and a unit with constant flow that allows the compensation of hydraulic losses and the command of actuator in order to change the geometric volume. The pump **PAV** feeds the non-adjustable rotary hydraulic motor **HM** which, in real system, either drives an electric generator or a load of mechanical nature **L**, through its shaft. In the test stand, the simulation of hydraulic rotary motor shaft load is achieved by the loading module, which consists of another hydraulic pump.

An important component of experimental stand is the automatic control loop, shown as block diagram in Figure 25.

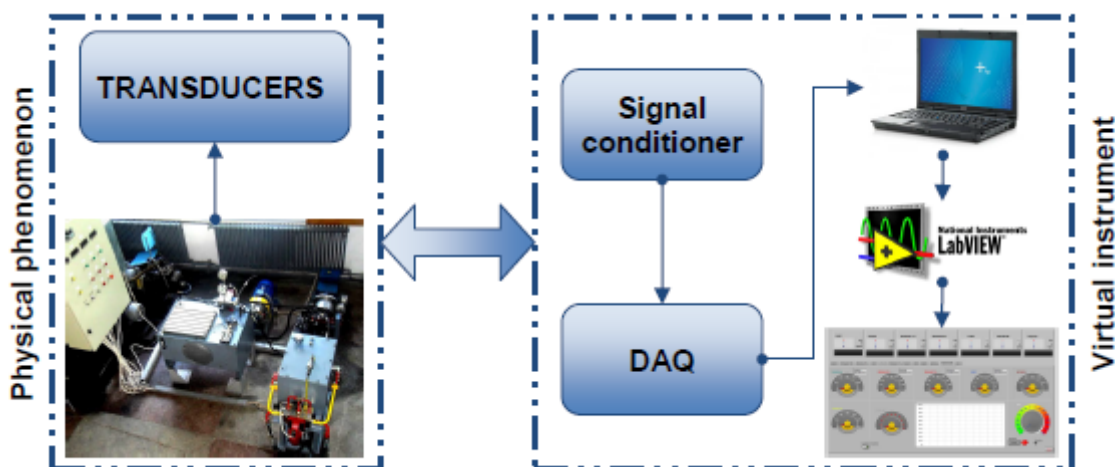


Fig. 25. Block diagram of automatic control loop

The transducers receive the physical phenomenon and convert physical parameters (pressure, flow etc.) in a unified type parameter, mainly voltage, the resulting signal being proportional to the variation of monitored parameters.

Conditioning modules transform electrical signals generated by transducers in a form that the DAQ (data acquisition) board can accept.

Acquisition board converts the electrical signals through its basic component: the analog-digital signal converter. A numerical value is attached to each voltage supplied by transducers, thus allowing interpretation of physical values by computing systems.

A lot of experimental tests have been made and there have been obtained a series of graphical variations for the main parameters of the system, presented in [3].

Experimental research has been conducted for a constant torque at the shaft of the rotary hydraulic motor, simultaneously with imposing the condition of constant rotation speed.

6. Conclusions

In the article were presented, first, some general data on the new technology of wind energy use in order to produce electricity, advantages and disadvantages of wind energy, wind potential in Romania, and the development of this technology worldwide.

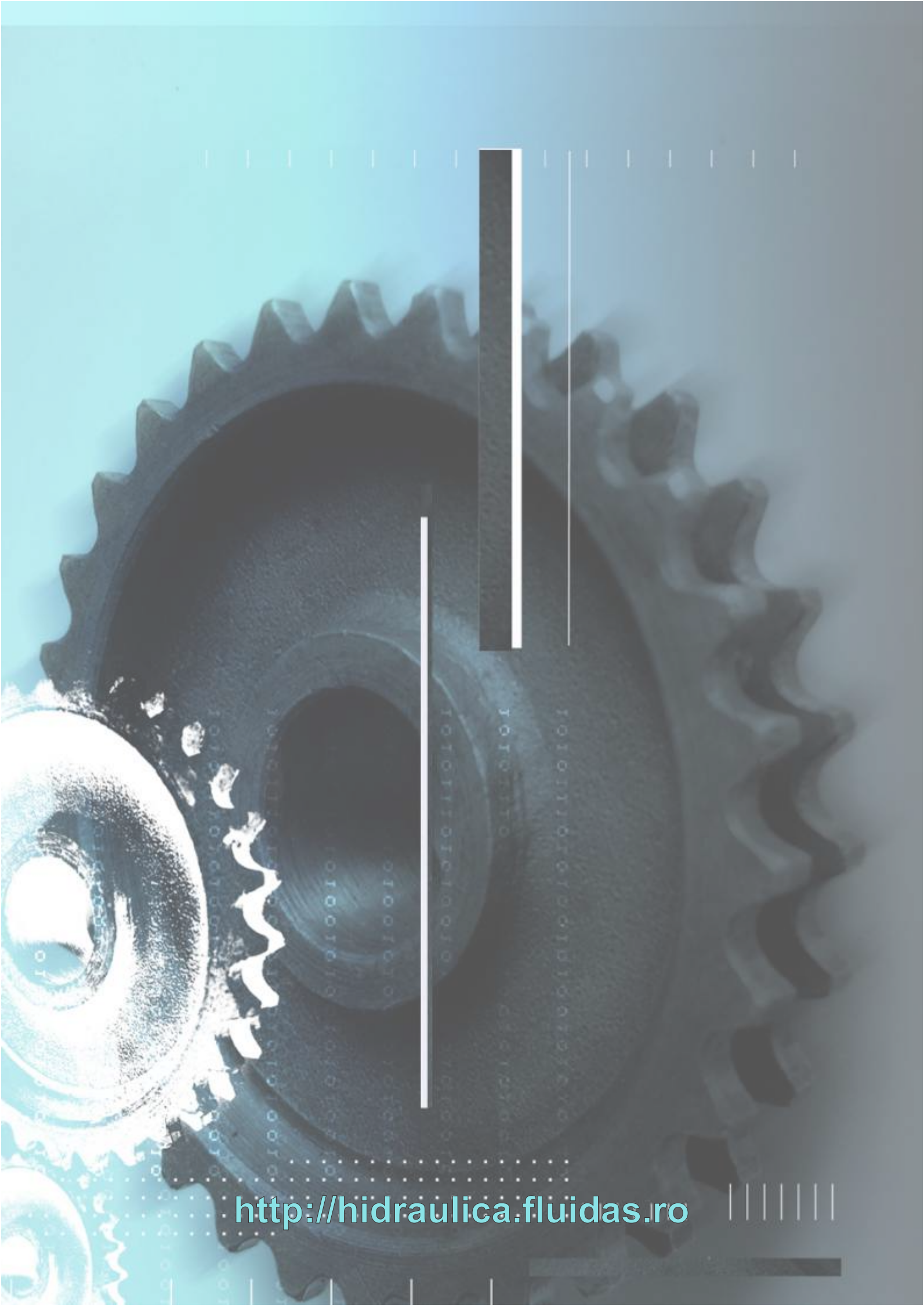
We then presented a number of specific issues concerning the conversion of wind energy into electricity, emphasizing the important role of intermediate transmissions between wind turbine itself and the electric generator itself, showing that one of the ways to increase energy efficiency is the use of hydrostatic transmissions.

There were presented the principles underlying the hydrostatic transmissions for wind turbines and were presented a series of concrete achievements both globally as well as in Romania, which have shown their advantages in adapting variable speed rates of wind turbine and control of constant speed to the electric generator.

Research on hydrostatic transmissions in wind power plants will continue in order to optimize the schematic diagrams and the ways for controlling the speed of the generator.

References

- [1] *** Energie Eoliană. In Wikipedia, http://ro.wikipedia.org/wiki/Energie_eolian%C4%83;
- [2] Roxana Petrescu, România, locul 10 în lume la capacitatea turbinelor eoliene instalate ... In : Ziarul Financiar, May 5, 2013, <http://www.zf.ro/zf-24/romania-locul-10-in-lume-la-capacitatea-turbinelor-eoliene-instalate-anul-trecut-china-si-usa-domina-piata-globala-a-vantului-10845810>;
- [3] D. Calarasu, C. Chirita, P. Drumea, B. Ciobanu. "Adaptive hydraulic transmission for small power wind turbine". In: Proceedings of 8th International Fluid Power Conference, pp. 383 – 397, Dresden, 2012;
- [4] Johannes Schmitz, Nils Vatheuer, Hubertus Murrenhoff. "Dynamic Analysis and Measurement of a Hydrostatic Transmission for Wind Turbines". In: CD / Proceedings of the 8th International Fluid Power Conference, Dresden, 2012;
- [5] Johannes Schmitz, Gunnar Matthiesen and Hubertus Murrenhoff. "Hydrostatic transmission for wind turbines – Comparison of different configurations and their applicability". In: Proceeding of the 9th International Fluid Power Conference, pp. 144 – 152, Aachen, 2014;
- [6] Niels Diepeveen, Antonio Jarquin Laguna. "Preliminary Design of the Hydraulic Drive Train for a 500kW Prototype Offshore Wind Turbine". In Proceedings of the 9th International Fluid Power Conference, pp.132– 143, Aachen, 2014.



<http://hidraulica.fluidas.ro>